Cellular and molecular mechanisms underlying srGAP2 function during neuronal development.

Sabrice Guy Guerrier

A dissertation submitted to the faculty of the University of North Carolina at Chapel Hill in partial fulfillment of the requirements for the degree of Doctor of Philosophy in the Department of Pharmacology.

Chapel Hill
2009

Approved by:

Franck Polleux, Ph.D.

John Sondek, Ph.D.

Eva Anton, Ph.D.

James Bear, Ph.D.

Keith Burridge, Ph.D.

Klaus Hahn, Ph.D.

Sabrice Guy Guerrier

Cellular and molecular mechanisms underlying srGAP2 function during neuronal development.

(Under the direction of Franck Polleux, Ph.D.)

During brain development, proper neuronal migration and morphogenesis is critical for the establishment of functional neuronal circuits. I have identified that srGAP2 negatively regulates neuronal migration and induces both neurite outgrowth and branching through the ability of its F-BAR domain to induce filopodia-like membrane protrusions resembling those induced by I-BAR domains in vivo and in vitro. Previous work has suggested that in non-neuronal cells, forced expression of proteins that promote filopodia decrease the rate of cell migration and the persistence of leading edge protrusions. srGAP2 knockdown reduces leading process branching and increases the rate of neuronal migration in vivo. Overexpression of srGAP2 or its F-BAR domain has the opposite effects, increasing leading process branching and dynamics and blocking migration. Finally, expression of a truncated form of the F-BAR domain that localizes to the membrane but fails to elicit filopodia-like membrane protrusions does not inhibit neuronal migration. This work highlights the functional importance of proteins directly regulating membrane deformation for proper neuronal migration and morphogenesis.

Dedication

To my loving wife, Dreka, I could not have done this without your great strength, love and support. You are my superwoman and I love you dearly.

Acknowledgements

James Bear, John Sondek, Keith Burridge, Eva Anton, Klaus Hahn, Sharon Milgram, Pat Brennwald, Vytas Bankaitis, Gary Johnson, Lisa Plummer, Marie Rougié, Julien Courchet, Rocky Cheung, Eldon Peters, Melody Lee, Janet Berrios, Jaqueline de Marchena-Powell, Ashton Powell, Meghan Morgan, Takayuki Sassa, Jaeda Coutinho-Budd, Dante Bortone, Randal Hand, Aurélie Gresset, Brenda Temple, Dionne Glast, Tiana Garrett, Ginnie Hench, Mike Lee, Anthony DePass, Rick McGee, Michelle Smith, Robert Sago, Adlar Simmons, Kerby Coulanges, Joseph Guerrier, Philippe Guerrier, Stephane Guerrier, Michele Guerrier, Franck Polleux, Dreka and Joshua Guerrier.

TABLE OF CONTENTS

LIST OF FIGURES

LIST OF ABBREVIATIONS

MGE	Medial Ganglionic Eminence
VZ	ventricular zone
CP	cortical plate
PP	preplate
MZ	marginal zone
dCP	deep cortical plate
SVZ	subventricular zone
IZ	intermediate zone
CDK5	cyclin dependent kinase 5
Ngn2	neurogenin 2
PI3K	phosphoinositide 3 kinase
JNK	c-jun N-terminal kinase
MTOC	microtubule organizing center
Lis-1	lissencephaly-1
DCX	doublecortin
FILIP	Filamin A interacting protein
BAR	Bin, Amphiphysin, Rvs
N-BAR	amphipathic (BAR)
FCH	Fer/Fes CIP4 homology
CC	coiled-coil
F-BAR	FCH- (BAR)
I-BAR	Inverse-(BAR)

GAP	GTPase activating/accelerating protein
GEF	guanine nucleotide exchange factor
srGAP	slit-robo GAP
LP	leading process

Chapter 1:

Introduction and Background

Overview of Cortical Development

The microcircuit underlying the function of the cerebral cortex is composed of two main neuronal sub-populations. The first, GABAergic interneurons are born in the medial ganglionic eminence (MGE) and migrate tangentially to the neocortex where they will provide inhibition to neuronal circuits (**Fig. 1.1**). The second, glutamatergic neurons are born in the ventricular zone (VZ) of the neocortex and migrate radially to the cortical plate (CP) where they will terminally differentiate displaying the proper dendritic morphology and extending axons to the proper locations (**Fig. 1.1**). These neurons will act as the excitatory neurons of the cortex. Defects in the ratio of excitatory to inhibitory neurons, results in severe developmental neuropathologies including from schizophrenia (Di Cristo, 2007) and epilepsy (Guerrini and Marini, 2006). As a result much work has been focused on identifying the genes that regulate the migration and differentiation of these two neuronal sub-populations during the development of the cerebral cortex.

In order to understand the consequences of impairment of the proper ratio of excitatory to inhibitory neurons in the cortex, one must first appreciate the manner in which the neocortex develops. The neocortex is a layered structure: neurons sharing a given function including axonal projection patterns, dendritic morphology, electrophysiological properties, etc... are grouped in separate layers. Between E10 and E11, the mouse neocortex consists of two layers, the ventricular zone (VZ) where progenitors undergo divisions and the preplate (PP) composed of the first postmitotic neurons present in the mammalian cortex (**Fig. 1.2**). At approximately E12, neurons migrate out of the VZ and split the PP into two layers (the marginal zone (MZ) and subplate (SP)) and thereby form the cortical plate (CP). The MZ contains a key population of neurons called Cajal-Retzius cells which secrete Reelin, a

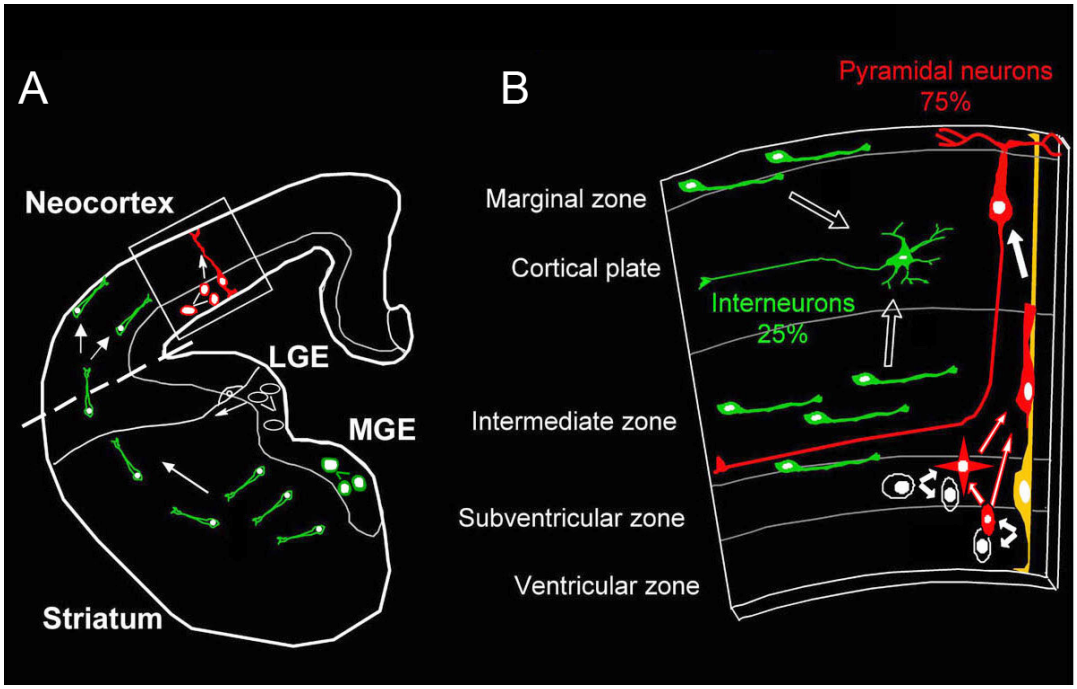

Figure 1.1: Overview of mammalian cortical development. A) Coronal view of developing telencephalon. The cerebral cortex is comprised of two neuronal subtypes: GABAergic interneurons (green) which are born in the ventricular zone (VZ) of the medial ganglionic eminence (MGE), migrate tangentially to the neocortex. Glutamtergic neurons (red) are born in the VZ of the neocortex and migrate radialy to their final destination in the cortical plate. B) More detailed view of radial migration. Glutamatergic neurons arise from asymmetrically dividing radial glial cells (yellow) in the VZ. The neurons then migrate to the subventricular zone where they undergo a phase in which they produce multiple neurites. Once the neurons polarize, they form a single leading process, attach to the radial glia and migrate by nucleokinesis to the cortical plate where they elaborate their dendrite and project their axon to the proper target.

large secreted glycoprotein playing a key role in cortical layer formation. These early postmitotic pyramidal neurons that form the immature CP constitute the future layer 6. This will be the deepest cortical layer. These cells migrate primarily via somal translocation whereby, their leading process remains attached to the basal membrane at the pial surface while its soma translocates from the VZ to the CP. The next wave of neurons born at E13 will generate layer 5 will then migrate from the VZ using radial glial progenitors as a substrate for migration. These layer 5 neurons will migrate passed the neurons that make up the CP and this process of the newest born neurons bypassing their predecessors will continue until about E18 (**Fig. 1.2**). This results in an "inside-out" development of the cortex where the youngest neurons constitute the most superficial layers and the oldest neurons constitute the deepest layers in the cortex. In the adult, this results in six cortical layers where layer 1 cells are most superficial and layer 6 cells are the deepest. Clearly, the cellular and molecular mechanisms controlling the precise timing of cell cycle exit, initiation of migration and proper translocation of neurons to the individual cortical layer are critical for the proper functional maturation of the cerebral cortex.

While somal translocation is thought to be the predominent mode of migration before E14 (Gupta et al., 2002), radial migration underlies the majority of layer formation during cortical development (E14-18; (Gupta et al., 2003)). Radial glial cells act as neuronal progenitors giving rise to neurons in the ventricular zone. Once the neuron exits the cell cycle, it migrates to the sub-ventricular zone (SVZ) where it undergoes a short multipolar phase, extending dynamic neurites in multiple directions (Noctor et al., 2004) before polarizing by forming a single leading process. The neurons then attach to and migrate along radial glia processes towards the CP using leading process attachment to pull the cell soma forward. This process is known as nucleokinesis. Once they reach the CP, radially migrating neurons detach from the radial glial scaffold and elaborate their apical and basal

dendrites. As one might expect much work has outlined the signaling pathways and molecules that control radial migration.

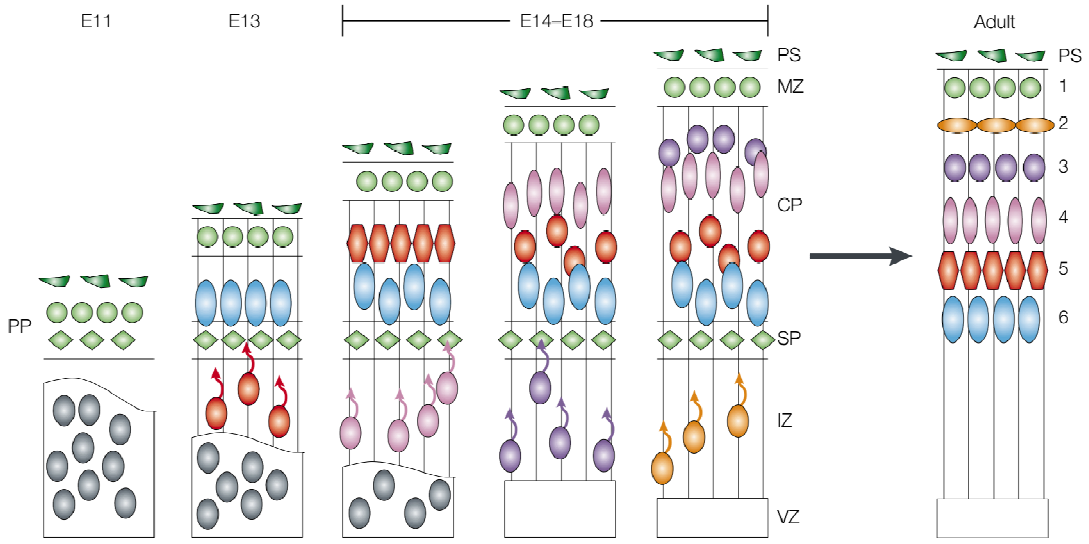

Figure 1.2. Overview of cortical lamination. During early cortical development (E11) the cortex consists of two layers: the ventricular zone and the preplate that was made by somally translocating post mitotic neurons. At E13, the preplate is split by a second wave of post-mitotic neurons resulting in the formation of the subplate and the marginal zone. These cells establish the cortical plate. From E14-E18 cells migrate through radial migration bypassing their predecessors as they migrate to the cortical plate resulting in the oldest born neurons being deep in the cortex and the newest born neurons being located superficially. This type of laminaiton is referred to as “inside out” development and results in the layer formation seen in the adult. (adapted from (Gupta et al., 2002))

Reelin regulates both glia independent and dependent forms of neuronal migration in the cortex

Reelin is an extracellular cue secreted by Cajal-Retzius cells resident in the marginal zone of the cortex (Curran and D'Arcangelo, 1998). Reeler mutant mice, show defective cortical lamination due to a mutation in the reelin gene (D'Arcangelo et al., 1995). Specifically these mice develop an inverted cortex, due to defective preplate splitting, resulting in the formation of the cortical plate beneath the neurons of the subplate and the appearance of an inverted cortex (Curran and D'Arcangelo, 1998). Interestingly, 2 additional mouse and rat lines with two spontaneously occurring mutations in mDAB1 (scrambler and yotari) share this phenotype with the Reeler mice (Sheldon et al., 1997) suggesting that reelin and Dab1 may act in the same pathway. In addition, the observation that loss of the very low density lipoprotein receptor (VLDLR) and apolipoprotein E receptor 2 (ApoER2) also shared this phenotype of no preplate splitting allowed for the identification of the reelin signaling pathway (Trommsdorff et al., 1999). Indeed, reelin binds to VLDLR and ApoER2 (Hiesberger et al., 1999) and this binding leads to tyrosine phosphorylation of mDAB1 by Src-family kinases (Benhayon et al., 2003). Taken together, this inability to split the preplate suggested that there is a defect in the ability of early somally translocating neurons to migrate. It should be noted however, that reelin signaling does not only affect somally translocating neurons. Reelin signaling also seems to affect radial glia-mediated neuronal migration since ectopic expression of reelin in the ventricular zone rescued the preplate splitting defect of the Reeler mouse but continued to present abnormal layer formation (Magdaleno et al., 2002). This suggested that reelin signaling could regulate radial migration independent of its function in preplate splitting. This data was later supported by work from Chris Walsh’s lab demonstrating that acute reduction of Dab1 by RNA interference increased the cell distance from the marginal zone suggesting an impairment of migration

(Olson et al., 2006).

CDK5 and radial migration

Cyclin dependent kinase 5 (CDK5) was shown to have no role in cell cycle progression, compatible with its expression and activity in postmitotic neurons (Lew et al., 1994). The activity of CDK5 is regulated by its coactivator p35 (Tsai et al., 1994), which is also highly expressed in postmitotic neurons but not neuronal progenitors (Chae et al., 1997; Tsai et al., 1994). Loss of p35 or CDK5 causes severe defects in neuronal migration and ultimately cortical lamination (Chae et al., 1997; Gilmore et al., 1998). The major defect here appears to be impairment of radial migration following preplate splitting, so that the newly born neurons cannot bypass their predecessors resulting in an inverted cortex with proper preplate splitting (Chae et al., 1997; Gilmore et al., 1998; Gupta et al., 2002). This is interesting since prior to preplate splitting neurons translocate by somal translocation whereas, post preplate splitting, neurons migrate primarily by nucleokinesis, suggesting that CDK5 primarily regulated radial glia-dependent migration. As a result, many subsequent studies have aimed to identify molecular substrates downstream of CDK5 that mediate these effects. In the subsequent sections I will discuss the molecules that regulate radial migration and describe those that are regulated by CDK5.

Rho family GTPases and radial migration

The role of Rho family GTPases in non-neuronal cell types has been studied extensively (Raftopoulou and Hall, 2004). Rho family GTPases are known to regulate a myriad of processes from cell polarity and migration to membrane trafficking and transcription. However, much less is known about the exact functions of Rho-GTPases

during neurodevelopment. As a result many recent studies have sought to understand the role of Rho-GTPases during development of the cortex.

RhoA is thought to primarily play role in cell contraction at the rear (Ridley et al., 2003). GTP bound RhoA activates rho-kinase, which leads to increase myosin light chain phosphorylation and finally increased myosin contractility (Ridley et al., 2003). This activity is thought to propel the cell rear forward during the migration cycle (Ridley et al., 2003). It appears that this RhoA pathway may be conserved in neurons (Ge et al., 2006; Hand et al., 2005; Heng et al., 2008). Hand et al. recently demonstrated that Neurogenin 2 (Ngn2), a bHLH proneural transcription factor, specificies the radial migration properties of cortical neurons. Mutation of tyrosine 241 of ngn2 to phenylalanine impaired migration and cells showed a defect in nuclear translocation. Interestingly, this defect could be partially rescued by dominant negative RhoA, suggesting the importance of RhoA activity in radial migration (Hand et al., 2005). Further work expanded on these observations by demonstrating that the rho effector, rho-kinase (ROCK) is required for radial migration (Nguyen et al., 2006a). Finally, it was recently shown that myosinII activity was required for forward nuclear movement during radial migration, since treatment with myosin inhibitor, blebbistatin inhibited nuclear movement (Tsai et al., 2007). These data suggest that the RhoA-ROCK-MyosinII pathway may be at work in radial migration.

While RhoA is thought to regulate contraction at the cell rear, Rac1 and Cdc42 are thought to act primarily by regulating actin dynamics at the leading edges of migrating cells (Ridley et al., 2003). Cdc42 in particular, has been shown to act both at the leading edge during migration, but also at the establishment of polarity before initiation of migration (Raftopoulou and Hall, 2004). Indeed, the ability of cdc42 to regulate cell polarity is also conserved during cortical development. Before radial migration occurs neurons are produced through both asymmetrical and symmetrical cell divisions (Nguyen et al., 2006b)

and the ability for these cells to divide is dependent upon the polarized localization of specific proteins (Costa et al., 2008). It turns out, that proper regulation of cdc42 is required for this polarization. Specifically, two groups indepently demonstrated that loss of cdc42 disrupted cell division and the localization of β-catenin and atypical protein kinase C (aPKC), two other proteins that are essential for neuronal polarity (Cappello et al., 2006; Chen et al., 2006). Because cdc42 conditional deletion reported in these studies were obtained through Cre-mediated recombination in neuronal progenitors, it is difficult to distinguish the function of cdc42 in cell migration from its function in cell division. However, recent work suggests that cdc42 may be directly involved in radial migration. Konno et al. recently showed using dominant-negative approaches that phosphoinositide 3 kinase (PI3K) activation was required for radial migration (Konno et al., 2005). Moreover, they showed that dominant negative cdc42 impaired radial migration after PI3K activation suggesting that cdc42 activation may be required for this activity.

Rac1 has also been implicated in regulating radial migration. Inhibition of Rac1 downstream of both PI3K and c-jun N-terminal kinase (JNK) blocked radial migration (Kawauchi et al., 2003; Konno et al., 2005). Moreover, the Rac GEF, P-Rex1 was also shown to be involved in radial migration (Yoshizawa et al., 2005). In addition, rac1/cdc42 effector p21 activated kinase (PAK)-1 was recently shown to be involved in radial migration. Expression of consituitively active form of PAK-1 severely impaired radial migration and reduction of PAK-1 had similar effects (Causeret et al., 2008).

While, RhoA, Rac1, and Cdc42 are the most commonly studied Rho-GTPases, it was recently shown that Rnd2 plays an important function in radial migration (Heng et al., 2008). Specifically, knockdown of Rnd2 transiently reduced radial migration and expression of low levels of Rnd2 was sufficient to significantly rescue the migration defect observed in the conditional Ngn2 knockout cortex (Heng et al., 2008).

Taken together these data highlight the potential importance of Rho family GTPase regulation in radial migration. However, much of this data comes from genetic studies and the use of constituitively active and dominant negative approaches. While these techniques provide useful information, they lack the resolution and specificity needed to truly analyze the specific role of these proteins in real time and with subcellular resolution. Future experiments should determine in real-time the subcellular activation of Rho family proteins using biosensors during neuronal migration. Moreover, shRNA studies would allow the study of cell autonomous effects of these proteins. Finally, we have developed tools to study the effects of gene manipulation specifically on neurons (Guerrier et al., submitted and (Heng et al., 2008)) that would allow one to bypass the effects of these proteins on cell division in order to observe the phenotypic consequences on radial migration.

Microtubule dynamics and microtubule associated proteins and their roles in radial migration

Microtubules play a key role in radial migration. This is due to the organization of microtubules which form a “cage” around the nucleus on one end of the microtubule organizing center (MTOC) and extend from the MTOC to the extreme end of the leading process (**Fig. 3**) and (Lambert de Rouvroit and Goffinet, 2001; Tsai and Gleeson, 2005). As a result, many groups have sought to identify proteins that regulate microtubule dynamics and as well as MTOC organization during radial migration. One such protein is lissencephally-1 or Lis-1. As the name suggests, loss of Lis-1 causes type 1 lissencephaly leading to a disorganization of the cortical layers during development as well as a lissencephalic (smooth, absence of gyrification) cortex (Guerrini and Marini, 2006). shRNA mediated reduction of Lis-1 has helped explain the lamination defect seen in patients with type-1 lissencephaly (Tanaka et al., 2004a; Tsai et al., 2005). Loss of Lis-1 affects cortical

development including cell division (Tsai et al., 2005). However, there were also significant effects on the ability of immature neurons to undergo transition from multipolar to bipolar (Tsai et al., 2005). Moreover, Lis-1 reduction led to impaired migration due to the inability of the cell soma to translocate (Tanaka et al., 2004a; Tsai et al., 2007; Tsai et al., 2005). Interestingly, the leading process of these cells continued to grow suggesting that Lis1 may be required to couple somal translocation with leading process growth. Indeed, a subsequent study demonstrated that Lis-1 knockdown impaired the movement of the centrosome, which could explain why the nucleus does not move forward when Lis-1 levels are reduced (Tanaka et al., 2004a). So how might Lis-1, a microtubule binding protein regulates the movement of the nucleus? Lis-1 associates with the minus end directed motor protein, dynein. The interaction between dynein and Lis1 is mediated by a protein called Nudel. Interestingly, Nudel function is highly conserved since it is critical for the proper migration of fungi (Tsai and Gleeson, 2005). Moreover, loss of 14-3-3 epsilon, which regulates Nudel localization, causes lissencephaly similarly to lis1 and the compound mutant (Lis1/14-3-3 double knockout) is more severe than the single knockout, again suggesting the functional importance of this pathway for neuronal migration (Toyo-oka et al., 2003). It was shown that like reduction of Lis1, reduction of dynein also impaired centrosome movement (Tanaka et al., 2004a; Tsai et al., 2007). It was demonstrated that dynein localized to the swelling present in front of the nucleus that forms prior to nuclear translocation and colocalized with centrosome. These data suggested that Lis1 may regulate forward movement of the nucleus by regulating dynein localization to the centrosome. Interestingly, it was shown that CDK5 can phophorylate Nudel (Niethammer et al., 2000) and that 14-3-3 epsilon could bind to phosphorylated Nudel to properly localize with Lis1 and dynein (Toyo-oka et al., 2003), thus providing one mechanism by which CDK5 could regulate radial migration.

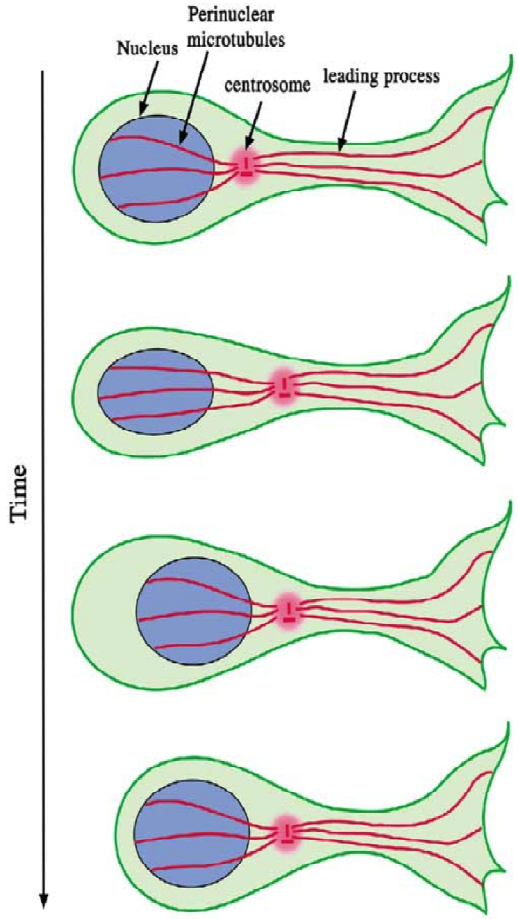

Figure 1.3. Nucleokinesis. Neuronal migration in the cortex is mediated by the centrosome's ability to connect microtubules to both the nucleus and leading process. As a result, leading process extension and adhesion leads to the centrosome being pulled forward. Motor proteins at that interact with microtubules at the centrosome can then pull the nucleus forward. Adapted from (Tsai and Gleeson, 2005)

Doublecortin (DCX), another microtubule associated protein, was identified as mutated in a form of X-linked lissencephally (des Portes et al., 1998; Gleeson et al., 1998). Its name comes from the fact that a sub-population of neurons accumulate in the white matter (band heterotopia) resulting in 'two gray matters' or "double cortex" (Guerrini and Marini, 2006). Like Lis1, shRNA studies revealed that reduction of DCX lead to a *bona fide* defect in radial migration (Bai et al., 2003). How does DCX regulate migration? DCX was shown to stabilize microtubules in vitro (Horesh et al., 1999) and to associate with microtubules in neurons (Francis et al., 1999; Gleeson et al., 1999). Its ability to associate with microtubules is phosphorylation dependent (Tanaka et al., 2004b). Interestingly, CDK5 was shown to phosphorylate DCX, and mutation of this phosphorylation site (serine 297) reduced interaction between DCX and microtubules. Moreover phosphorylated DCX localization to the microtubule cage around the nucleus in cortical neurons (Tanaka et al., 2004b) suggesting that DCX may act to regulate microtubule pulling of the nucleus forward. Moreover it was shown that DCX can interact with Lis1 biochemically (Caspi et al., 2000) and DCX expression can rescue the migration defect caused by lis1 reduction in cerebellar granule neurons (Tanaka et al., 2004a). More specifically DCX expression rescued the dissociation of centrosome/nucleus coupling caused by Lis1 and dynein reduction suggesting that DCX could facilitate their association with the cage around the nucleus and thereby regulate nucleokinesis and neuronal migration (Tanaka et al., 2004a). These data provide a mechanism whereby Lis1 couples with DCX to regulate nucleokinesis.

Regulators of actin dynamics and radial migration

As one might expect, the regulation of actin polymerization is required for proper cortical development. Mutation of the actin bundling protein, filamin A, results in periventricular heterotopia (Fox et al., 1998). This appears to be due to a migration defect

that causes accumulation of neurons in the ventricular zone (Fox et al., 1998). Filamins are thought to act as actin bundling proteins and allow the association of F-actin with plasma membrane (Stossel et al., 2001). Careful studies in migrating cortical neurons have begun to determine exactly how filamins might regulate migration during cortical development. First, the actin binding activity of filamin A is required for its ability to regulate radial migration (Nagano et al., 2004). Interestingly, these cells displayed a round shape with no leading process extending from the cell body suggesting that f-actin bundling and stabilization may be required for proper leading process formation (Nagano et al., 2004). In addition, time-lapse analyisis of neurons expressing this actin binding deficient mutant of filamin a, showed that indeed leading processes were produced however they were extremely dynamic and cells never transitioned to a bipolar state (Nagano et al., 2004). Since impairment of filamin A activity inhibited leading process formation, it was plausible to think that increased filamin A may cause more efficient leading process formation. Cortical neurons seem to tightly regulate the levels of filamin A present in the cells since it was found that Filamin A expression levels in cortical neurons was tightly regulated by the protein FILIP (Filamin A interacting protein) (Nagano et al., 2002). FILIP expression was shown to decrease Filamin A levels in cells and expression of FILIP siRNA or overexpression Filamin A lead to increased radially oriented leading processes (Nagano et al., 2004). Moreover, time-lapse of FILIP siRNA treated neurons showed increased transition from multipolar to bipolar state suggesting that increased filamin A promotes a radially oriented leading process. In addition to filamin A, the actin severing protein, cofilin, was recently shown to be required for radial migration (Bellenchi et al., 2007). The genetic deletion of cofilin resulted in cortical laminaiton defects (Bellenchi et al., 2007). These defects were due to effects both on cell division and migration. Moreover, Kawauchi et al, showed that expression of dominant negative cofilin resulted in impaired radial migration (Kawauchi et al., 2006).

Finally, Ena/Vasp proteins have recently been shown to regulate cortical development. Deletion of Ena/Vasp proteins inhibited neurite initiation in cortical neurons. In addition, these mutants demonstrated thicker cortical layers where Ena/Vasp null cells migrated past wild type neurons, suggesting that migration is enhanced in these cells (Kwiatkowski et al., 2007). This is consistent with the role of Ena/Vasp proteins in fibroblast migration since reduction of Ena/Vasp actiivty in fibroblast results in increase leading edge persistence and an increase rate of cell migration (Bear et al., 2000; Bear et al., 2002). Taken together, these data suggest an important role for the regulation of actin dynamics in migrating neurons, however there is much work needed to understand exactly how the dynamics are regulated and the specific role that actin is playing in radial migration.

Membrane deforming proteins and their potential role in neuronal migration

Recently, in addition to the well-established role of the cytoskeleton in producing forces to generate plasma membrane protrusions and invaginations, many membrane-associated proteins have also been shown to directly sculpt and deform biological membranes. It is now generally accepted that there are many different forms of membrane remodeling controlled by specialized families of proteins which regulate a vast array of important biological processes such as (1) endomembrane trafficking, exocytosis and membrane fusion as well as (2) plasma membrane deformation including membrane protrusions(lamelipodia and filopodia dynamics) and membrane invaginations (endocytosis, macropinocytosis, etc…) (**Fig. 1.4E-F**; reviewed in (Doherty and McMahon, 2008)).

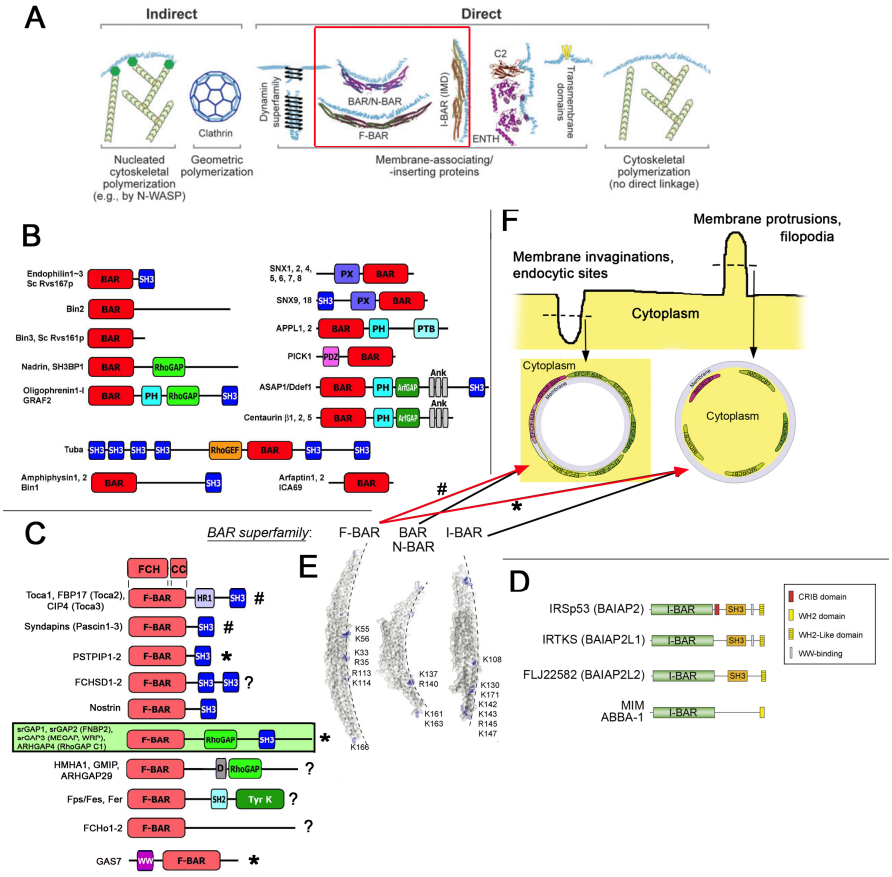

Figure 1.4. Mammalian BAR superfamily of membrane-deforming proteins. (**A**) Diagram adapated from (Doherty and McMahon, 2008) showing the different protein families involved in direct or indirect membrane deformation. The red square show the BAR-superfamily. (**B-D**) Domain structure of all members of the BAR/N-BAR (B), F-BAR (C) and I-BAR (D) subfamilies of proteins. (**E**) Ribbon-diagram representation of the crystallized dimers of these subfamilies (from left to right the F-BAR domain of FCHo2, the BAR domain of Amphiphysin and I-BAR domain of IRSp53 (Scita et al., 2008). The amino acid residues shown in blue correspond to the lysine (K) or arginine (R) which are positively charged residues that confer binding to negatively charged phophlipids at the plasma membrane. Note that they are located in the concave side of F-BAR and BAR examples, but on their convex side of the I-BAR example. This is thought to be the main structural basis of the membrane tubulation and invagination (endocytic sites) for F-BAR and BAR/N-BAR domains as well as

membrane protrusion and filopodia formation for I-BAR domains (**F**). Note that several other predicted F-BAR containing proteins (including PSTPIP1-2 and GAS7) are potent inducers of filopodia formation in various cell lines (stars in C-F;) (Chitu et al., 2005; Chitu and Stanley, 2007; She et al., 2002)}. Panels in B is adapted from (Itoh and De Camilli, 2006) and panels in E-D-F are modified from (Scita et al., 2008).

These proteins generate membrane curvature through insertion of hydrophobic or amphiphatic motifs into the membrane to induce bilayer asymmetry and through the formation of membrane-bound protein scaffolds with intrinsic curvature (Itoh and De Camilli, 2006). I will now review the current knowledge on one of the protein superfamiles, the BAR domain-containing proteins.

BAR domain superfamily: regulators of membrane curvature involved in membrane invagination and membrane protrusion

- The BAR (Bin, Amphiphysin, Rvs) domain superfamily is a large family (>30) of proteins playing central roles in membrane remodeling in all eukaryotes (**Fig. 1.4B**). Mutations in genes encoding BAR domain proteins have been linked to several diseases (Billuart et al., 1998; Endris et al., 2002), and inactivation of these proteins in cells and animals is often characterized by severe phenotypes resulting from altered membrane dynamics (reviewed in (Itoh and De Camilli, 2006; Scita et al., 2008)). Based on structural features and phylogenetic relationships, the BAR domains can be divided into distinct subfamilies (Frost et al., 2007). The canonical BAR domain is a dimeric module, where three kinked antiparallel α-helices of each monomer form a banana-shaped dimeric 6-helix bundle (Peter et al., 2004). BAR domains interact with cellular membranes through their concave surface, which typically contains charged amino acids. A subset of BAR domains (N-BARs) also contain an N-terminal amphiphatic helix that folds upon membrane interaction and penetrates into the bilayer. In a number of proteins, the BAR domain is also functionally linked to other membrane-binding motifs such as PH or PX domains (Itoh and De Camilli, 2006). Thus, although the curved shape of BAR domains appears to be critical for membrane tubulation, in many cases the membrane curvature- sensing/generation activity is enhanced by additional lipid-

binding motifs (Itoh and De Camilli, 2006).

- F-BAR domains (**Fig. 1.4C**) were originally identified as a FER-CIP4 homology (FCH) domain in the N-terminal region of many actin-regulating proteins. Subsequent studies by Pietro DeCamilli's group and others revealed (1) most FCH-containing proteins contain a coiled-coil (CC) region at variable distance from the C-terminal end of the FCH domain and (2) overall secondary structure homology between [FCH+CC] and BAR domains and demonstrated that the combination of FCH+CC domains or F-BAR (FCH and BAR) domains tubulate membranes in vitro and in vivo like BAR domains (Itoh et al., 2005; Tsujita et al., 2006). The structure of F-BAR domain differs from the canonical BAR domain by containing five α-helices per monomer. Importantly, being more elongated and gently curved (Fig. 2E), F-BAR domains induce larger-diameter membrane tubules in comparison to BAR domains (Henne et al., 2007; Shimada et al., 2007). A recent cryo-EM study demonstrated that F-BAR domains self-assemble into a helical coat around the membrane tubules, providing evidence that these domains use a combination of scaffolding and cooperative assembly to induce membrane curvature (Frost et al., 2008).
- The I-BAR domain (**Fig. 1.4D**), which is also known as IM (IRSp53/MIM homology) domain, was first identified as an F-actin crosslinking domain at the N-terminal region of mammalian IRSp53 and missing-in-metastasis (MIM) proteins (reviewed in (Mattila and Lappalainen, 2008; Scita et al., 2008)). However, subsequent studies suggested that I-BAR/IM domains do not significantly crosslink actin filaments under physiological conditions and revealed that the domain displays structural homology to BAR domains. I-BAR/IM monomer consists of three α–helices that dimerize into an antiparallel structure, which resembles a zeppelin or inverse BAR (I-BAR) domain shape. Biochemical studies demonstrated that I-BAR domains of MIM and

IRSp53 directly bind and deform membranes into tubules in vitro. However, in contrast to the concave-shaped lipid-binding interface of BAR and F-BAR domains, the positively charged lipid-binding surface of I-BAR domains displays a convex geometry. This provided a possible structural explanation for why I-BAR domains induce membrane protrusions rather than invaginations when expressed in cells. However, direct evidence for this ‘‘inverse mechanism’’ has not been demonstrated yet. Furthermore, possible differences in the membrane deformation properties within the I-BAR domain family are likely.

What is the evidence that membrane-deforming proteins may be involved in neuronal migration? Interestingly, FBP17, a F-BAR containing protein regulates neurite branching downstream of Rnd2 activation (Heng et al., 2008). In addition, a screen for downstream transcriptional targets of Ngn2 identified slit-robo GAP2 (srGAP2) as a potential downstream transcriptional target of Ngn2 (Mattar et al., 2004). srGAP2 belongs to the srGAP family of Rho GTPase activating proteins identified by Yi Rao’s group as cytoplasmic interactors of the Robo receptor using a yeast-two-hybrid approach (Wong et al., 2001).

Analysis of the domain organization of the srGAP family showed that srGAPs possess an N-terminal F-BAR domain, a RhoGAP domain and a C-terminal SH3 domain. srGAP1-3 expression is enriched in the developing CNS where they show partially overlapping patterns of expression (**Fig. 1.5**). Interestingly, in the embryonic cortex, srGAP1 is not detected whereas srGAP2 and 3 are expressed in progenitors and post-mitotic regions. The SH3 domains of srGAPs were shown to associate with mouse formin 1 (Chan et al., 1996). The SH3 domain of srGAP2 and srGAP3 have been shown to interact with WASP and WAVE respectively (Chan et al., 1996; Linkermann et al., 2009; Soderling et al., 2002) placing these molecules in an ideal position to act at the interface between the plasma

membrane and the actin cytoskeleton. Finally, recent work has implicated this family in the regulation of cell migration since srGAP3 was recently shown to regulate cell migration in cancer cells (Simpson et al., 2008). However the role of this family of proteins in the regulation of radial migration remains poorly understood. As a result, the focus of this thesis is to determine the function of srGAP2 during cortical development and specifically to determine its effects on radial migration.

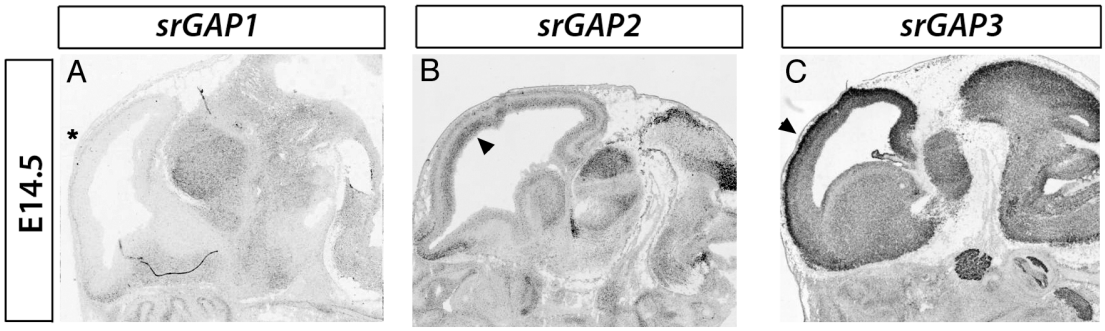

Figure 1.5. Pattern of expression of srGAP1-3 in the developing telencephalon. *In situ* hybridization on sagittal sections of E14.5 mouse embryos showing the mRNA expression of srGAP1 (A), srGAP2 (B) and srGAP3 (C). Rostral is left, dorsal is up. Note that srGAP1 is not expressed at detectable level in the cortex (star in A) whereas both srGAP2 and srGAP3 are expressed at higher levels in the cortex (arrowheads in B-C).

Chapter 2 (Manuscript Re-Submitted to *Cell* for publication (3/19/2009).)

srGAP2 regulates neuronal migration through the ability of its F-BAR domain to induce filopodia-like membrane protrusions

Sabrice Guerrier [1,2], Jaeda Coutinho-Budd [2], Takayuki Sassa [2], Aurelie Gresset[1], Nicole Vincent Jordan[1], Adam Frost[3], and Franck Polleux [1,2 #]

[1] Department of Pharmacology - School of Medicine- UNC-Chapel Hill
[2] Neuroscience Research Center- UNC-Chapel Hill
[3] Department of Molecular Biophysics and Biochemistry, Interdepartmental Neuroscience Program, Yale University- School of Medicine

[#] Address correspondence to:
Franck Polleux, Ph.D.
University of North Carolina- Chapel Hill
Neuroscience Center
Department of Pharmacology
115 Mason Farm Road
Room 8109C
CB-7250
Chapel Hill, NC
USA

Phone 919-966-1449 (office)
Fax 919-966-9605
Email polleux@med.unc.edu

Running title: **Membrane dynamics and neuronal migration**

INTRODUCTION

During brain development, neural progenitor proliferation, neuronal migration and differentiation require considerable changes in cell shape involving coordinated cytoskeletal and membrane remodeling (Ayala et al., 2007; Luo, 2002). In particular, during mammalian cortical development, neurons born through asymmetric division of radial glial progenitors have to migrate over long distances to reach their final destination in the cortical plate where they will undergo terminal differentiation, which includes axonal and dendritic growth as well as synapse formation. The cellular mechanisms by which cortical neurons migrate involve the coordinated extension and adhesion of the leading process (LP) along radial glial processes with the forward translocation of the nucleus (Ayala et al., 2007; Lambert de Rouvroit and Goffinet, 2001; Tsai and Gleeson, 2005). These events are currently thought to primarily depend on centrosome and microtubule dynamics involving the function of proteins such as Lis1, Doublecortin, and Nudel among others (Niethammer et al., 2000; Reiner et al., 1995; Tanaka et al., 2004b; Tsai et al., 2005). However, recent genetic studies have identified molecules that regulate leading process morphology and as a consequence, cell migration. Specifically, deletion of cyclin dependent kinase 5 (CDK5) (Ohshima et al., 2007) or its activator p35 (Gupta et al., 2003) resulted in an increase in LP branching and impaired migration. These studies demonstrate a functional link between LP morphology and proper neuronal migration.

The basis of neurite initiation, outgrowth and branching is rooted in the ability of the cytoskeleton to undergo dynamic changes (Luo, 2002). The actin cytoskeleton, in particular, has been shown to regulate axon and dendritic outgrowth and branching (Luo, 2002). While several different actin structures contribute to these activities, bundled, filamentous actin present in filopodia seem to be particularly important for neurite morphogenesis (Gupton and Gertler, 2007; Mattila and Lappalainen, 2008). Filopodia have been shown to play a role

in growth cone morphology (Burnette et al., 2007; Gallo and Letourneau, 2004) and neurite outgrowth (Luo, 2002) and branching (Dent et al., 2004; Gallo and Letourneau, 1998). In addition, recent evidence suggests that filopodia formation is required for neurite initiation (Dent et al., 2007; Kwiatkowski et al., 2007). Downregulation of the actin anti-cappers, ENA/VASP proteins, which are potent inducers of filopodia using either functional interference or a genetic approach, resulted in loss of filopodia and failed neurite initiation. Interestingly, loss of ENA/VASP proteins also resulted in defects in cortical lamination (Kwiatkowski et al., 2007) suggesting a complex functional relationship between filopodia formation, neurite initiation and neuronal migration. However, at this point, the molecular mechanisms underlying the function of filopodia dynamics in neurite initiation and branching during neuronal migration are still poorly understood.

Classically, filopodia formation is thought to be dependent on mechanisms that regulate actin polymerization at the barbed end of actin filaments and proteins that act to bundle branched actin in order to form parallel bundles (Gupton and Gertler, 2007). However, recent work has demonstrated that proteins that act on lipids at the plasma membrane seem to play a role in filopodia formation as well (Gupton and Gertler, 2007). LPR1, a lipid phosphatase related protein, was shown to induce filopodia independent of many of the classical filopodia pathways including ENA/VASP proteins and Cdc42 and its effectors (Sigal et al., 2007). In addition, IRSp53, a protein known to bind to and deform phospholipids membrane has also been shown to induce filopodia formation independent of its ability to bundle F-actin (Mattila et al., 2007). These and other recent results strongly suggest that changes in cell shape including filopodia dynamics or membrane invagination and endocytosis require the function of membrane binding proteins that couple membrane deformation and F-actin dynamics. However, the functions of proteins that deform membranes in the form of protrusions in vivo, remain poorly understood.

Here we identify slit-robo GTPase Activating Protein (srGAP2) as a potent inducer of filopodia in neurons and an important regulator of neuronal migration and morphogenesis. srGAP2 is expressed throughout the cortex during and after radial migration (Mattar et al., 2004; Yao et al., 2008). It contains three functional domains: a predicted FCH-Bin/Amphiphysin/Rvs domain (F-BAR domain), Rho GTPase accelerating/activating (GAP) domain, and a Src Homology 3 (SH3) domain. Crystal structures of the F-BAR domains of FBP17, CIP4, and FCHo2 demonstrated that these domains are elongated homodimers characterized by a shallow curvature formed by the anti-parallel interaction of two alpha-helical coiled coils (Henne et al., 2007; Shimada et al., 2007). In addition to sharing the general fold and quaternary organization of the BAR domain superfamily as a whole, these domains were found to share functional properties with 'classical' BAR domains, most notably the ability to bind and deform membranes in vitro and in living cells (Frost et al., 2008; Kakimoto et al., 2006; Shimada et al., 2007). However, to date, the in vivo functions of F-BAR domain-containing proteins, including the srGAPs, have not been assessed.

RhoGAP domains inactivate Rho family GTPases by increasing their relatively slow intrinsic rate of GTP hydrolysis. RhoGAP containing proteins are known to regulate cell polarity, morphology, and migration in many cell types (Billuart et al., 1998; Moon and Zheng, 2003; Ng et al., 2002). Finally, SH3 domains are polyproline-biding motifs mediating protein-protein interactions. Interestingly, the SH3 domain of the related proteins, srGAP1 and srGAP3, have been shown to interact with the Robo1 receptor, a known axon guidance receptor (Li et al., 2006; Wong et al., 2001), and the WAVE-1 complex, an actin-polymerizing complex (Soderling et al., 2002). In addition the SH3 domain of srGAP2 was shown to interact with N-WASP (Linkermann et al., 2009) placing the srGAP family of proteins in an ideal position to regulate neurite outgrowth.

Here we show that srGAP2's ability to regulate neuronal migration and morphology requires the unexpected ability of its N-terminal F-BAR containing domain to induce filopodia-like membrane protrusions resembling those induced by the I-BAR domains of IRSp53 and MIM. Interestingly, the RhoGAP and SH3 domains also participate in srGAP2's regulation of neuronal migration. Taken together, these results highlight the functional importance of proteins directly regulating membrane deformation for proper neuronal migration and morphogenesis.

RESULTS

Expression of srGAP2 in the Developing Cortex

To begin our study of the role of srGAP2 in cortical development, we first examined its pattern of expression. srGAP2 mRNA is expressed throughout the developing cortex and is found both in proliferative zones (ventricular and subventricular zones, VZ and SVZ respectively) at E13 and E15 and in postmitotic regions (cortical plate, CP) at E15 and P1 (Fig. 2.1A). In order to determine the pattern of srGAP2 protein expression, we obtained a polyclonal antibody raised against the C-terminus of srGAP2 (Fig. 2.1B-C; (Yao et al., 2008). srGAP2 protein is expressed throughout cortical development culminating at postnatal day 1 (P1) corresponding to the peak of neuronal migration in the cortex. Its expression is maintained at P15 and reduced, but still present, in adult cortex (**Fig. 2.1C**).

srGAP2 expression pattern was examined by immunofluorescent staining showing that it is ubiquitously expressed in the cortical wall (**Fig. 2.1D**) being found both in Nestin-positive neuronal progenitors in the VZ (**Fig. 1H-J**) and MAP2-positive post-mitotic neurons in the CP (**Fig. 2.1E-G**). Finally, we determined the subcellular localization of endogenous srGAP2 in acutely dissociated E15 cortical neurons. SrGAP2 localizes to the extreme

periphery of immature cortical neurons (**Fig. 2.1K-M** arrows) and was often localized to F-actin-rich filopodia-like protrusions (arrowhead in **Fig. 2.1K-M** and **Fig. 2.1N-P**).

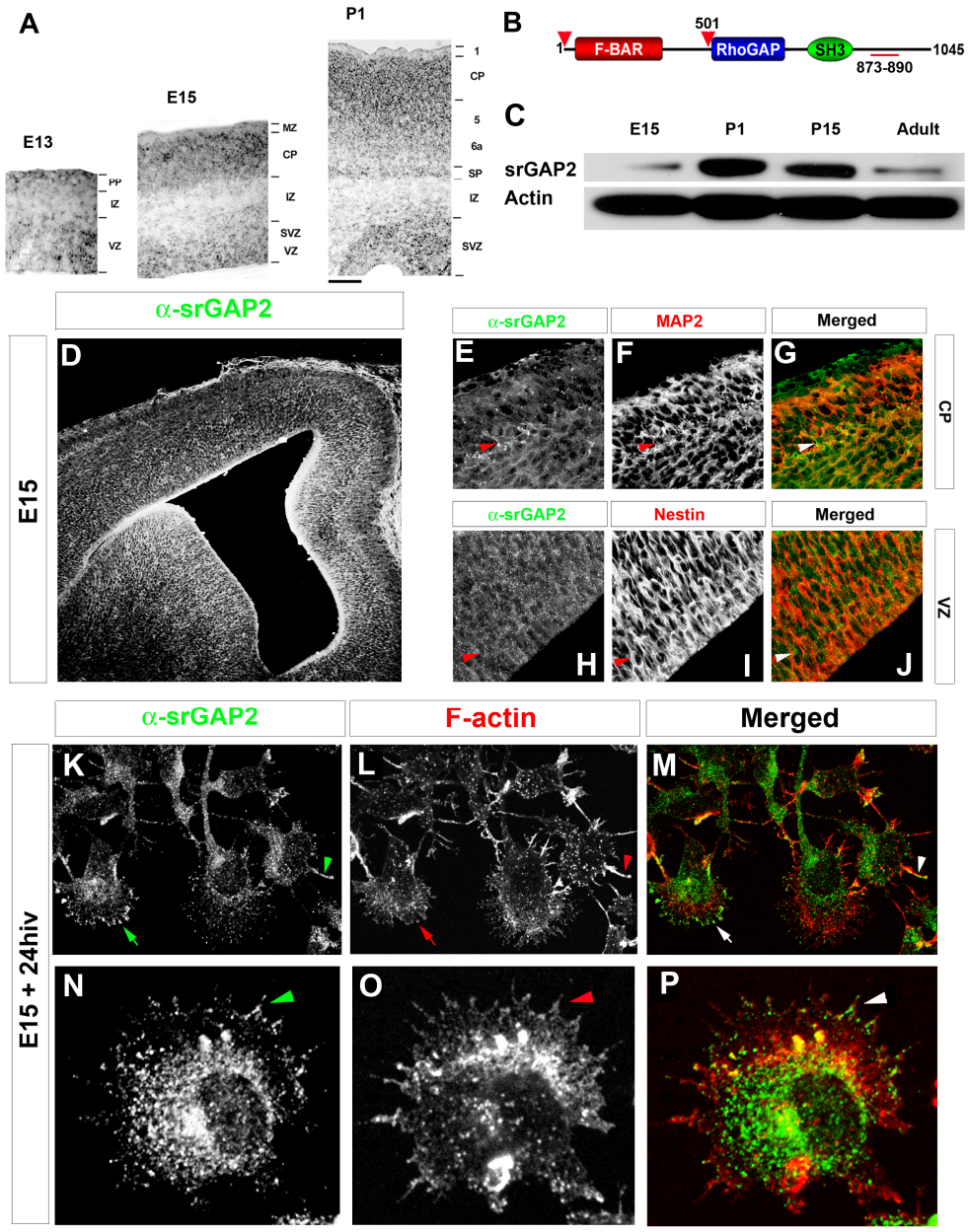

Figure 2.1. srGAP2 is expressed in neuronal progenitors and post-mitotic neurons and localizes to sites of membrane protrusion.

(A) *In situ* hybridization for *srGAP2* in developing cortex at embryonic day (E)13 and E15 and postnatal day (P)1. *srGAP2* mRNA is expressed within the ventricular and subventricular zones where neuronal progenitors are dividing and initiating migration respectively at E13 and E15. It is also

found in the cortical plate (CP) at E15 and P1 where neurons differentiate and form axon and dendrites. (B) Domain organization of srGAP2 which contains an F-BAR domain, a RhoGAP and a SH3 domain from N- to C-terminal ends (1-1045 aa, predicted MW 118kDa). The black bar indicates the localization of the antigen (A2, aa 873-890) used to affinity purify the srGAP2-specific polyclonal antibody to the C-terminal end of srGAP2 (Yao et al., 2008). (C) Western blot for srGAP2 protein levels during cortical development. Cortical lysate where obtained at the indicated time points (E15, P1, P15 and Adult) and proteins separated by SDS-PAGE followed by immunoblotting with A2-rabbit polyclonal antibody recognizing srGAP2 protein. Blotting against actin is used to verify equal protein loading. (D-J) Immunofluorescence staining of srGAP2 protein expression on fixed coronal sections of E15 mouse cortex. srGAP2 protein colocalizes (arrowheads) with MAP2 (postmitotic neuron marker) in the CP (D-F) and also colocalizes with Nestin (arrowheads) (neuronal precursor marker) in the VZ (G-I). (K-P) Immunofluorescence staining of srGAP2 protein in early dissociated cortical neuron cultures (E15+ 24 hours *in vitro* –hiv). srGAP2 protein is found close to the plasma membrane of immature cortical neurons (arrow in K-M) and to F-actin-rich filopodia (stained with Alexa546-phalloidin; arrowheads in K-M and N-P).

Full-length srGAP2 and its F-BAR Domain Induce Filopodia Formation

Over-expression of F-BAR domain-containing proteins such as FBP17 or CIP4 have been shown to cause membrane invagination and tubulation in cell lines (Itoh et al., 2005; Tsujita et al., 2006). To determine if srGAP2 and its predicted F-BAR domain had similar properties, we expressed srGAP2 in COS7 cells. Surprisingly, expression of srGAP2 did not induce any membrane invaginations but instead, induced filopodia formation (**Fig. 2.2D-F, 2.2P**). This effect requires its F-BAR domain since deletion of the F-BAR domain (srGAP2$^{\bullet\Delta F\text{-}BAR}$-EGFP) resulted in normal COS7 cells morphology (**Fig. 2.2G-I, 2.2P**).

Interestingly, expression of the F-BAR domain of srGAP2 did not inhibit endocytosis, assessed using Alexa546-Transferrin uptake assay (**Fig. 2.3**), as do the F-BAR domains of FBP17 and CIP4 (Itoh et al., 2005). Furthermore, expression of the isolated F-BAR domain fused to EGFP induced filopodia formation just as full-length srGAP2 (**Fig. 2.2J-K, 2.2P**). Of note, the F-BAR domain is a very potent membrane-targeting motif (**Fig. 2.2J**). These data suggest that the F-BAR domain of srGAP2 is necessary and sufficient for membrane localization and the induction of filopodia-like membrane protrusions.

In order to distinguish the membrane targeting function of the F-BAR domain from its membrane deformation activity, we identified a small truncation of the C-terminal 49 amino-acids of the F-BAR domain (corresponding to two short alpha-helices in the C-terminal part of the F-BAR domain) that we called F-BAR$^{\otimes\Delta 49}$ (**Fig. 2.4A**). Expression of F-BAR$^{\otimes\Delta 49}$-EGFP in COS7 cells results in membrane targeting but fails to elicit filopodia formation in COS7 cells (**Fig. 2.2M-O, 2.2P**). We do not know the structural basis for the inability of this truncation to elicit filopodia formation but it may be due to an effect on oligomer formation since it is thought that the c-terminal end of F-BAR domains are required for this activity. Interestingly, these 49 amino acids reside in α6-8 (**Fig. 2.4A**) within the srGAP family that is C-terminal to the minimal, predicted F-BAR domain (amino acids 1-358, **Fig. 2.4B**)

suggesting that the F-BAR domain of srGAP2 may contain additional sequences. Indeed, we were unable to obtain stable protein expression of the minimal F-BAR domain. Furthermore, as shown for other F-BAR domains (Frost et al., 2008; Itoh et al., 2005; Kakimoto et al., 2006; Shimada et al., 2007), srGAP2 forms a stable dimer in solution as assessed by light scattering assays (**Fig. 2.4C**) and deletion of the FCH domain (green box **Fig. 2.4A**) which represents a significant portion of the dimerization interface, destroys the ability of srGAP2 to induce filopodia formation in COS7 cells (data not shown). Altogether, these data suggest that all 8 alpha helices are likely to be required for formation of the functional F-BAR domain of srGAP2.

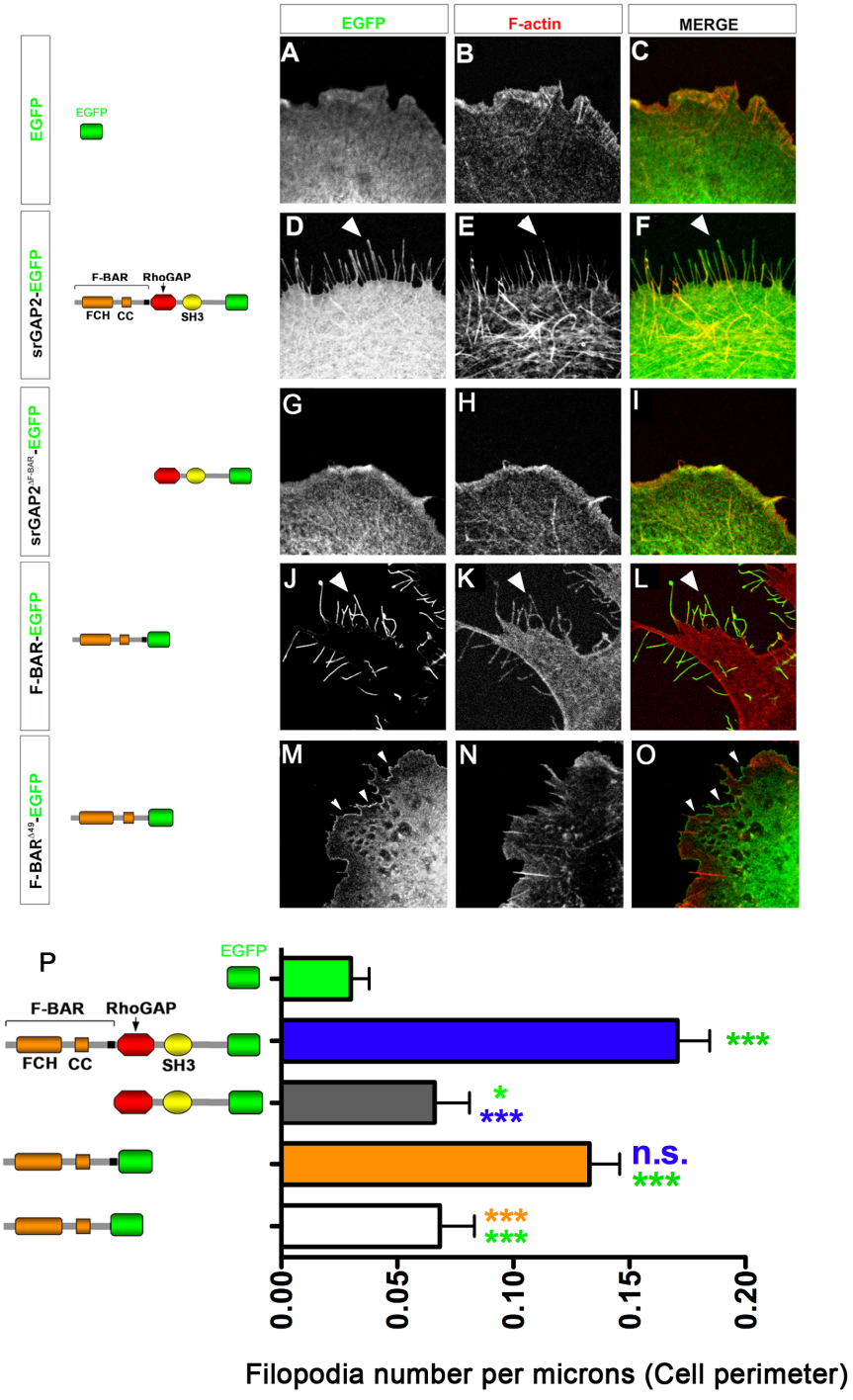

Figure 2.2. SrGAP2 induces filopodia formation in a F-BAR-dependent manner in COS7 cells.

(A-C) COS7 cell expressing EGFP counter stained with phalloidin for F-actin (red).

(D-F) COS7 cell expressing srGAP2-EGFP fusion protein for F-actin-rich filopodia (arrowheads in D-F).

(G-I) Expression of srGAP2$^{\Delta\Delta F\text{-}BAR}$-EGFP fusion protein does not promote filopodia formation.
(J-L) Expression of the F-BAR-EGFP fusion protein is sufficient to promote filopodia formation in COS7 cells. Note the significant increase in membrane targeting extreme periphery of the cell (J-L) and induces the formation of long actin rich protrusions (J-L) like full-length srGAP2. Thus expression of the F-BAR domain of srGAP2 is sufficient to induce filopodia. Moreover this activity is not simply dependent on localization to the plasma membrane since expression F-BAR$^{\Delta\Delta 49}$-EGFP (M-O), which localized nicely to the plasma membrane, did not cause a significant increase in filopodia.
(P) Quantification of the effects described in A-O. (EGFP, n=41 cells; srGAP2-EGFP, n=52 cells; srGAP2$^{\Delta\Delta F\text{-}BAR}$-EGFP, n=21 cells; F-BAR-EGFP, n=21 cells; F-BAR$^{\Delta\Delta 49}$-EGFP, n= 15 cells. Cells were taken from 3 independent experiments and analyzed using Mann-Whitney Test * $p<0.05$; ** $p<.001$; *** $p<0.001$. Green color indicates comparison to EGFP and blue color indicates comparison to srGAP2-EGFP and orange indicated comparison to F-BAR-EGFP)

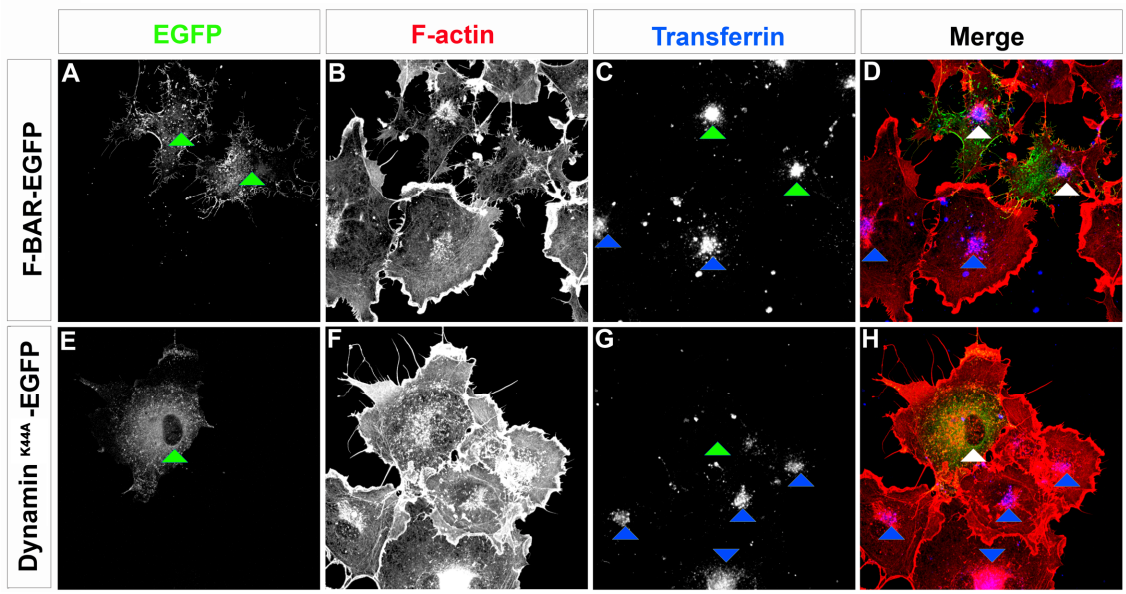

Figure 2.3. Expression of the F-BAR domain of srGAP2 in COS7 cells does not inhibit endocytosis.

(A-D) COS7 cells expressing the F-BAR-EGFP fusion protein were incubated with Alexa 647-conjugated transferrin then fixed and permeabilized and stained with Alexa546-phalloidin to label F-actin (B). This transferrin-uptake assay reveals no significant difference in the level of endocytosis between F-BAR-EGFP-expressing cells (white arrowheads in D) and untransfected cells (blue arrowheads in D).

(E-H) COS7 cells expressing Dynamin^{K44A}-EGFP (dominant negative) were used as a positive control for inhibition of endocytosis as these cells were unable to endocytose transferrin (white arrowheads in H).

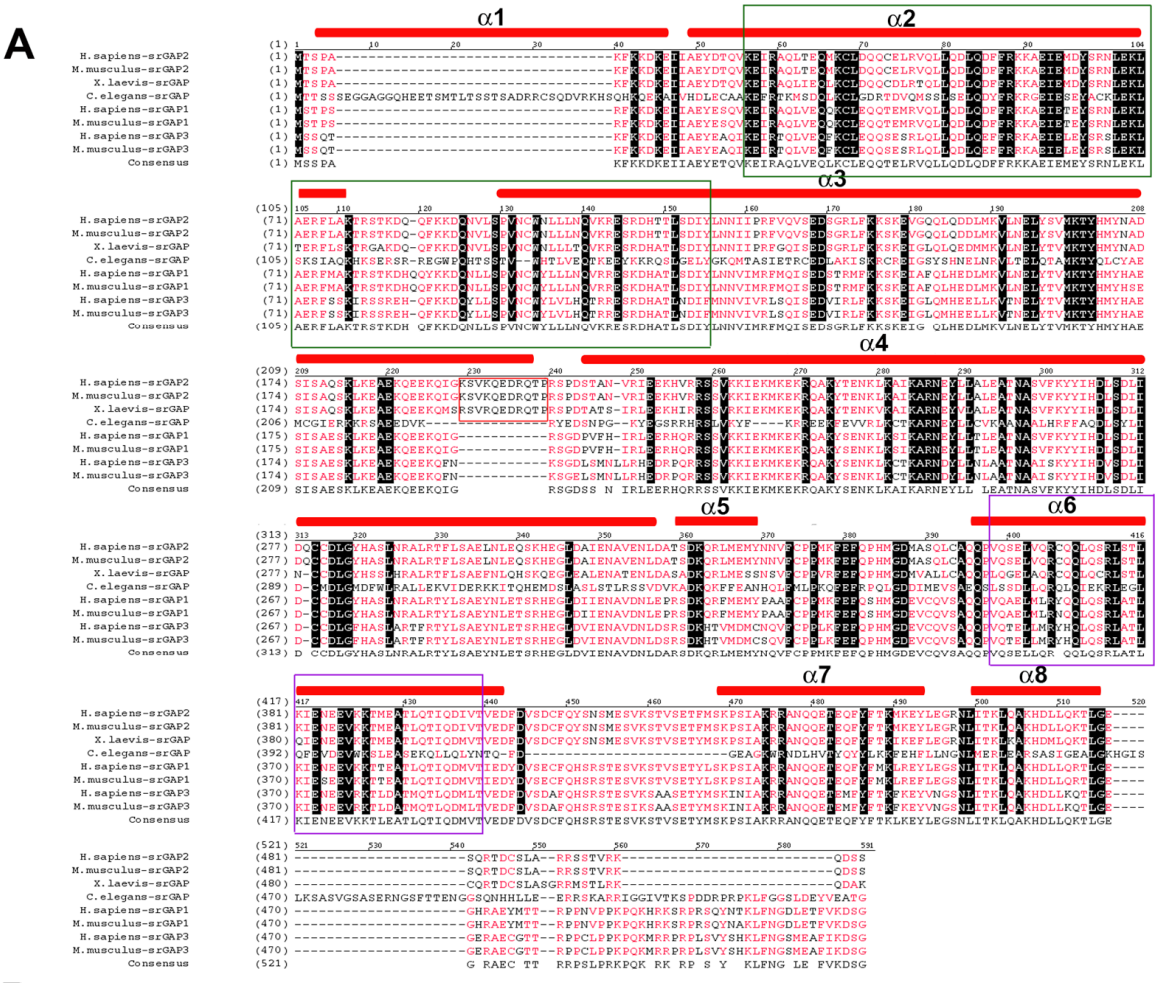
A
α1
α2
α3
α4
α5
α6
α7
α8
H.sapiens-srGAP2
M.musculus-srGAP2
X.laevis-srGAP
C.elegans-srGAP
H.sapiens-srGAP1
M.musculus-srGAP1
H.sapiens-srGAP3
M.musculus-srGAP3
Consensus

B

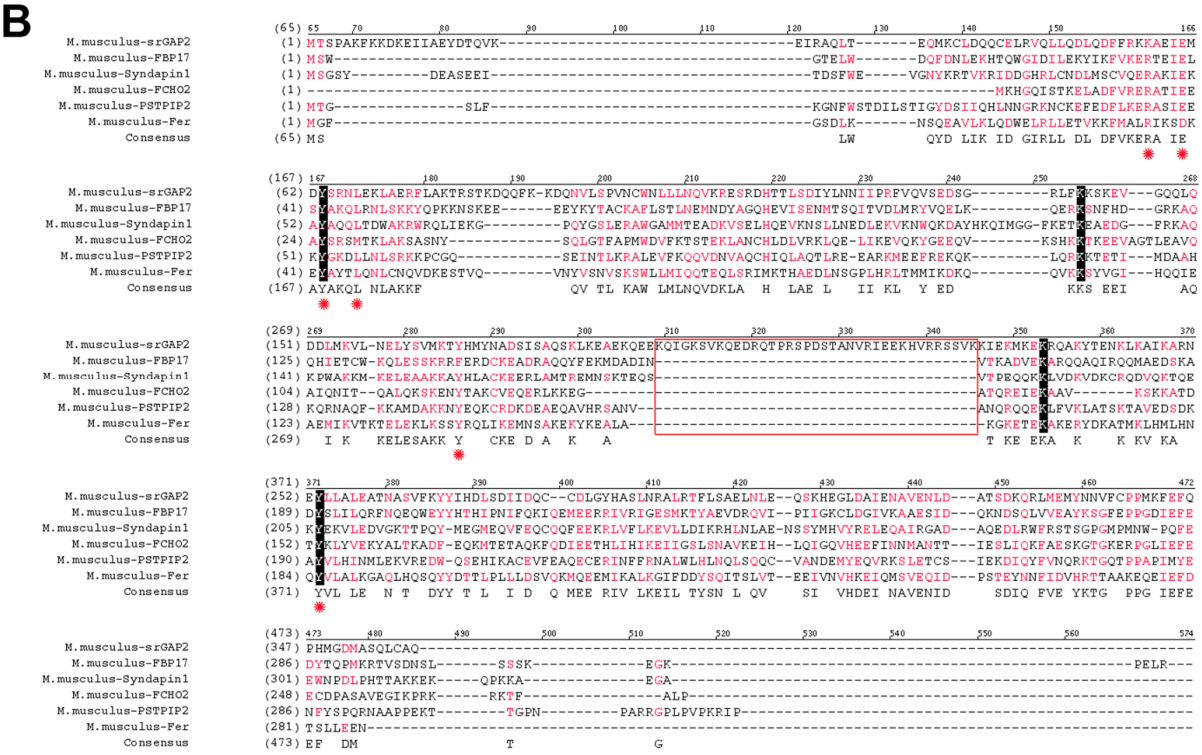
M.musculus-srGAP2
M.musculus-FBP17
M.musculus-Syndapin1
M.musculus-FCHO2
M.musculus-PSTPIP2
M.musculus-Fer
Consensus

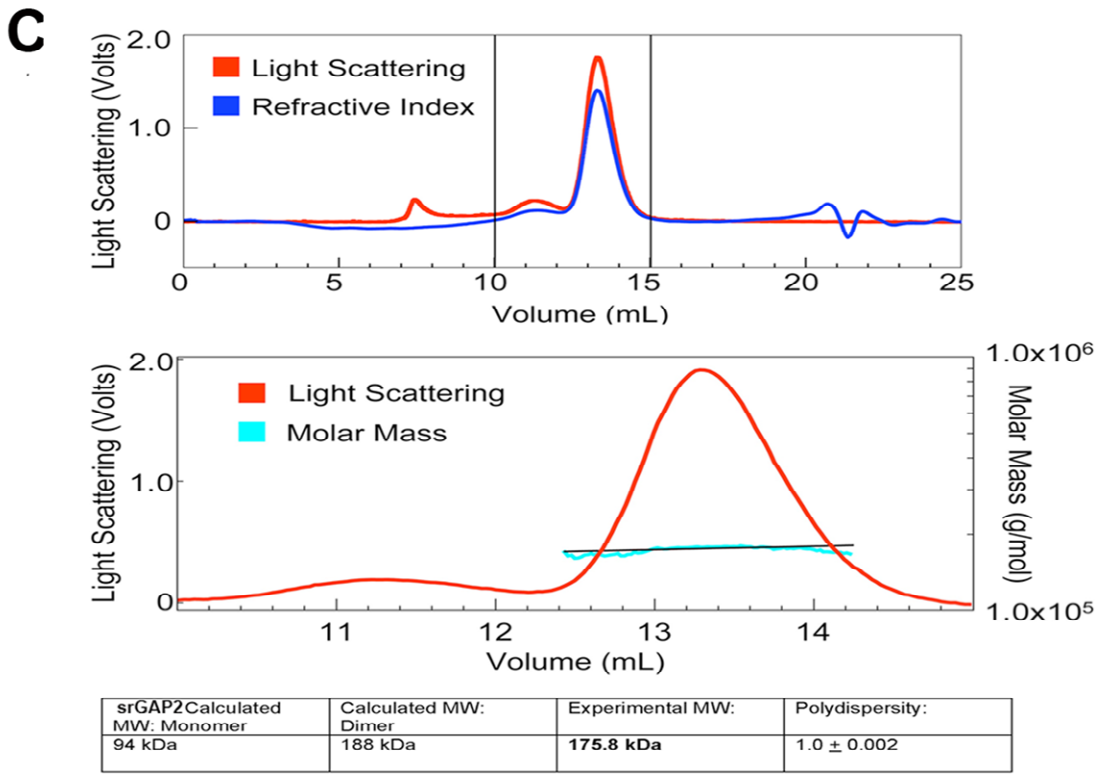

srGAP2Calculated MW: Monomer	Calculated MW: Dimer	Experimental MW:	Polydispersity:
94 kDa	188 kDa	**175.8 kDa**	1.0 ± 0.002

Figure 2.4. SrGAP2 is an F-BAR domain containing protein.

(A) Sequence alignment of the srGAP family from various species. Residues labeled in white on black background are identical. Red residues represent groups of conserved amino acids. SrGAP2-specific insertion is boxed in red. Predicted alpha-helices are depicted as red bars (secondary structure prediction was obtained using hhpred (Soding et al., 2005) (http://toolkit.tuebingen.mpg.de/hhpred) and Bioinfobank metaserver (http://meta.bioinfo.pl). The F-BAR domain is defined by the alpha helices 2-4. However, three additional alpha-helices are predicted C-terminal of the 'minimal' F-BAR domain and precede the GAP domain.

(B) Structural alignment of mouse srGAP2 with representative mouse F-BAR domains was performed using PromalS3D (Pei et al., 2008) (http://prodata.swmed.edu/promals3d/promals3d.php) and hhpred. Residues colored white on black background are identical between sequences. Red residues represent conserved groups of amino acids. Red stars depict amino acids shown to reside at the dimer interface. Green boxes represent FCH domain as defined by SMART (/smart.embl-

heidelberg.de/). Purple boxes represent predicted coiled coil. Red box identifies srGAP-specific insertion.

(C) Top panel: purified full-length srGAP2 protein (aa 1-786 containing F-BAR, GAP and SH3 domains) (300 □g) was loaded onto a Superose 6 column and separated by size exclusion chromatography. Lower panel: expanded view of the light scattering curve (red) in brackets, with the predicted molar mass depicted in cyan. The molecular weight of srGAP2 in solution was determined to be 175.8 kDa by fitting the molar mass curve to a linear function using Astra software.

The F-BAR domain of srGAP2 deforms membrane like an I-BAR domain

The ability of srGAP2 or its F-BAR domain to induce filopodia in COS7 cells is reminiscent of the activity of the structurally related, Inverse (I)-BAR domain-containing proteins such as IRSp53 and Missing-in-Metastasis (MIM) (Mattila and Lappalainen, 2008; Mattila et al., 2007; Saarikangas et al., 2009; Scita et al., 2008). The filopodia induced by I-BAR domains are dependent upon their ability to interact with and to deform the membrane (Mattila et al., 2007). Interestingly, F-actin depolymerization prevents the dynamics and formation of new filopodia but does not affect the maintenance of pre-existing filopodia induced by the I-BAR domains of IRSp53 or MIM (Mattila et al., 2007). We tested if this property of I-BAR proteins is shared by srGAP2 and its F-BAR domain. Untreated COS7 cells expressing the F-BAR domain of srGAP2 developed F-actin rich filopodia (**Fig. 2.5A-C**). While COS7 cells treated with cytochalasin-D were depleted of F-actin, this treatment had no effect on membrane localization of the F-BAR domain or on the maintenance of filopodia-like protrusions (**Fig. 2.5D-F**).

We next wanted to determine if the dynamics of the filopodia induced by srGAP2 were dependent on F-actin. F-BAR-induced filopodia were highly dynamic in COS7 cells protruding and retracting within less than a minute (**Fig. 2.5H-2K**, and **Movie S1**). In contrast, F-BAR-induced filopodia formed prior to cytochalasin-D treatment were totally resistant to F-actin depolymerization (**Fig. 2.5L-O,** and **Movie S2**). These data suggest that the F-BAR domain of srGAP2 functions as an I-BAR domain in living cells, by inducing filopodia that require F-actin for their dynamics but is independent of F-actin for their structural maintenance.

In order to directly test the membrane deformation properties of the F-BAR domain of srGAP2, we incubated purified F-BAR domain with preformed liposomes. As visualized by

negative stain transmission electron microscopy (TEM), this did not result in liposome outward tubulation as has been reported for other F-BAR domains (see control experiment using F-BAR domain of FBP17 added to an intact, preformed liposome **Fig. 2.6**). Rather, the F-BAR domain of srGAP2 induced an inward dimpling or "scalloping" of the liposome surface (**Fig. 2.5P-Q**), which is reminiscent of the activity of I-BAR domains in the same conditions (Suetsugu et al., 2006), suggesting that F-BAR domain of srGAP2 can induce "inverse" membrane tubulation.

This suggested the possibility that if the purified F-BAR domain of srGAP2 could be exposed to the inside surface of liposomes, then protrusive tubules would form (**Fig. 2.5R**). To test this hypothesis, mixtures of the F-BAR domain with intact, large unilamellar vesicles (LUVs) were briefly sonicated (5sec) which presumably resulted in transient pore formation in liposomes and introduction of the recombinant F-BAR inside LUVs. Following a wash, liposomes were fixed, negatively stained and imaged using TEM. As predicted by the I-BAR model, this resulted in numerous long tubular extensions emerging from LUVs (**Fig. 2.5S**). Consistent with the dimensions of tubules induced by other members of the F-BAR and I-BAR families (Frost et al., 2008; Mattila et al., 2007), the srGAP2 F-BAR-induced tubules were 83 nm +/- 15 nm (average +/- SD, n=38) in diameter when imaged after variable degrees of "flattening" in negative stain conditions. Importantly, at higher magnification, the tubules observed by negative staining electron microscopy after sonication do no have an obvious protein coat surrounding the liposomes (**Fig. 2.5S**). This is in contrast with tubules observed by other F-BAR and BAR domains that are known to coat the outer surface of the tubule as shown in **Fig. 2.6** (Frost et al., 2008; Shimada et al., 2007). Together, these results suggest that unlike previously characterized F-BAR domains, the F-BAR domain of srGAP2 induces tubular extensions, not invaginations, of the membrane and is therefore a potent inducer of filopodia-like membrane protrusions comparable to the recently

characterized I-BAR domain-containing proteins MIM and IRSp53 (Mattila et al., 2007; Suetsugu et al., 2006).

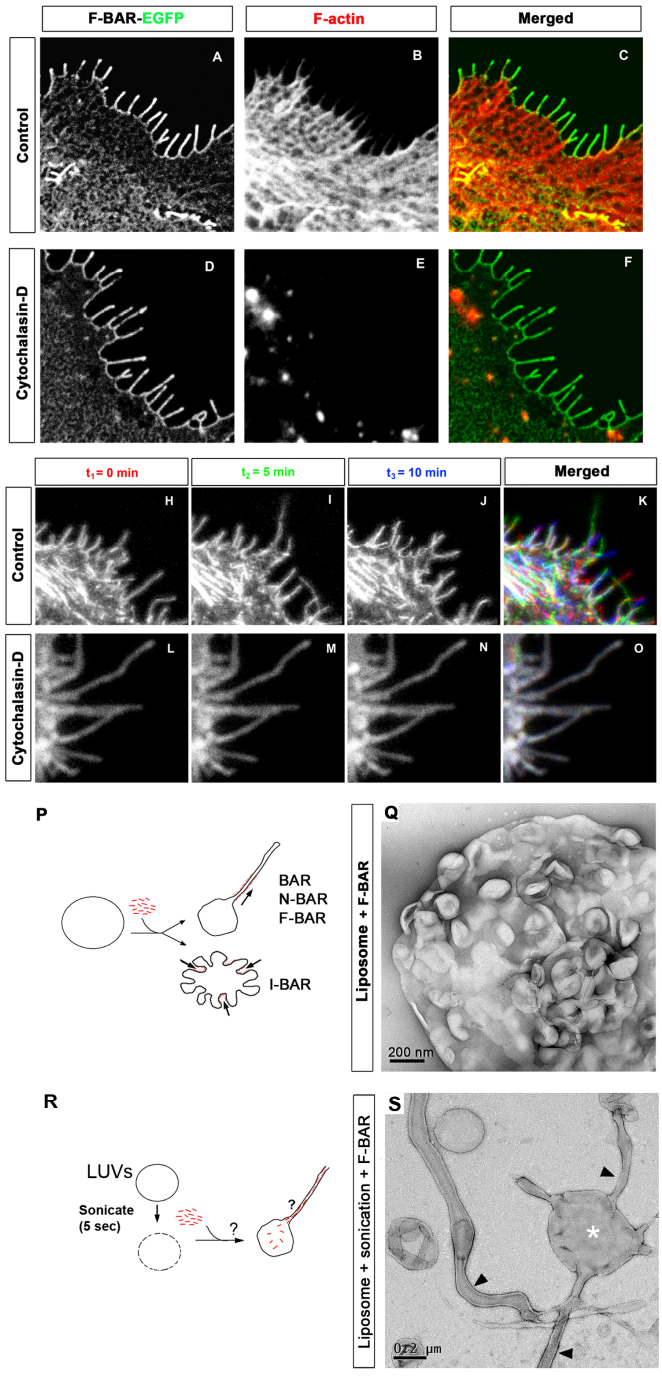

Figure 2.5. F-BAR induced filopodia required F-actin for their dynamic formation but not for their structural maintenance.

(A-C) COS7 cell expressing the F-BAR-EGFP fusion protein not treated with cytochalasin D (control). Note the cortical localization of the F-BAR domain and the numerous F-actin-rich filopodia (phalloidin in B and C).

(D-F) COS7 cell expressing the F-BAR-EGFP fusion protein incubated with 400μM cytochalasin D for 30 minutes. Note that the complete loss of F-actin (phalloidin; E) had no effect on the localization of the F-BAR domain or on the structure of the F-BAR mediated protrusions.

(H-K) Time series showing the dynamics of F-BAR-EGFP-induced filopodia in COS7 cells. Time 0, 5, and 10 minutes are pseudo-colored in red, green, and blue respectively. Note there is little colocalization of filopodia at the cell periphery (K). This is in stark contrast to COS7 cells expressing F-BAR-EGFP treated with cytochalasin- D (30 minutes) (L-O) where the protrusions remain static and do not grow or retract for the same period of time shown in control cells.

(P) Schema depicting tubulation assay in Q.

(Q) F-BAR domain of srGAP2 added to preformed liposomes. Note the inward dimpling or "scalloping" of the liposome surface. (R) schema depicting tubulation assay in (S) where F-BAR domain of srGAP2 was added to liposomes after extrusion. This results in a fraction of the F-BAR domain resident inside the liposome. Note the formation of tubule protrusion from the liposome.

(S) High magnification of liposome/F-BAR mixture after sonication. Note the absence of striations or an obvious protein coat on the lipid tubule, a hallmark of canonical F-BAR tubulation. These tubules are 83 nm +/- 15 nm (average +/- SD, N=38) after being partially flattened by the negative staining procedure.

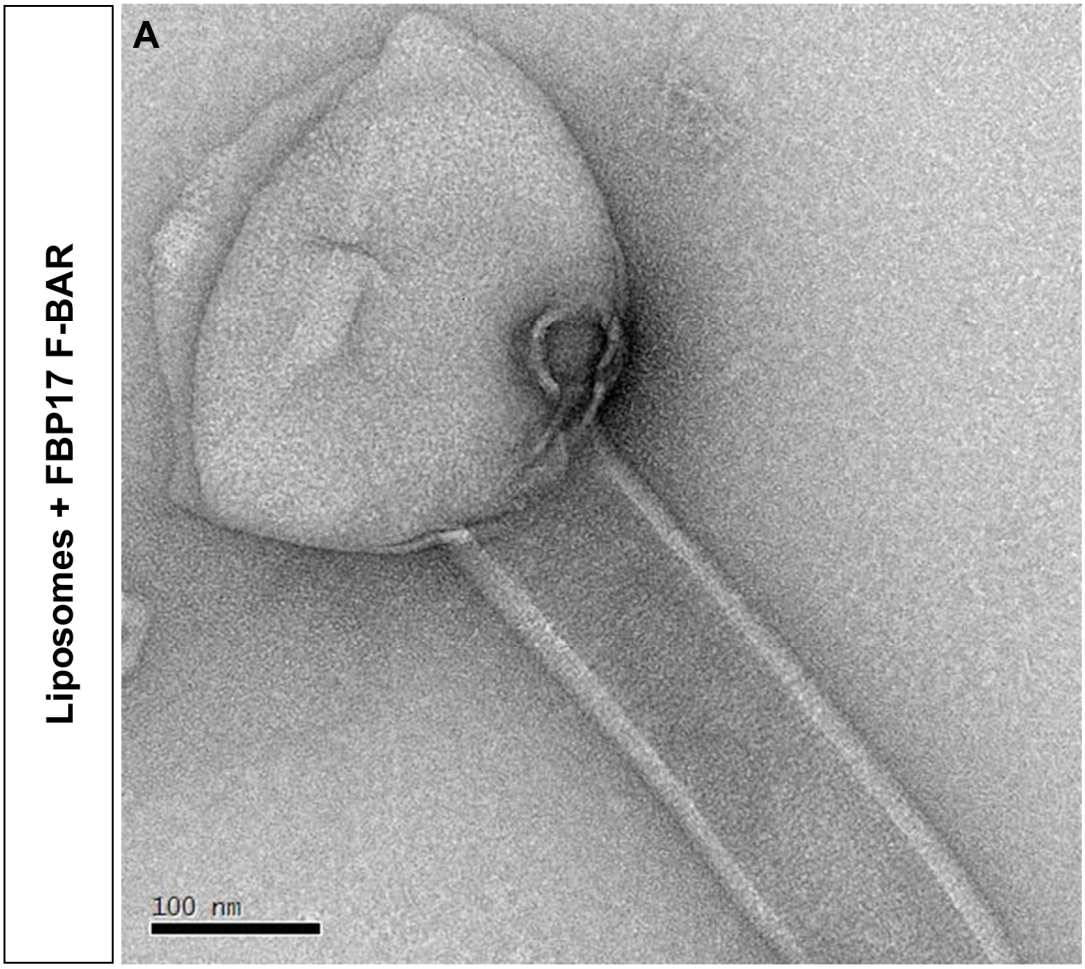

Figure 2.6. Control FBP17 F-BAR tubulates liposome.

A) F-BAR domain of FBP17 incubated with preformed liposomes.

srGAP2 regulates neurite formation and branching through the ability of its F-BAR domain to form filopodia

The effects of srGAP2 on COS7 cells and liposomes as well as its localization to the cell periphery in dissociated cortical neurons prompted us to ask if srGAP2 is required for proper neuronal morphology. Therefore we first tested the function of srGAP2 in neuronal morphogenesis by designing short-hairpin interfering RNA (shRNA) in order to acutely knockdown srGAP2 expression (**Fig. 2.7A**). We found that srGAP2 knockdown in E15 cortical neurons led to a significant decrease in both axonal (**Fig. 2.7C-D and 2.7F**) and dendritic branching after 5 div (**Fig. 2.7G-H and 2.7J**). Both of these effects were rescued by co-transfection of an untargetable version of srGAP2 (**Fig. 2.7E and 2.7I; 2.7F and 2.7J**) demonstrating that this is not an off-target effect. The fact that srGAP2 knockdown reduced branching in cortical neurons, a process previously shown to require filopodia formation (Dent et al., 2004), suggest that srGAP2 may promote neurite branching through its ability to induce filopodia in neurons.

In order to determine if srGAP2 promoted filopodia formation and neurite initiation and branching through its F-BAR domain, we performed structure/function analysis using electroporation of E15 cortical progenitors with various srGAP2 constructs followed by dissociation, which induces rapid differentiation. First, we restricted our analysis to Stage 1 neurons (Dotti et al., 1988), which corresponds to the time point when immature neurons produce a significant number of filopodia-like protrusions (Dent et al., 2007; Kwiatkowski et al., 2007). Our analysis confirmed our previous results in COS7 cells, showing that expression of full-length srGAP2 induced a significant increase in filopodia-like protrusions in Stage 1 cortical neurons compared to control EGFP (**Fig. 2.8A-B and 2.8F**). This effect requires the F-BAR domain since deletion of the F-BAR domain (srGAP2$^{\Delta F\text{-}BAR}$) significantly reduced the ability of srGAP2 to induce filopodia in Stage 1 neurons (**Fig. 2.8C and 2.8F**).

As in COS7 cells, expression of the F-BAR domain alone potently induced filopodia formation (**Fig. 2.8D and 2.8F**). Again, the effect of the F-BAR domain requires its membrane deformation properties and not simply its membrane targeting property since expression of F-BAR$^{\Delta 49}$ does not induce filopodia in Stage 1 cortical neurons (**Fig. 2.8E and 2.8F**) and instead induces large lamellipodia (arrowhead in **Fig. 2.8E**). These data suggest that srGAP2, through its F-BAR domain, induces filopodia in primary cortical neurons.

We then analyzed Stage 2 neurons defined by the presence of short neurites prior the polarized emergence of a single axon (Dotti et al., 1988) in order to test if srGAP2 and its F-BAR domain were sufficient to promote the transition between filopodia-like membrane protrusions and elongating neurites. As shown in **Figure 2.8G-K**, both full-length srGAP2 and the F-BAR domain significantly increased the total number of primary neurites emerging from the cell body as well as the number of primary branches per neurite (**Fig. 2.8L**). Expression of srGAP2$^{\Delta F\text{-}BAR}$ as well as F-BAR$^{\Delta 49}$ fail to increase primary neurite number and neurite branching compared to control EGFP (**Fig. 2.8G and 2.8K and 2.8L**) showing that (i) the F-BAR domain is sufficient to increase neurite initiation and branching and (ii) that the membrane deformation properties of the F-BAR domain are required for srGAP2's ability to induce neurite initiation and branching.

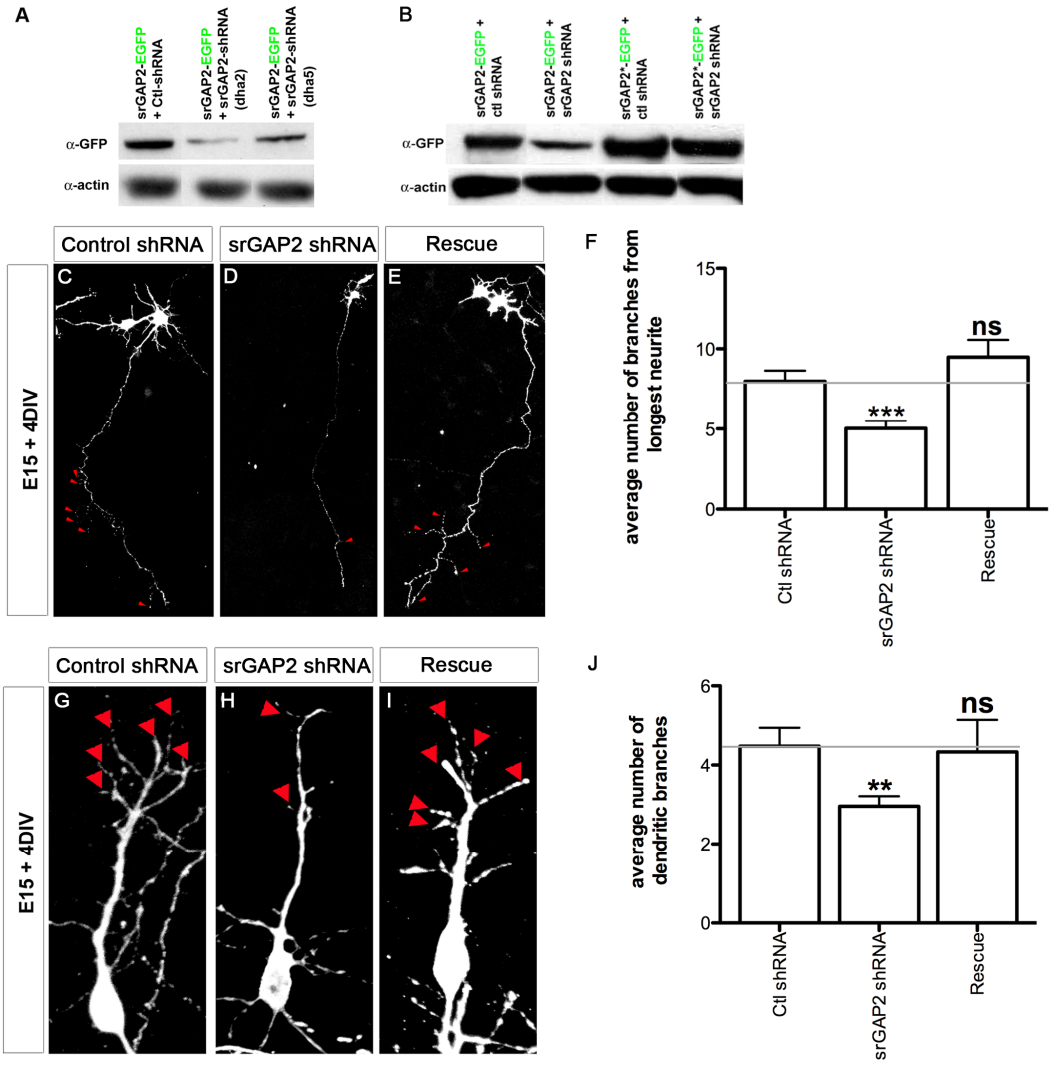

Figure 2.7. Knockdown of srGAP2 in cortical neurons reduces axonal and dendritic branching.
(A) Western blot probed with ant-GFP and anti-actin antibodies from COS7 cells co-transfected with either control shRNA plus srGAP2-EGFP (lane 1), srGAP2 shRNA plus srGAP2-EGFP (Dha2, lane 2) or (Dha5, lane3) (B) Western blot probed with anti-GFP and anti-actin antibodies from COS7 cells co-transfected with either control shRNA plus srGAP2-EGFP (lane 1), srGAP2 shRNA plus srGAP2-EGFP (lane 2), a mutated form of srGAP2*-EGFP (resistant to srGAP2 shRNA) plus control shRNA (lane 3), or srGAP2*-EGFP plus srGAP2 shRNA (lane 4). srGAP2 shRNA significantly knocks down srGAP2 expression compared to control shRNA which can be rescued by expression of srGAP2*-EGFP (compare lanes 3 and 4).
(C-E, G-I) E15 dissociated cortical neurons were cultured for 4 days after ex vivo electroporation with control shRNA, srGAP2 shRNA, or srGAP2 shRNA + srGAP2*-EGFP. Control shRNA transfected

neurons display frequent primary branches from the axon (arrowheads in B) and the primary dendrite (arrowheads in F). Both effects were markedly reduced in srGAP2 shRNA transfected neurons (D and H) and rescued by co-transfection of srGAP2 shRNA with srGAP2*-EGFP (E and I).
(F) Quantification of the number of branches from the longest neurite (axon) as shown in C-E.
(J) Quantification of the number of primary dendritic branches as shown in G-I. (ctl shRNA, n=42 cells; srGAP2 shRNA, n=95 cells; srGAP2*-EGFP + srGAP2 shRNA, n=39 cells. Cells were taken from 3 independent experiments and analyzed using Mann-Whitney Test $p<.05$ = , $p<.01$=**, $p<.001$=***).

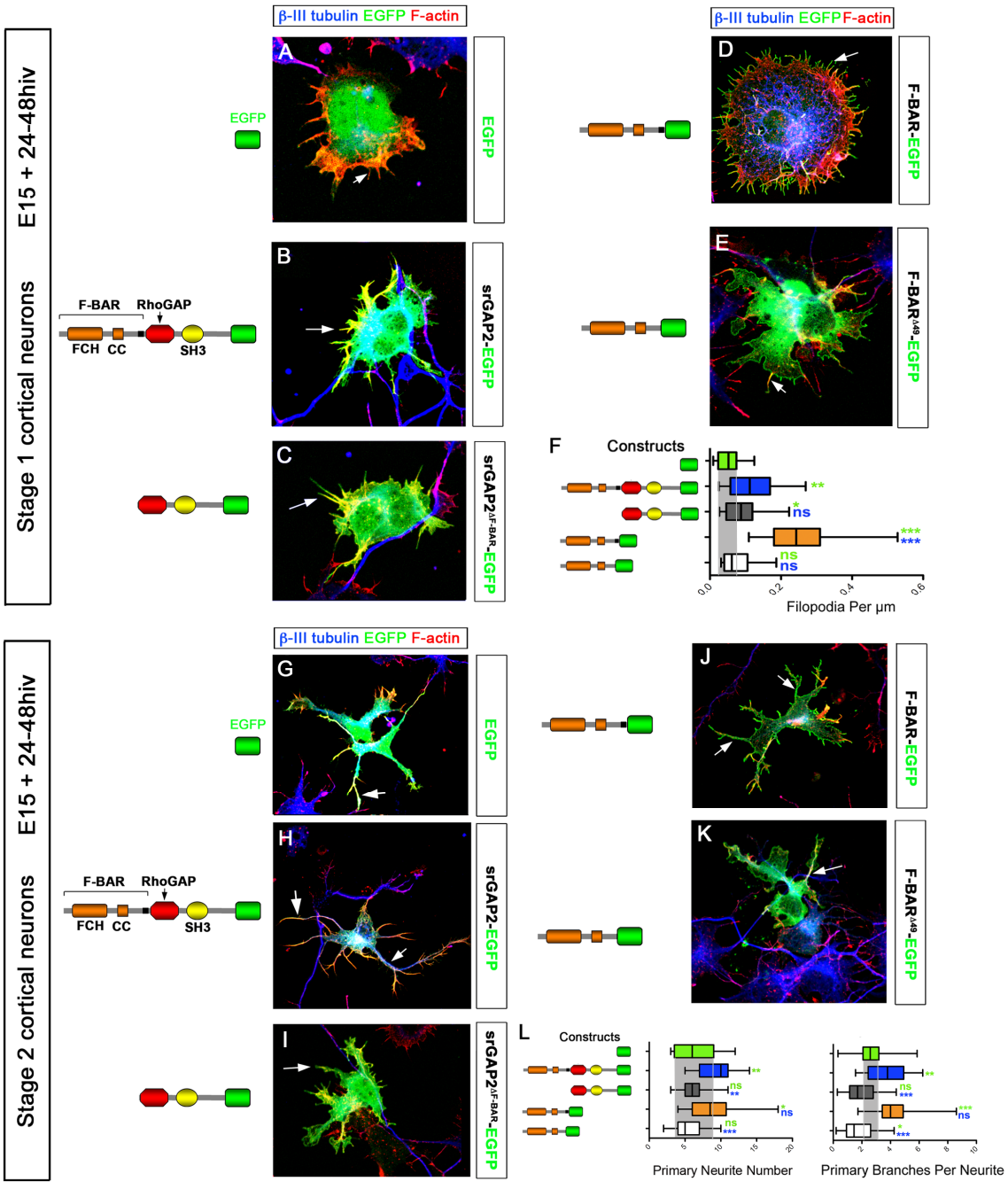

Figure 2.8. srGAP2 promotes filopodia formation and neurite outgrowth in an F-BAR dependent manner.

(A-E) Stage 1 cortical neurons expressing various srGAP2 constructs. All cells are stained with β-III tubulin to indicate that it is a neuron and phalloidin to visualize F-actin.

Control stage 1 neurons (EGFP (A)) normally display filopodia at cell periphery. However expression of srGAP2-EGFP (B, white arrow) significantly increased the number of filopodia. This effect required

the F-BAR domain since srGAP2$^{\Delta F\text{-}BAR}$-EGFP (C) expressing cells displayed filopodia at control levels whereas expression of F-BAR-EGFP (D) displayed a significant number of filopodia. This was not simply sue to the F-BARs ability to localize to the membrane (D) since F-BAR$^{\Delta 49}$ (E) localized nicely to the plasma membrane but did not cause an increase in the number of filopodia.

(F) Quantification of filopodia per micron in all conditions. Note srGAP2 and F-BAR are potent inducers of filopodia formation while srGAP2$^{\Delta F\text{-}BAR}$ and F-BAR$^{\Delta 49}$ are not. (EGFP n= 20 cells; srGAP2-EGFP n= 21 cells; srGAP2$^{\Delta F\text{-}BAR}$-EGFP n= 20 cells; F-BAR-EGFP n= 20 cells; F-BAR$^{\Delta 49}$-EGFP n= 20 cells. Cells were taken from 3 independent experiments and analyzed using Mann-Whitney Test * $p<0.05$; ** $p<.001$; *** $p<0.001$. Green color indicates comparison to EGFP and blue color indicates comparison to srGAP2-EGFP)

(G-K) Stage 2 cortical neurons expressing various srGAP2 constructs. All cells are stained with β-III tubulin to indicate that it is a neuron and phalloidin to visualize F-actin. EGFP (G) expressing neurons and stage 2 display several neurites (white arrows) and some branching. Expression of srGAP2 (H) caused a significant increase in both neurite formation (white arrows) and branching (white arrowheads). Similar to stage 1, expression of the F-BAR domain alone (J) also increased neurite formation (white arrows) and branching (white arrowheads), while deletion of the F-BAR domain in full length srGAP2 (I) or expression of F-BAR$^{\Delta 49}$ (K) did not increase primary neurite number or branching.

(L) Quantification of neurite number per cell in all conditions and primary branch number per neurite. Note srGAP2 and F-BAR are potent inducers of neurite outgrowth while srGAP2$^{\Delta F\text{-}BAR}$ and F-BAR$^{\Delta 49}$ are not. (EGFP n= 21 cells; srGAP2-EGFP n= 23 cells; srGAP2$^{\Delta F\text{-}BAR}$-EGFP n= 23 cells; F-BAR-EGFP n= 20 cells; F-BAR$^{\Delta 49}$-EGFP n= 20 cells. Cells were taken from 3 independent experiments and analyzed using Mann-Whitney Test * $p<0.05$; ** $p<.001$; *** $p<0.001$. Green color indicates comparison to EGFP and blue color indicates comparison to srGAP2-EGFP)

Reduction of srGAP2 expression promotes neuronal migration

To determine more generally the function of srGAP2 during cortical development, we introduced our shRNA constructs directed against srGAP2 (Dha2 and Dha5; **Fig. 2.7A**) into radial glial progenitors at E15 using ex vivo electroporation coupled with organotypic slice culture (Hand et al., 2005). This assay represents a powerful tool to test the role of specific genes in neuronal migration and differentiation. Interestingly, after 3 days in culture, at a time point when only few control-shRNA electroporated neurons have migrated (**Fig. 2.9A and 2.9C-D**), slices expressing srGAP2 shRNA showed a significant increase in the percentage of neurons that have reached the dense cortical plate (dCP) and a corresponding decreased percentage of neurons in the intermediate zone (IZ) (**Fig. 2.9B, and 2.9C-D**) suggesting that reduction of srGAP2 expression promoted radial migration.

We next wanted to directly determine if srGAP2 knockdown increased neuronal migration by regulating the rate of neuronal translocation. To do this we used time-lapse confocal microscopy to visualize neurons coexpressing nuclear-(n) EGFP (to ease cell tracking) and control (**Fig. 2.9E-H and Movie S3**) or srGAP2 shRNA **(Fig. 2.9E-L and Movie S4**) in slice culture. We observed that srGAP2 shRNA expressing neurons migrated approximately 23% faster than those expressing control shRNA (**Fig. 2.9M**) suggesting that reduction of srGAP2 increased cell speed.

Excessive LP branching in migrating cortical neurons can have strong inhibitory effects on neuronal migration (Gupta et al., 2003; Ohshima et al., 2007). As a result we wanted to determine if knockdown of srGAP2 reduced LP branching. Indeed, high magnification reconstruction of the morphology of control shRNA or srGAP2 knockdown neurons in layers 5/6 co-transfected with cytoplasmic EGFP, showed that their LP was significantly less complex, less branched when compared to control migrating neurons (**Fig.**

2.9N-P). Control neurons displayed approximately twice as many LP branches compared to srGAP2 shRNA-expressing neurons (**Fig. 2.9P**). These data strongly suggest that srGAP2 may negatively regulate the rate of radial migration by regulating LP branching and dynamics.

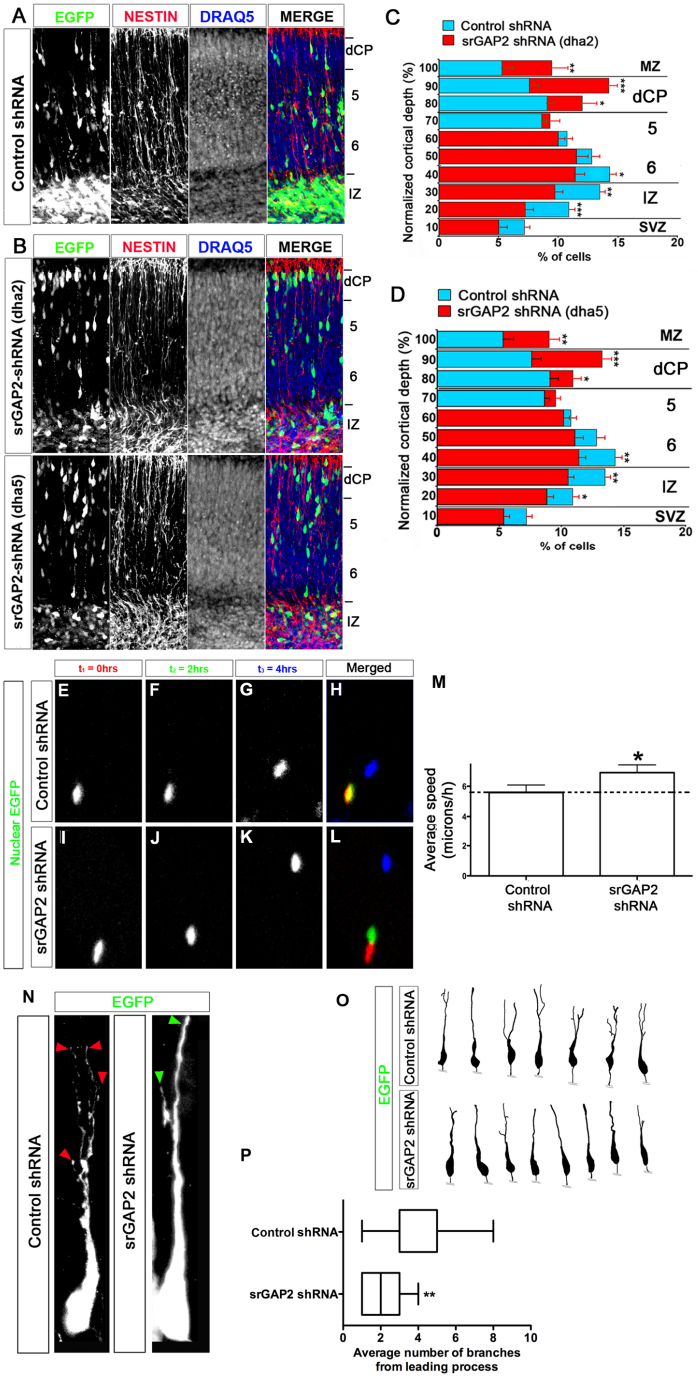

Figure 2.9. Knockdown of srGAP2 promotes neuronal migration and reduces leading process branching.

(A) E15 cortical slices cultured for 3 days after electroporation with EGFP + control shRNA. Slices were stained with anti-Nestin antibody revealing radial glial scaffold and Draq5 to illustrate cytoarchitecture. Note that neurons have just begun to migrate but have yet to reach the cortical plate.

(B) E15 cortical slices cultured for 3 days after electroporation with EGFP + Dha2 (B, top panel) or Dha5 (B lower panel). Slices were stained with anti-Nestin antibody revealing radial glial scaffold and Draq5 to illustrate cytoarchitecture. Note that knockdown of srGAP2 using either Dha2 or Dha5 shRNA decreased the number of migrating neurons found in the IZ and compared to CP at 3div compared to control.

(E-L) E15 cortical slices cultured for 2 days *ex vivo* after electroporation with Nuclear EGFP (3NLS) along with control shRNA (E-H) or srGAP2 shRNA (I-L) were imaged using time-lapse confocal microscopy. Neurons transfected with srGAP2 shRNA undergo faster translocation within 4 hrs (I-L and no colocalization in L) than control shRNA-transfected neurons.

(M) Quantification of effects of srGAP2 knockdown on cell speed. SrGAP2 knockdown cells migrated approximately 23% faster (6.91 microns/h compared to 5.59microns/h) compared to control shRNA-transfected neurons. (ctl shRNA, n=95 cells; srGAP2 shRNA n=84 cells. Cells were taken from 3 independent experiments and analyzed using Mann-Whitney Test p<.05 = * **,** p<.01=**, p<.001=***).

(N) High magnification images of control shRNA (left panel) or srGAP2 shRNA (right panel) expressing neurons from layers 5/6. Note the branched morphology of the leading process of control shRNA expressing neurons (red arrowheads pointing to leading process tips) whereas srGAP2 shRNA expressing neurons displayed a much simpler, unbranched morphology (green arrowhead pointing to single leading process tip). This type of morphology could lead to more rapid cell migration.

(O) Computer-based reconstruction of representative quantified control and srGAP2 shRNA expressing neurons demonstrating the leading process branching effect.

(P) Quantification of the average leading process branch number in control or srGAP2 shRNA expressing neurons. (ctl shRNA, n=19 cells; srGAP2 shRNA n=17 cells. Cells were taken from 3 independent experiments and analyzed using Mann-Whitney Test * p<0.05; ** p<.001; *** p<0.001). Note the difference in the overall distribution of the box plot for each condition.

The F-BAR domain is necessary and sufficient for srGAP2-mediated inhibition of radial migration

Since reduction of srGAP2 expression enhanced migration and reduced LP branching, we hypothesized that over-expression of srGAP2 or its F-BAR domain should be sufficient to block migration by increasing filopodia formation and LP dynamics. Indeed, overexpression of srGAP2 severely inhibited radial migration compared to control EGFP-expressing slices electroporated at E15 and cultured for 5 div (**Fig. 2.10E-H**). We first quantified the extent of migration by determining the average number of neurons per unit surface area in the CP, where pyramidal neurons complete migration and in the IZ, where they initiate migration (see **Fig. 2.11** for definition of the cytoarchitecture of the slices at 5div). This CP/IZ ratio (**Fig. 2.10U**) is significantly decreased by srGAP2 overexpression (**Fig. 2.10E-H**) when compared to control EGFP expressing neurons (**Fig. 2.10A-D**) demonstrating that srGAP2 overexpression reduces neuronal migration.

We next wanted to test if the F-BAR domain was involved in the effect of srGAP2 on neuronal migration. Expression of srGAP2$^{\Delta F\text{-}BAR}$ does not significantly reduce the CP/IZ ratio compared to EGFP control **(Fig. 2.10I-L, 6U**) and is significantly different from the ratio measured by srGAP2 overexpression (**Fig. 2.10U**) suggesting that the F-BAR domain is required for srGAP2's ability to inhibit migration. Moreover, expression of the F-BAR domain alone was sufficient to reduce neuronal migration to the same extent than srGAP2 while expression of F-BAR$^{\Delta 49}$ had no effect on the ability of neurons to migrate (**Fig. 2.10M-P and Fig. 2.10Q-T and 2.10U**) suggesting that the ability of the F-BAR domain to induce filopodia is required for the ability of srGAP2 to inhibit neuronal migration.

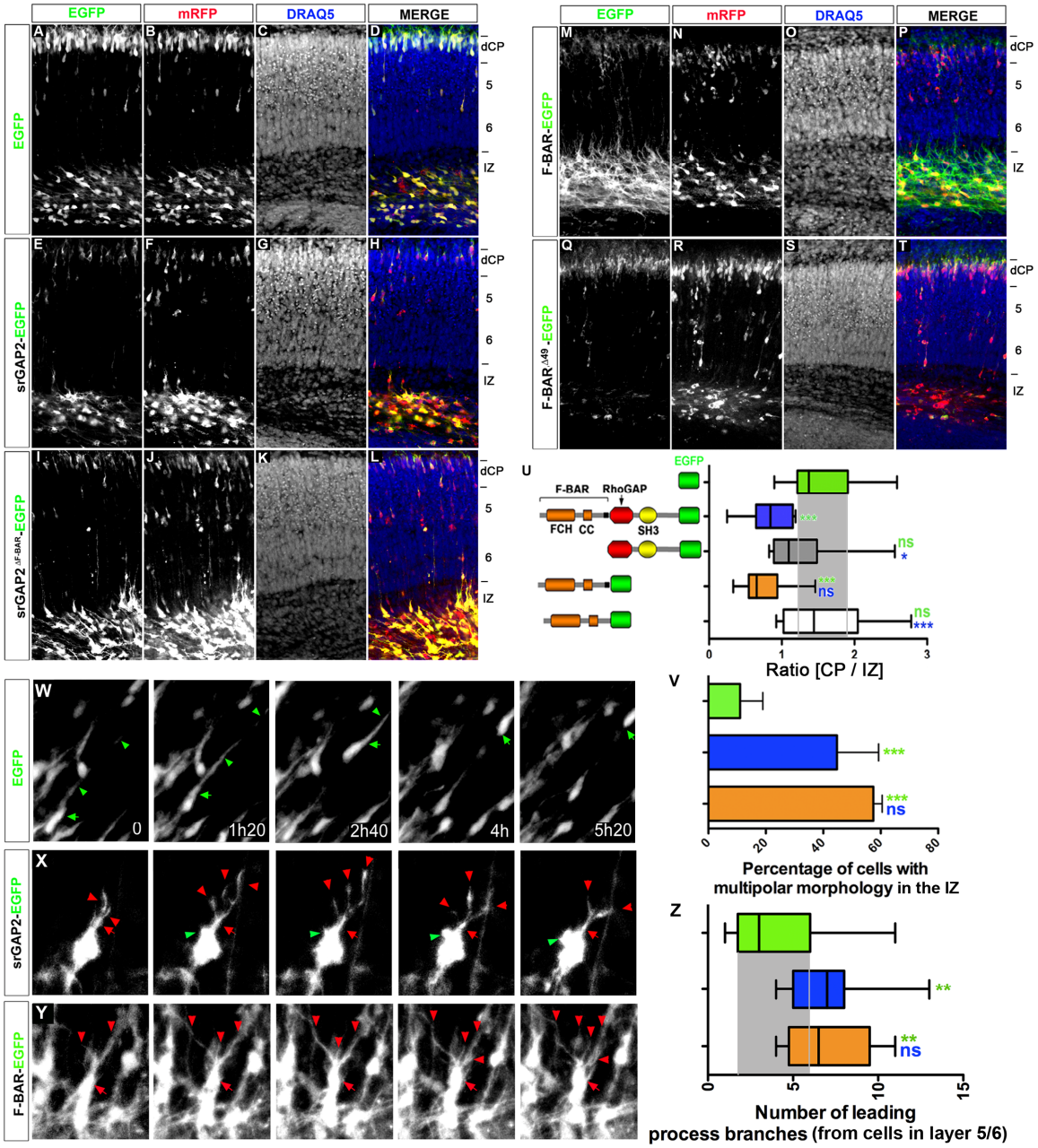

Figure 2.10. SrGAP2 mediated inhibition of migration requires F-BAR mediated membrane deformation.

(A-T) E15 cortical slices cultured for 5 days after electroporation with various srGAP2 constructs and mRFP. Slices were stained with Draq5 in order to demonstrate cytoarchitecture. While EGFP expressing neurons efficiently migrated from the IZ to CP (A-D), srGAP2-EGFP expressing neurons

did not (E-H), showing decreased neurons in the CP and increased neurons in the IZ. This affect was abrogated by removing the F-BAR domain (I-L). Interestingly, expression of the F-BAR domain alone had similar effect as srGAP2 (M-P) while expression of F-BARD49 had no effect on migration (Q-T) suggesting that the membrane deformation ability of the F-BAR domain is important for this effect.
(U) Quantification of CP/IZ ratio. (EGFP n= 13 slices; srGAP2-EGFP n= 14 slices; srGAP2$^{\Delta F\text{-}BAR}$-EGFP n= 8 slices; F-BAR-EGFP n= 10 slices; F-BAR$^{\Delta 49}$-EGFP n= 6 slice Slices were taken from 4 different experiments and analyzed using Mann-Whitney Test * $p<0.05$; ** $p<.001$; *** $p<0.001$. Green color indicates comparison to EGFP and blue color indicates comparison to srGAP2-EGFP).
(V) Quantification of percentage of cells with multipolar morphology in EGFP, srGAP2, or F-BAR transfected slices. Multipolar cells were defined as cells possessing $\geq$ 3 processes. (EGFP n= 66 cells; srGAP2-EGFP n= 42 cells; F-BAR-EGFP n= 57 cells. Cells were taken from 3 different experiments and analyzed using Fisher's exact test * $p<0.05$; ** $p<.001$; *** $p<0.001$. Green color indicates comparison to EGFP and blue color indicates comparison to srGAP2-EGFP).
(W-Y) Time series E15 cortical slices cultured for 3 days after electroporation with EGFP, srGAP2-EGFP, or F-BAR-EGFP. EGFP expressing neurons displayed a unipolar morphology (green arrowhead pointing at single leading process) and the cell body translocated a significant distance within 5 hours (green arrows (W)). In contrast, srGAP2-EGFP or F-BAR-EGFP expressing neurons displayed multiple leading processes (red arrowheads (X and Y)) and did not translocate their cell body (red arrows (X and Y)). This is likely due to the fact that no stable leading process is established (multiple arrowheads in X and Y). Finally notice the high degree of membrane dynamics occurring at the cells body (X green arrowhead) further demonstrating the ability of srGAP2 to facilitate membrane protrusions.
(Z) Quantification of leading process branching from cells expressing EGFP, srGAP2-EGFP, or F-BAR-EGFP in layer 5/6. (EGFP n= 17 cells; srGAP2-EGFP n= 21 cells; F-BAR-EGFP n= 9 cells. Cells were taken from 3 different experiments and average branch number was analyzed using Mann-Whitney Test * $p<0.05$; ** $p<.001$; *** $p<0.001$. Green color indicates comparison to EGFP and blue color indicates comparison to srGAP2-EGFP)

srGAP2 inhibits migration by increasing leading process dynamics and branching

The accumulation of neurons expressing srGAP2 or its F-BAR domain in the IZ suggested that the neurons might be partially blocked in the multipolar to unipolar transition (Noctor et al., 2004). Indeed quantification of the percentage of multipolar cells (cells displaying $\geq$ 3 neurites) in the IZ in slices electroporated srGAP2 or the F-BAR domain revealed a significant increase in the percentage of neurons with multiple processes emerging from the cell body compared to control slices expressing EGFP only (**Fig. 2.10V**). This is consistent with the ability of srGAP2 to induce filopodia and neurite initiation/branching in dissociated neurons (see **Fig. 2.8**).

To investigate the dynamic changes of neuronal morphology during migration, we used time-lapse confocal microscopy in our electroporated slice culture assay. Control neurons engaging radial migration in the IZ, form a stable LP upon initiating radial migration (green arrowheads in **Fig. 2.10W and Movie S5**) and undergo efficient cell body translocation (green arrows in **Fig. 2.10W and Movie S5**). In contrast, neurons overexpressing srGAP2 or the F-BAR domain alone, do not undergo cell body translocation (red arrows in **Fig. 2.10X and 2.10Y and Movies S6 and S7**), and instead of forming a single, stable LP, they form multiple processes that are highly dynamic and unstable (red arrowheads in **Fig. 2.10X and 2.10Y and Movies S6 and S7**). Moreover, the plasma membrane of these cells appears highly dynamic showing large, transient protrusions (green arrowheads in **Fig. 2.10X**). While many neurons accumulate in the IZ, some neurons did manage to translocate into layers 5/6 (**Fig 2.10E-H and 2.10M-P**). To determine the consequence of srGAP2 expression on these neurons we obtained high magnification images of their leading processes. Interestingly, expression of srGAP2 or its F-BAR domain caused significant increased in LP branching compared to EGFP control (**Fig 2.10Z and**

Fig. 2.11E-G). This data is consistent with our previous result showing that srGAP2 knockdown reduced LP branching and that srGAP2 or F-BAR overexpression increased filopodia formation, neurite initiation and branching in dissociated neuronal culture. Taken together these data suggest that srGAP2 increases neurite initiation and branching through the ability of its F-BAR domain to induce filopodia, which in turn negatively regulates neuronal migration.

Finally, to ensure that the reduction in the number of migrating neurons was not due to an indirect effect of srGAP2 on progenitor proliferation and/or cell cycle exit, we designed a vector allowing us to express srGAP2 in early post-mitotic neurons using the 2.2kB NeuroD promoter (**Fig. 2.12A**). NeuroD is a bHLH transcription factor and a direct transcriptional target of Ngn2 (Hand et al., 2005; Heng et al., 2008) thereby inducing cDNA expression in intermediate progenitors and early post-mitotic neurons in the SVZ and IZ (**Fig. 2.13E-H**) but not by Nestin+ radial glial progenitors in the VZ as obtained by our regular chicken β-actin promoter (**Fig. 2.13A-D**). Furthermore, the level of protein expression in neurons obtained with this promoter is much lower than using the chicken β-actin promoter (data not shown; (Heng et al., 2008)). Expression of srGAP2 using this NeuroD promoter significantly reduced the number of cells reaching the cortical plate compared to control EGFP (**Fig. 2.12B-I and 2.12J**). These data reinforce the fact that srGAP2 acts as a negative regulator of neuronal migration in the cortex.

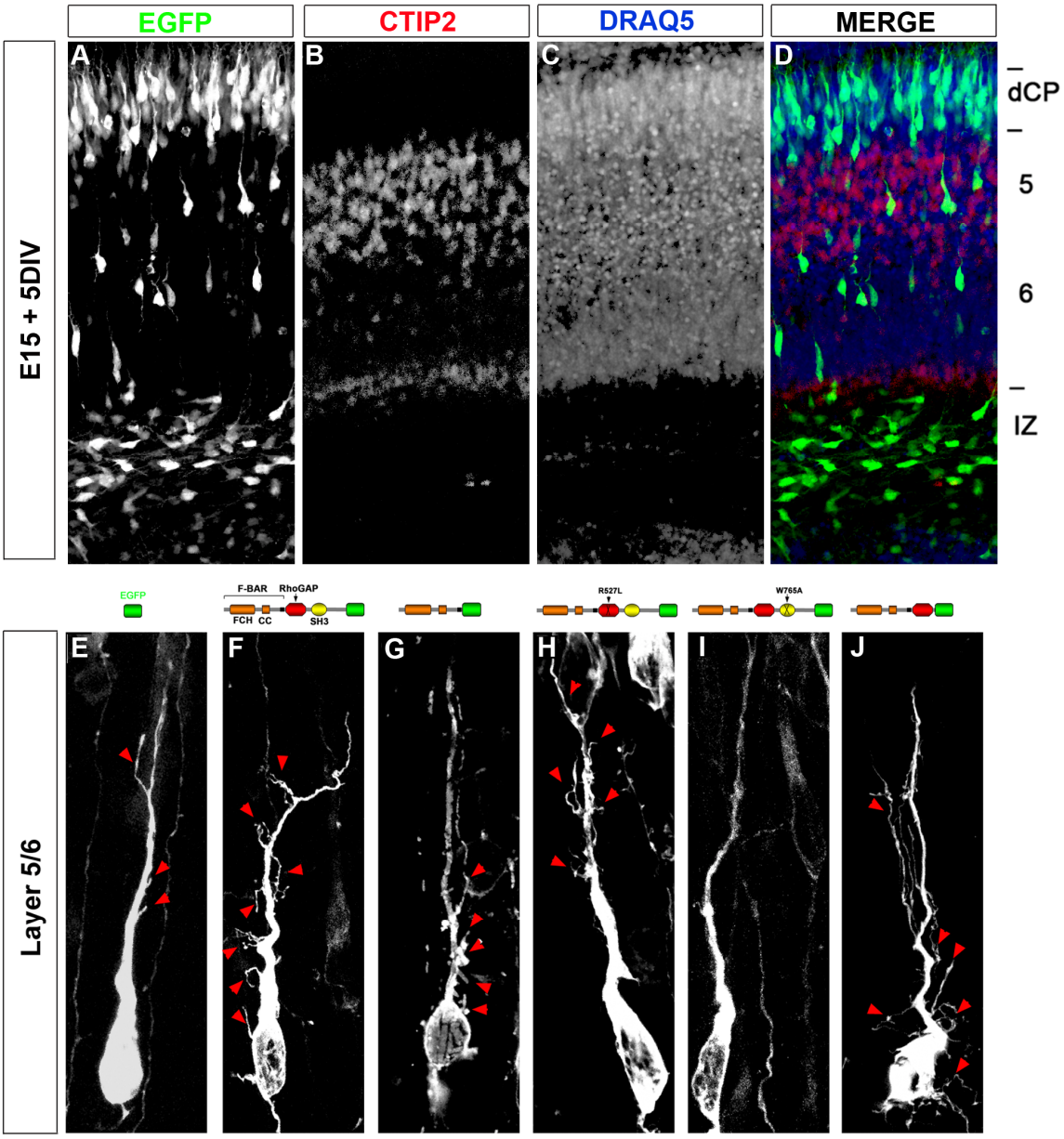

Figure 2.11. srGAP2 increases leading process branching in F-BAR dependent manner.

(A-D) E15 cortical slices cultured for 5 days after electroporation with EGFP and slices were stained with CTIP2 (layer 5/6 marker) and Draq 5 in order to demonstrate cytoarchitecture.

(E-J) Representative images of neurons in layer 5/6 after electroporation with srGAP2 constructs containing an F-BAR domain. EGFP (E) expressing neurons displayed a slightly branched morphology. Expression of srGAP2 (F) caused a marked increase in leading process branching, as

did expression of F-BAR-EGFP (G) and srGAP2^{R527L}-EGFP (H) expressing neurons. Interestingly, srGAP2^{W765A}-EGFP (SH3 domain mutant) expressing neurons did not show a significantly branched leading process despite having an F-BAR domain. However deletion of the c-terminus (srGAP2$^{\Delta C\text{-term}}$-EGFP) including the SH3 domain restored the branching activity (J).

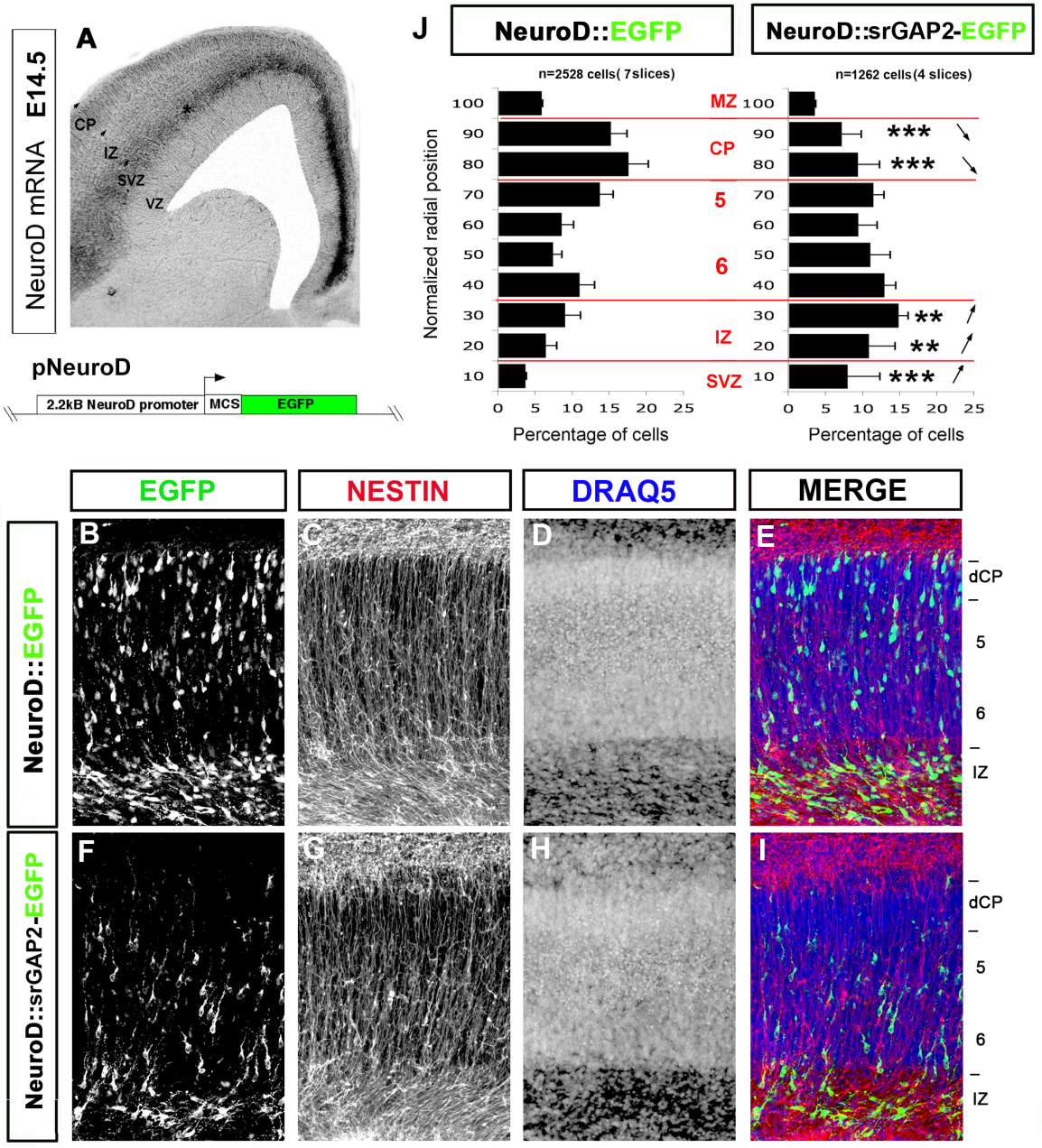

Figure 2.12. Expression of srGAP2 in post mitotic neurons inhibits radial migration.

(A) In situ hybridization of *NeuroD mRNA* in the developing neocortex of an E15 mouse embryo. NeuroD mRNA is expressed at the SVZ/IZ border but not in the VZ. Schematic representation of the construct used to express EGFP-fusion proteins under the control of the 2.2kB promoter region of NeuroD, which drives cDNA expression exclusively in post-mitotic neurons.

(B-I) E15 cortical slice cultured for 5 days after transfection with pNeuroD-EGFP or pNeuroD-srGAP2-EGFP. EGFP expressing neurons migrate nicely to the cortical plate (B-E). In contrast, srGAP2-

EGFP expressing neurons migrate poorly to the cortical plate (F-I). Slices were stained with anti-nestin to reveal the radial glial scaffold and Draq5 to illustrate the cytoarchitecture.
(K-L) Quantification of B-G showing that a greater proportion of neurons reach the cortical plate in control (EGFP transfected) conditions than in srGAP2 transfected neurons (note decrease proportion of cells in CP and increase proportion in IZ (denoted by arrows) when compared to control). (EGFP n= 7 slices and srGAP2 n= 5 slice).
Statistical significance: Mann-Whitney test, * $p<0.05$; ** $p<.001$; *** $p<0.001$.

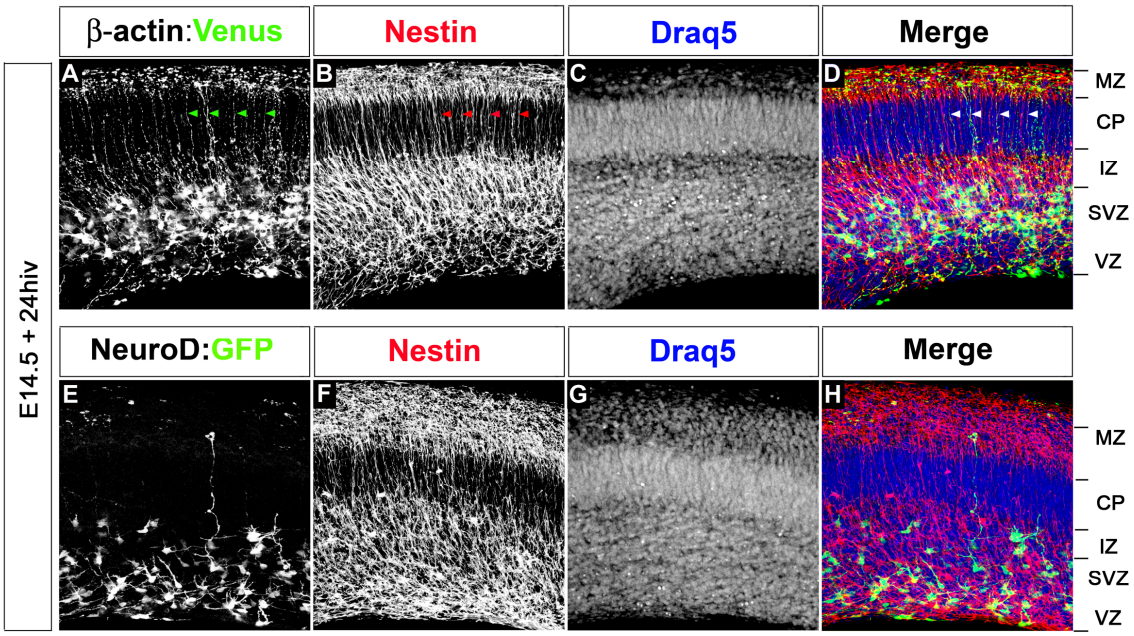

Figure 2.13: NeuroD drives expression gene expression in post mitotic neurons.

(A-D) E15 cortices were electroporated chicken-β-actin driven Venus construct sliced and cultured for 24 hrs. After 24 hrs venus positive cells were also positive for anti-nestin (radial glia marker, green arrow heads in A, red arrow heads in B and white arrow heads in D). Also note the long radial glial like morphology of cells.

(F-H) In contrast NeuroD drive EGFP showed no radial glial like morphology and no localization with anti-nestin, supporting the idea that the NeuroD promoter drives expression in postmitotic neurons.

srGAP2 partially requires its RhoGAP and SH3 domains to inhibit migration

We next wanted to determine the contributions of the RhoGAP and SH3 domains to srGAP2 function in neuronal migration and morphogenesis. In order to determine the substrate specificity of the GAP domain of srGAP2, we first purified its GAP domain as a GST-fusion (**Fig. 2.14A**). We then performed fluorescence-based GTP hydrolysis assays (**Fig. 2.14B**; (Shutes and Der, 2006)). The GAP domain of srGAP2 increased the rate of GTP hydrolysis on Rac1, but had no effect on RhoA or Cdc42 (**Fig. 2.14B**) or RhoG (data not shown). In addition, full-length srGAP2 strongly interacted with activated Rac1 ($Rac1^{Q61L}$) but only weakly interacted with activated $Cdc42^{Q61L}$ (**Fig. 2.14C**) and activated $RhoA^{Q63L}$ (data not shown). These two independent approaches demonstrate that the GAP domain of srGAP2 is specific for Rac1 but not Cdc42 or RhoA.

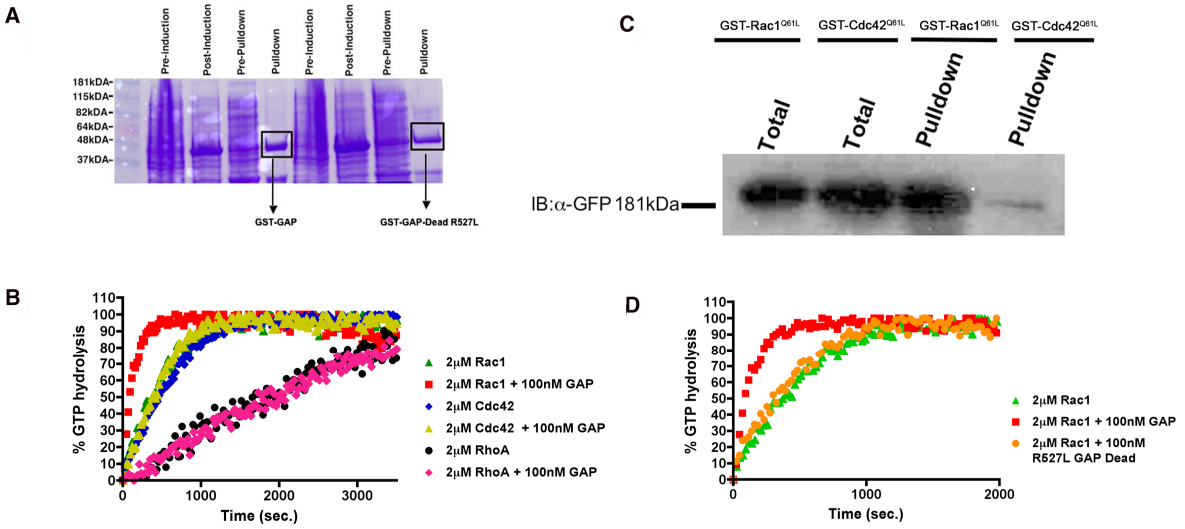

Figure 2.14. The RhoGAP domain of srGAP2 is specific for Rac1.

(A) GST-purification of the wild-type GAP and GAP^{R527L} forms of the RhoGAP domain of srGAP2. Coumassie-stained gel showing the yield recombinant proteins obtained before and after induction (lanes 1-2 and 5-6) in bacteria as well as before and after glutathione-elution of GST-GAP (lanes 3-4) and GST-GAP^{R527L} (lanes 7-8). The boxed areas correspond to the purified recombinant proteins used for the subsequent GTP hydrolysis assays in panel B-C.

(B) Fluorescent-based GTP hydrolysis assay as a function of time (seconds) for 2μM purified Rac1, Cdc42, RhoA in the presence or absence of 100nM of the recombinant GAP-domain of srGAP2. Note that the GAP domain of srGAP2 only accelerates the rate of GTP hydrolysis of Rac1 but not Cdc42 or RhoA.

(C) Same as B expect that 2μM purified Rac1 is incubated alone or in the presence of 100nM of recombinant wild-type GAP domain or GAP^{R527L}. Note that this point mutation abolishes the accelerating effect of the GAP domain on Rac1 GTP hydrolysis.

(D) GST pulldown of srGAP2-EGFP from COS7 cells using constitutively active forms of Rac1 ($Rac1^{Q61L}$) or Cdc42 ($Cdc42^{Q61L}$). GST-Rac^{Q61L} pulls down significantly higher amounts of srGAP2 compared to GST-$Cdc42^{Q61L}$ confirming that this is a Rac1-specific GAP.

To determine the contribution of the Rac1-GAP domain on srGAP2's ability to regulate neuronal morphogenesis and migration, we engineered a catalytically-inactive form of srGAP2 (srGAP2^{R527L}). Indeed this mutant was unable to accelerate GTP hydrolysis of Rac1 (**Fig. 2.14D**). Expression of the 'GAP-dead', srGAP2^{R527L} was as potent as srGAP2 at inducing filopodia-like membrane protrusions in Stage 1 cortical neurons (compare **Fig. 2.15B** and **2.15C**; quantified in **2.15F**) and at promoting primary neurite initiation (**Fig. 2.15H** and **2.15I;** quantified in **2.15L**). While, this mutant was competent to induce an increase neurite outgrowth, there were significantly fewer (2-fold) srGAP2^{R527L} expressing neurons at stage 2 when compared to srGAP2 (**Fig. 2.16**). In addition, srGAP2^{R527L} displays a reduced ability to induce neurite branching when compared to srGAP2 (**Fig. 2.15L**), suggesting that the Rac1-GAP activity of srGAP2 may be required for some aspects of neurite dynamics such as neurite branching.

We next wanted to determine the contribution of the Rac1-GAP activity of srGAP2 in its ability to inhibit neuronal migration. Expression of srGAP2^{R527L} in E15 cortical progenitors followed by 5 days in slice culture significantly inhibits migration compared to control EGFP (**Fig. 2.17A-D and 2.17I-L and 2.17U**) although not as potently as full-length srGAP2 over-expression (**Fig. 2.17E-H and 2.17U**) suggesting that the Rac1-GAP activity of srGAP2 contributes to its ability to inhibit migration. In addition, similarly to srGAP2, expression of srGAP2^{R527L} increased the percentage of multipolar cells in the IZ (**Fig. 2.17V**) and increased LP branching of radially migrating neurons in layer 5/6 (**Fig. 2.17X and 2.11H**). These data suggest that the Rac1-GAP activity may act to modulate protrusion formation induced by the F-BAR domain of srGAP2, but is not absolutely required since expression of the F-BAR domain is sufficient to form protrusions and inhibit migration.

Finally, to test the contribution of the SH3 domain, we engineered a mutant to a conserved tryptophan residue (srGAP2^{W765A}), which was shown to be required for the ability

of the SH3 domains of srGAP1 to bind to Robo1 and for the SH3 domain of srGAP3 to bind to WAVE-1 (Li et al., 2006; Soderling et al., 2002). Expression of srGAP2^{W765A}, unlike the expression of full-length srGAP2 or its F-BAR domain, did not efficiently induce filopodia-like membrane protrusions in Stage 1 cortical neurons (**Fig. 2.15D** and **2.15F**), and had a significantly decreased ability to induce primary neurite branching compared to full-length srGAP2 (**Fig. 2.15J** and **2.15L**). Like srGAP2^{R527L}, expression of srGAP2^{W765A} increased primary neurite initiation, however showed a significantly reduced percentage (2 fold) of neurons transitioning from Stage 1 to Stage 2 compared to srGAP2 (**Fig. 2.16**) suggesting that full-length (i.e. all domains functionally intact) srGAP2 is required for the transition from stage 1 to stage 2 i.e. for transition between filopodia-like protrusions to elongating neurites.

Interestingly, using our slice migration assay, expression of srGAP2^{W765A} had no effect on cortical neuron migration (**Fig. 2.17M-P** and **2.17U**), although there was a slight increase in cells with multipolar morphology in the IZ compared to EGFP (**Fig. 2.17V**). The lack of effect of srGAP2^{W765A} over-expression on the CP/IZ ration prompted us to use time-lapse microscopy to observe LP dynamics in radially migrating neurons. This analysis revealed that migrating neurons expressing srGAP2^{W765A} did not display increased leading process branching and dynamics but instead had a single, stable leading processes (red arrowheads **Fig. 2.17W and Movie S8**) and translocated efficiently (green arrowheads **Fig. 2.17W and Movie S8**) which is strikingly different from neurons overexpressing full-length srGAP2 (**Fig. 2.17X**). Moreover analysis of neurons in layer 5/6 showed no significant increase in LP branching as demonstrated with other constructs containing an F-BAR domain (**Fig. 2.10 and Fig. 2.17X and Fig. 2.11**).

The fact that srGAP2^{W765A} showed weak filopodia formation compared to full-length srGAP2 and no increase in neurite branching suggested that the F-BAR domain function in srGAP2^{W765A} might be inhibited. By analogy to the molecular mechanisms controlling the

activation of other Rho-GAP and Rho-GEF proteins (Eberth et al., 2009; Mitin et al., 2007; Yohe et al., 2007), we hypothesized that srGAP2 might normally be in an inactive, auto-inhibited conformation through structural interaction between the N-terminal F-BAR domain and of the C-terminal region (including the SH3 domain) (see model in **Fig. 2.18A**) that is released upon binding of protein interactors to its SH3 domain.

To test this model, we designed a C-terminal deletion of srGAP2 (srGAP2$^{\Delta C\text{-term}}$), which deletes the entire C-terminal portion starting from the SH3 domain to the C-terminal end of the protein leaving only the F-BAR and Rac1-GAP domains. Indeed, expression of srGAP2$^{\Delta C\text{-term}}$ very potently induced filopodia formation in stage 1 neurons (**Fig. 2.15E** and **2.15F**) and neurite outgrowth and branching in Stage 2 neurons (**Fig. 2.15K-L**). Finally we tested the effects of this mutant on neuronal migration. In sharp contrast to srGAP2^{W765A}, expression of srGAP2$^{\Delta C\text{-term}}$ potently inhibited migration (**Fig. 2.17Q-T and 2.17U**) resulting in increased multipolar cells in the IZ (**Fig. 2.17V**). Finally, analysis of the morphology of neurons translocating through layer 5/6 shows that expression of srGAP2$^{\Delta C\text{-term}}$ increased LP branching similarly to other F-BAR containing constructs but unlike srGAP2^{W765A} (**Fig. 2.17X and Fig. 2.11J**). These data suggest that the ability of the F-BAR domain to promote membrane protrusions in the form of filopodia and neurite branches may be regulated by the C-terminal domain of srGAP2, and release from this auto-inhibition might require binding of protein interactors to the SH3 domain during neuronal migration and morphogenesis.

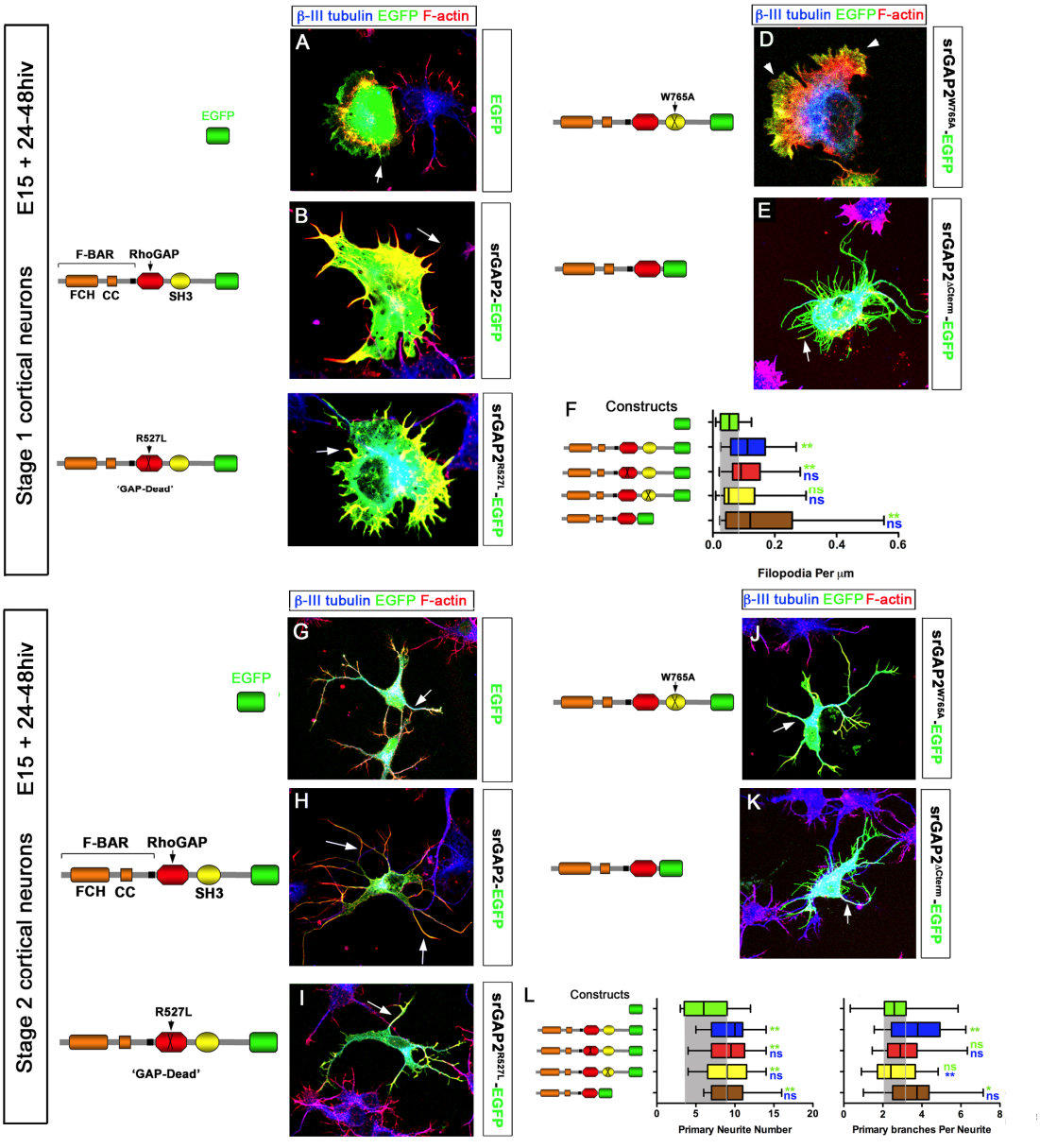

Figure 2.15. The GAP and SH3 domains participate in srGAP2's ability to promote filopodia formation in neurons.

(A-E) Stage 1 cortical neurons expressing various srGAP2 constructs. All cells are stained with β-III tubulin to indicate that it is a neuron and phalloidin to visualize F-actin.

Control stage 1 neurons (EGFP (A)) normally display filopodia at cell periphery. However expression of srGAP2-EGFP (B) significantly increased the number of filopodia. Mutation of the GAP domain (srGAP2^{R527L}-EGFP (B)) did not appear to affect the ability of srGAP2 to make filopodia but did appear to increase lamellapodia formation. The SH3 domain mutant (srGAP2^{W765A}-EGFP (D)) completely abrogated srGAPs ability to induce filopodia formation while deletion of the c-terminus (E) (including the SH3 domain, srGAP2$^{\Delta C\text{-term}}$-EGFP) was able to induce filopodia.

(F) Quantification of A-E. (EGFP n= 20 cells; srGAP2-EGFP n= 21 cells; srGAP2^{R527L}-EGFP n= 21 cells; srGAP2^{W765A}-EGFP n= 21 cells; srGAP2$^{\Delta C\text{-term}}$-EGFP n=20 cells. Cells were taken from 3 different experiments and analyzed using Mann-Whitney Test * $p<0.05$; ** $p<.001$; *** $p<0.001$. Green color indicates comparison to EGFP and blue color indicates comparison to srGAP2-EGFP)

(G-K) Stage 2 cortical neurons expressing various srGAP2 constructs. All cells are stained with β-III tubulin to indicate that it is a neuron and phalloidin to visualize F-actin.

As shown previously expression of srGAP2 (H) caused increase neurites initiation and branching compared to EGFP (G) expressing neurons at stage 2. Expression of srGAP2^{R527L}-EGFP (I); srGAP2^{W765A}-EGFP (J); and srGAP2$^{\Delta C\text{-term}}$ -EGFP (K) all caused increased neurite initiation. While, srGAP2$^{\Delta C\text{-term}}$ -EGFP expression caused significant increases in neurite branching (K), srGAP2^{W765A}-EGFP expression (I) had no effect. Expression of srGAP2^{R527L}-EGFP did cause an increase in neurite branching, but not as significant as srGAP2.

(L) Quantification of G-K. (EGFP n= 20 cells; srGAP2-EGFP n= 21 cells; srGAP2^{R527L}-EGFP n= 22 cells; srGAP2^{W765A}-EGFP n= 21 cells; srGAP2$^{\Delta C\text{-term}}$-EGFP n=23 cells. Cells were taken from 3 independent experiments and analyzed using Mann-Whitney Test * $p<0.05$; ** $p<.001$; *** $p<0.001$.)

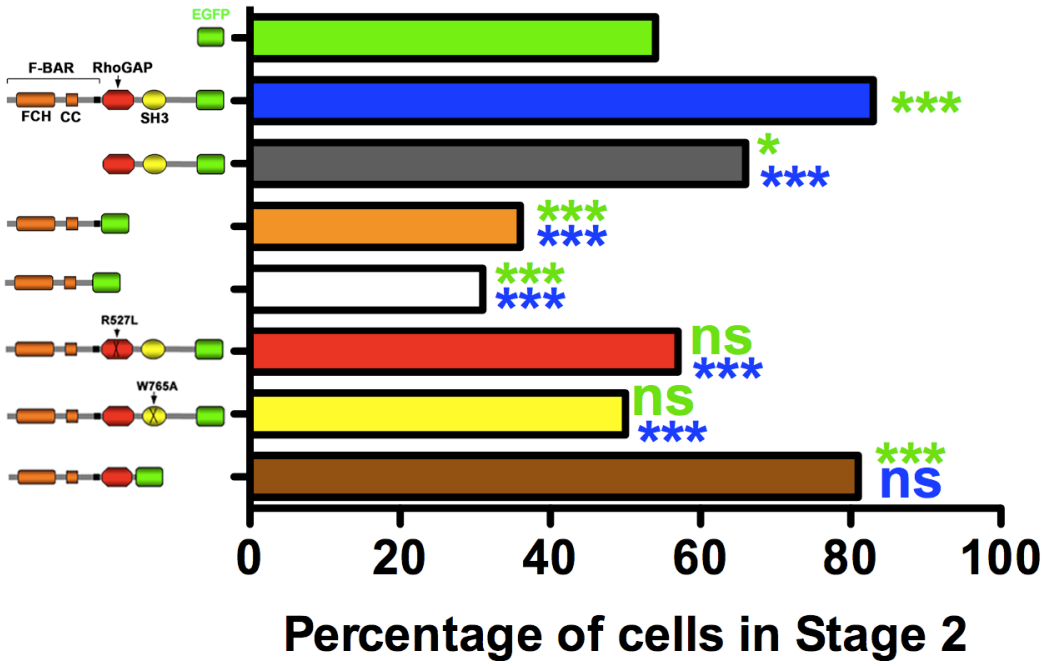

Figure 2.16. srGAP2 expressing cells accumulate in Stage 2

Analysis of the percentage of cells that accumulate at stage 2 after transfection of various srGAP2 constructs

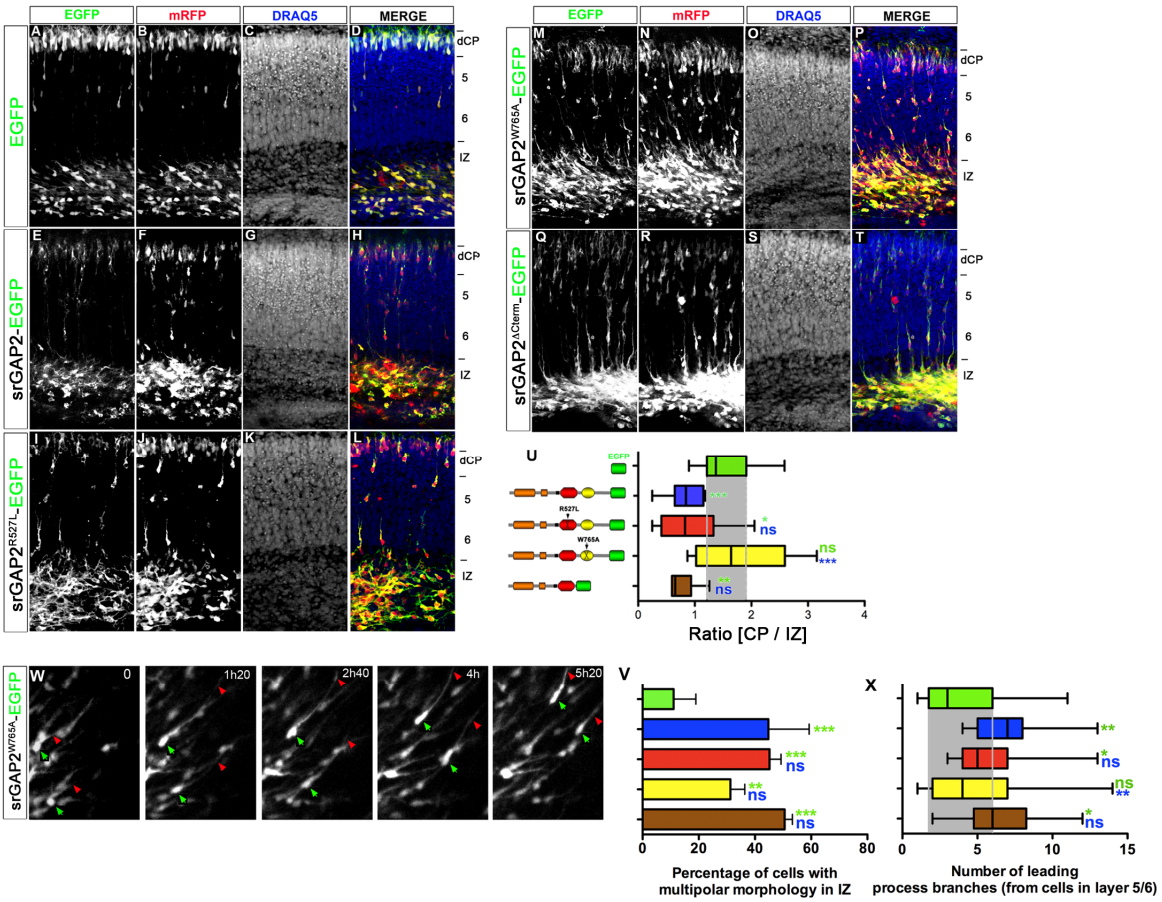

Figure 2.17. The GAP and SH3 domains participate in srGAP2's ability to inhibit migration.

(A-T) E15 cortical slices cultured for 5 days after electroporation with various srGAP2 constructs and mRFP. Slices were stained with Draq5 in order to demonstrate cytoarchitecture. As shown previously srGAP2 expressing neurons migrate very poorly to the cortical plate (E-H)

Impairment of the GAP activity of srGAP2 (srGAP2^{R527L}) inhibits migration albeit not to the degree of full-length srGAP2 (I-L). Moreover, mutation of the SH3 domain (srGAP2^{W765A}) (M-P) had no effect on the ability of neurons to migrate, in that it does not inhibit migration like full-length srGAP2. However, expression of the c-terminal deletion of srGAP2 (srGAP2$^{\Delta C\text{-term}}$-EGFP) does impair migration (Q-T).

(U) Quantification of effects displayed in A-L. (EGFP, n= 13 slices; srGAP2-EGFP n= 14 slices; srGAP2^{R527L}-EGFP n= 11 slices; srGAP2^{W765A}-EGFP n= 8 slices; srGAP2$^{\Delta C\text{-term}}$-EGFP n= 6 slices.

Slices were taken from 4 independent experiments and analyzed using Mann-Whitney Test p<.05 =* **,** p<.01=**, p<.001=***. Green color indicates comparison to EGFP and blue color indicates comparison to srGAP2-EGFP).

(V) Quantification of percentage of cells with multipolar morphology in EGFP, srGAP2, or F-BAR transfected slices. Multipolar cells were defined as cells possessing $\geq$ 3 processes. (EGFP n= 66 cells; srGAP2-EGFP n= 42 cells; srGAP2^{R527L}-EGFP n= 47 cells; srGAP2^{W765A}-EGFP n= 52 cells; srGAP2$^{\Delta C\text{-term}}$ -EGFP n= 50 cells. Cells were taken from 3 independent experiments and analyzed using Mann-Whitney Test * p<0.05; ** p<.001; *** p<0.001. Green color indicates comparison to EGFP and blue color indicates comparison to srGAP2-EGFP).

(W) Time-series of E15 cortical slices cultured for 3 days after electroporation with srGAP2^{W765A}-EGFP. These neurons showed a unipolar morphology with a single unbranched leading process (red arrowhead) and translocated very efficiently (green arrowhead).

(X) Quantification of leading process branching from cells expressing EGFP, srGAP2-EGFP, srGAP2^{R527L}-EGFP, srGAP2^{W765A}-EGFP, or srGAP2$^{\Delta C\text{-term}}$ -EGFP in layer 5/6. (EGFP n= 17 cells; srGAP2-EGFP n= 21 cells; srGAP2^{R527L}-EGFP n= 18 cells; srGAP2^{W765A}-EGFP n= 26 cells; srGAP2$^{\Delta C\text{-term}}$-EGFP n= 18 cells. Cells were taken from 3 independent experiments and analyzed using Mann-Whitney Test * p<0.05; ** p<.001; *** p<0.001. Green color indicates comparison to EGFP and blue color indicates comparison to srGAP2-EGFP)

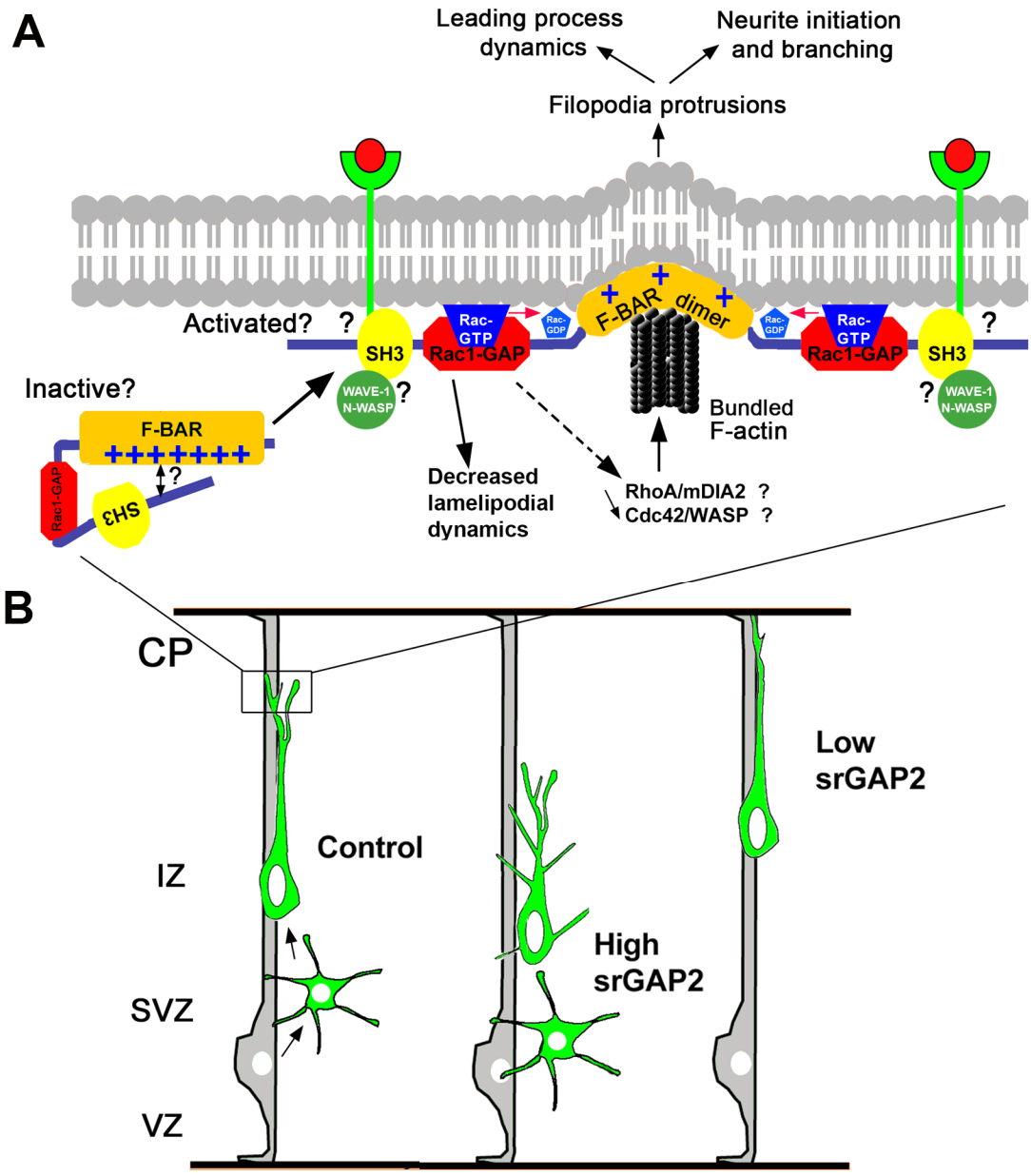

Figure 2.18. Model for srGAP2 regulated membrane protrusion in neuronal migration.

(A) Hypothetical Model for srGAP2 mediated membrane protrusions. When ligand binds receptor at the plasma membrane of migrating neuron, srGAP2 is recruited to this site through interactions between the receptor and the SH3 domain. Binding of the SH3 domain releases inhibition of srGAP2 exposing F-BAR and GAP domains. The F-BAR then interacts with negatively charged phospholipids at the plasma membrane, where it begins to induce curvature. Meanwhile the GAP domain reduces

active Rac1 locally at this site resulting in either Cdc42 activation leading to Wasp activation or RhoA activation leading mDIA2 activation. Either pathway results in F-actin polymerization, which fills in the tubes generated by F-BAR activation. In addition, interactions between SH3 domain with other regulators of actin polymerization, such as WAVE-1 or N-WASP may also participate in this process. (B) Summary of srGAP2 effects on radial migration during cortical development. Normally neurons migrate radially to CP with a slightly branched leading processes. When there is too much srGAP2, leading process outgrowth is dynamic and unstable. In addition the cells grow many neurites and neurite branching is increased resulting in an inhibition of migration. Finally, if srGAP2 levels are low, leading process branching is decreased and which may produce a more persistent leading process and neurons migrate.

Chapter 3: Discussion

Summary of results

In this study, we provide loss-of-function, gain-of-function as well as structure-function analysis demonstrating that srGAP2 is a novel, negative regulator of neuronal migration and a positive regulator of neurite initiation and branching through the ability of its F-BAR domain to induce filopodia-like membrane protrusions. We find that reduction of srGAP2 expression leads to a decrease in LP complexity in migrating neurons and increased rate of neuronal migration. Overexpression of srGAP2 had the opposite effects increasing LP dynamics and complexity and inhibiting radial migration. Finally, we show that these effects are largely mediated by the ability of the F-BAR domain to cause filopodia-like membrane protrusions. *Taken together, my thesis work demonstrates for the first time the function of an F-BAR domain-containing protein in cell migration and morphogenesis* in vivo *and more generally this work highlights the functional importance of proteins directly regulating membrane deformation during brain development.*

srGAP2 is a novel F-BAR domain-containing protein

It is well-established that cytoskeletal dynamics produce forces to generate plasma membrane protrusions and invaginations, however recent evidence suggest that many membrane-associated proteins directly sculpt and deform biological membranes (Doherty and McMahon, 2008). Here we report that srGAP2 regulates neuronal migration as well as neurite initiation and branching through the ability of its F-BAR domain to deform membranes and form filopodia-like membrane protrusions. This is a surprising finding since F-BAR domains have been mostly characterized for their ability to induce membrane invaginations (Frost et al., 2008; Habermann, 2004; Henne et al., 2007; Itoh and De Camilli, 2006; Peter et al., 2004; Shimada et al., 2007). How might we explain the ability of srGAP2's F-BAR domain to induce filopodia protrusion rather than membrane invagination/inward

tubulations? F-BAR domains are composed of a series of alpha-helices forming a strong dimerization motif, which allow the homodimers to adopt a quaternary 'banana-like' structure. Positively charged amino acids resident on the concave surface of the homodimer can interact with negatively charged phospholipids at the plasma membrane. Oligomerization and the inherent, concave curvature of the molecule are thought to regulate membrane curvature and induce membrane tubules of a fixed diameter *in vitro* and *in vivo* (Frost et al., 2008; Henne et al., 2007; Peter et al., 2004; Shimada et al., 2007). Therefore, one possibility for how srGAP2's F-BAR domain may cause filopodia-like protrusions is by having a different curvature as well as a different surface distribution of positively charged residues than canonical F-BAR domains. Indeed, the structurally related I-BAR domain present in proteins such as IRSp53 or MIM, form stable dimers and has the ability to deform lipid membranes just as F-BAR domains (Mattila et al., 2007; Saarikangas et al., 2009). However, the I-BAR homodimers form less curved, straighter structures instead of the typical curved 'banana-shaped' homodimers present in BAR, N-BAR and F-BAR domains (Scita et al., 2008). Interestingly, I-BAR domains are very potent inducers of filopodia (Lim et al., 2008; Mattila et al., 2007; Saarikangas et al., 2009; Suetsugu et al., 2006) and it is thought that this is due to the inherent curvature of the I-BAR homodimer. We hypothesize that the dimer formed by the F-BAR domain of srGAP2 displays a general quaternary structure and charge distribution comparable to I-BAR domains. While this can only be proven by structural information, we provide several lines of evidence supporting an I-BAR like behavior: (1) we show that like I-BAR induced filopodia, those induced by the F-BAR domain of srGAP2 are resistant to F-actin depolymerization, (2) we show that unlike other F-BAR domains of FPB17 and CIP4, over-expression of the F-BAR domain of srGAP2 does not inhibit endocytosis, (3) we show that the F-BAR domain of srGAP2 induces similar liposome deformations compared to IRSp53 (Suetsugu et al., 2006), (4) finally, we show

that exposure of the F-BAR to the inner surface of liposomes resulted in protrusive tubes which would be expected if it were behaving like an I-BAR.

How could srGAP2 achieve this alternative membrane curvature i.e. membrane protrusion instead of membrane invagination? The F-BAR domain of srGAP2 appears to be larger than canonical F-BAR domains (**Fig. 2.18**). In order to achieve stable expression we had to express a large portion of the c-terminal extension that goes beyond the region of highest structural homology to 'classical' F-BAR domain of FBP17 or CIP4 (approx. aa 1-350; Itoh et al. 2005), which adds an additional 150 amino acids which are predicted to contain 3 alpha helices (**Fig. 2.18**). This additional sequence could have significant structural consequences on protein folding and therefore on the type of curvature induced by the F-BAR domain.

Recently, it was shown that the PX-BAR of Sorting Nexin 9 domain could adopt different curvatures compared to the full length molecule suggesting that additional sequences could indeed affect the size of membrane tubules (Wang et al., 2008). In order to determine exactly how srGAP2's F-BAR domain induces membrane curvature, future studies will have to focus on characterizing the structure of this F-BAR domain with atomic resolution. Ideally, we would like to crystallize both full-length srGAP2 and its F-BAR domain alone. In the short-term, we might gather some useful information by using small angle x-ray scattering (SAXS) to elucidate differences in the conformation of the F-BAR domain and full-length protein in solution (see for example (Wang et al., 2008)).

Interestingly, the F-BAR domain of srGAP2 is not the only F-BAR-containing protein inducing filopodia formation. Gas7 and PSTPIP2 (MAYP) have also been predicted to contain a F-BAR domain (combination of a FCH domain and a coiled-coil domain) and have been shown to induce filopodia (Chitu et al., 2005; She et al., 2002). Both proteins have also been shown to associate with F-actin suggesting that part of srGAP2's effects could be due

to F-actin binding/bundling. However, these proteins and more importantly their predicted F-BAR domains have not been directly tested for their ability to deform membranes.

Our data and data cited above suggest that F-BAR domains could be functionally diverse and that this functional diversity regarding the type of membrane deformation properties they display might be due to small structural differences. As described previously, the F-BAR domain of srGAP2 is larger than the canonical F-BAR domains. We found that the additional 150 amino acids of srGAP2 are predicted to form three distinct alpha helices (α6-8). The structural alignments of this region demonstrate homology to F-actin binding proteins including Talin and myosin, suggesting that srGAP2 may indeed contain an actin-binding site. Future experiments using structure function analysis to determine the role of these additional structures will help us to understand how the F-BAR domain induces filopodia in cells.

While I-BAR's have been shown to induce filopodia for sometime, there is no mechanism as to how filopodia induced by I-BARs or the F-BAR domain of srGAP2. One intriguing possibility may be the effect of small, local membrane curvature on the barbed end of F-actin. The dendritic nucleation model suggests that actin filament barbed ends are juxaoposed to the plasma membrane (Pollard and Borisy, 2003). Through Brownian motion the filaments detach from the membrane exposing their barbed ends (presumably losing capping protein as well). This exposes the barbed end and actin monomer might be added facilitating actin polymerization. I propose that the role of I-BARs and F-BARs like srGAP2 might be to create space in between F-actin and the plasma membrane through their ability to deform membranes. This should result in a net increase in free barbed ends and should result in actin polymerizaiton. Moreover, these proteins could then bundle F-actin (I-BARs and the F-BAR, MAYP are thought to have bundling activity (Aspenstrom et al., 2006; Scita et al., 2008)) and simultaneously bind the membrane as the protrusion forms. It will be

interesting to see if local changes in membrane curvature are sufficient to induce actin polymerization. Of course, many F-BAR and I-BAR containing proteins contain SH3 domains that have been shown to interact with WASP and WAVE-1, regulators of Arp2/3 and formins (Chan et al., 1996; Linkermann et al., 2009; Soderling et al., 2002), so not only could they bundle and facilitate actin polymerization through the increase of free barbed ends, but in the case of formins, they could recruit proteins that facilitate this.

The role of srGAP2 during cortical development

Neurite outgrowth is key property of developing neurons since it is required for the formation of the leading process that guides migrating neurons to their proper location as well for the morphogenesis of dendrites and axons that determine brain circuitry. We demonstrate here that srGAP2 is a novel promoter of neurite initiation and branching and that this property plays a negative role in the regulation of neuronal migration. This activity seems to be dependent on the ability of the F-BAR domain to induce filopodia-like membrane protrusions. It is well established that filopodia promote neurite outgrowth and it was recently shown that filopodia were required for neurite initiation in cortical neurons (Dent et al., 2007). However, knockdown of srGAP2 did not affect neurite initiation but reduced both axon and dendrite branching, processes known to require filopodia formation. The absence of an effect of srGAP2 knockdown on neurite initiation is likely due to the presence of many other proteins involved in filopodia formation; I-BAR-containing proteins such as IRSp53 or ABBA (Mattila et al., 2007; Saarikangas et al., 2008) or other classes of proteins that promote filopodia formation and neurite initiation through distinct mechanisms such as the ENA/VASP proteins. It was recently shown that MENA/Evl/VASP proteins are required for neurite initiation in cortical neurons (Dent et al., 2007; Kwiatkowski et al., 2007).

These proteins are still present in our assays and therefore could support filopodia formation in the absence of srGAP2. In support of this idea, Dent et al. demonstrated that while MENA/Evl/VASP triple knockout neurons plated on poly-L-lysine were unable to form neurites, plating on laminin or expression of other inducers of filopodia (such as formins) could support neurite formation even in the absence of ENA/VASP proteins (Dent et al., 2007). This suggests that neurons possess several alternative pathways for filopodia formation and neurite initiation. We have recently obtained gene trapped mouse for srGAP2 in which b-gal fusion has been knocked into intron 2, disrupting the srGAP2 gene. This genetic loss of function of srGAP2 may allow us to observe early defects in polarity caused by this disruption. The lack of a phenotype on neurite intitiation after srGAP2 may also be due to compensation by other srGAPs. SrGAP3 in particular, is expressed in the ventricular zone at E15 just as srGAP2. Moreover, srGAP3 was first identified as a Rac1 GAP and its down regulation has been shown to increase cell migration. It will be interesting to observe the effects of knockdown of both srGAP2 and srGAP3 to see if this sufficient to block neurite initiation.

The ability of srGAP2 to promote neurite initiation and branching appears to also be important for its regulation of migration (**Fig. 2.18B**). Knockdown of srGAP2 increased the percentage of migrating neurons as well as the overall rate of migration and significantly reduced leading process complexity and branching (**Fig. 2.18B**). This could potentially explain the increase in the rate of cell migration since it has been shown in fibroblast, reduction of ENA/VASP proteins activity (i.e. proteins that promote filopodia formation) increased lamellipodia persistence and increased cell speed (Bear et al., 2000; Bear et al., 2002). In addition, it was recently shown that loss of ENA/VASP proteins in cortical neurons lead to more superficial laminar position, which could be an effect of increased migration (Goh et al., 2002; Kwiatkowski et al., 2007). Therefore decreased branching in srGAP2

knockdown neurons may support increased leading process persistence and increased migration. Finally, in recent work, Simpson et. al, used an siRNA screen to identify genes that regulate cancer cell migration (Simpson et al., 2008). Interestingly, downregulation of the srGAP2 homolog, srGAP3 was also associated with an increased rate of cell migration suggesting that negative regulation of cell migration may be a conserved function of the srGAP family.

Conversely, we show that expression of srGAP2 strongly inhibited migration by producing excessive neurite protrusions. Importantly, these effects are mediated by the membrane deformation properties of the F-BAR domain since expression of F-BAR$^{\Delta 49}$, which can target to the membrane but cannot induce filopodia-like membrane protrusions had no effect on cell migration or leading process branching. Excessive leading process branching has previously been associated with defects in neuronal migration. Loss of p35, the activator of CDK5, was shown to induce significant LP branching leading to impaired migration (Gupta et al., 2003). The authors interpreted this impairment of migration as an effect of leading process branching causing radial glia-independent migration. While we have not observed any change in the interaction between migrating neurons and the radial glia scaffold (data not shown), it would be interesting to test for any functional interactions between the CDK5 pathway and srGAP2. In addition these studies may highlight a role for leading process branching in regulating the timing in which cortical neurons reach their proper cortical layer. It appears that the timing of migration is important for proper radial migration since reduction of FILIP, which regulates the level of Filamin protein expession, caused increase in radially oriented processes. This suggests that Filamin levels are kept low until migration needs to be initiated (Nagano et al., 2004).

Regulation of srGAP2: GAP and SH3 domains

The BAR superfamily of proteins are involved in a wide range of functions and this diversity arises from the different functional domains associated with BAR-like domain (Itoh and De Camilli, 2006). srGAP2 is an F-BAR domain containing protein that contains a GAP domain as well as an SH3 domain. We demonstrate that srGAP2 is a Rac1-specific GAP and much recent work has highlighted the importance of Rac1 regulation in neuronal development (Govek et al., 2005). Mutation of the Rac1/Cdc42 GEF, ARHGEF6 (also called Cool-2, α-pix) results in X-linked mental retardation suggesting the importance of properly regulating Rac1 activity during neuronal development (Kutsche et al., 2000). Interestingly, the BAR domain containing protein oligophrenin-1 as well as the F-BAR containing protein srGAP3 (also called MEntal retardation GAP or MEGAP), are both Rac1-GAPs and have been involved in severe forms of mental retardation (Billuart et al., 1998; Endris et al., 2002; Govek et al., 2004).

Not surprisingly, Rac1 has also been implicated in regulating radial migration. Inhibition of Rac1 downstream of both phosphoinositide 3 kinase (PI3K) and c-jun N-terminal kinase (JNK) blocked radial migration (Kawauchi et al., 2003; Konno et al., 2005). Moreover, the Rac GEF, P-Rex1 was also shown to be involved in radial migration (Yoshizawa et al., 2005). These data suggests the importance of small GTPase signaling, particularly Rac1, in fine-tuning radial migration. Surprisingly, the GAP activity seemed to be largely dispensable for srGAP2's ability to promote filopodia formation and neurite outgrowth. The fact that protrusions remain even in when there is no GAP activity does not suggest that the GAP activity is not involved in protrusion formation but rather suggests that the presence of the F-BAR domain is sufficient to induce protrusions. The GAP domain may not be required for filopodia-like protrusion formation but may help modify the environment for this to occur. Indeed, recent work has demonstrated that Rac1 down regulation increased filopodia

formation in neuronal growth cones (Rajnicek et al., 2006). Therefore the GAP domain of srGAP2 could participate in filopodia formation in two ways: (1) local inactivation of Rac1 could result increased Cdc42 activity. Cdc42 could in turn activate pathways that promote bundled F-actin which are required for filopodia formation (Raftopoulou and Hall, 2004); (2) Alternatively, Rac1 inactivation could lead to increased activation of RhoA (since Rac1 activation has been shown to inactivate RhoA (Nimnual et al., 2003; Rajnicek et al., 2006), which in turn could lead to the activation of the formin, mDia2. mDia2 could then lead to actin nucleation. In either case the Rac GAP activity would result in growth of bundled F-actin that is funneled into membrane protrusions deformed by the F-BAR domain (Fig. 2.18A). This could be an important modulatory mechanism for regulating F-BAR mediated protrusion. Since Rac1 activation is known to be required for proper radial migration and neurite outgrowth (Causeret et al., 2008; Govek et al., 2005; Kawauchi et al., 2003; Yoshizawa et al., 2005), one way Rac1 might regulate neuronal migration and neurite outgrowth might be to regulate how efficiently srGAP2 promotes filopodia formation.

One striking feature of F-BAR domain-containing proteins is that a significant number also possess SH3 domains (Itoh and De Camilli, 2006). These SH3 domains bind a myriad of effectors from regulators of endocytosis (Itoh and De Camilli, 2006) and regulators of the actin cytoskeleton (Aspenstrom et al., 2006; Chitu and Stanley, 2007) to cell surface receptors (Wong et al., 2001). The SH3 domain of srGAP2 has been shown to bind the Robo1 receptor (Wong et al., 2001) and has also been shown to bind N-WASP (Linkermann et al., 2009), but the functional relevance of these interactions has yet to be determined. We show that abrogating the effector binding property of the SH3 domain severely reduces the ability of srGAP2 to induce membrane protrusions and inhibit migration. In fact, of the constructs that contain an F-BAR domain, it is the only one that did not promote protrusions (**Fig. 2.11E-J**). This suggested the possibility that srGAP2 is auto-inhibited as resting state

and in this conformation the F-BAR domain might be inhibited. Indeed, deletion of the C-terminal end of srGAP2 (including the SH3 domain) restored the ability of F-BAR domain to promote filopodia-like protrusions, neurite initiation and branching and to inhibit neuronal migration, supporting the idea that the F-BAR domain of srGAP2 may be inhibited by the C-terminal domain of srGAP2. It was recently shown that the BAR domain containing proteins GRAF and oligophrenin-1 existed in an auto-inhibited state (Eberth et al., 2009) suggesting that other BAR domain-containing proteins may share a similar mechanism of activation. We propose that srGAP2 exists in an autoinhibited state where the c-terminus of srGAP2 interacts with the N-terminal F-BAR domain. This interaction could be mediated by 2 patches negatively-charged residues that flank the SH3 domain (data not shown), which would allow the c-terminus to interact with positively charged residues in the F-BAR domain. The inhibition could then be released by effector binding to the SH3 domain exposing the F-BAR and GAP domains to facilitate membrane protrusion (**Fig. 2.18A**). Future experiments will test this model and determine the type of structural and functional interactions underlying the cooperativity between the three main functional domains of srGAP2 and how these interactions influence srGAP2 function during neuronal migration and morphogenesis.

Future Directions

This thesis presents the novel observation that srGAP2 regulates neuronal migration and morphogenesis through the ability of its F-BAR domain to cause membrane protrusions. Several of these findings presented in this study will be interesting to pursue:

1- The ability of the F-BAR domain to induce filopodia. Future studies will be aimed at determining the crystal structure of srGAP2 and identifying the molecular

mechanisms underlying its ability to induce filopodia including the potential interaction of the F-BAR domain with actin.

2- srGAP2 regulates filopodia formation and neurite initiation/branching in cortical neurons. We would like to explore the signaling pathways that mediate neurite initiation/branching upstream of srGAP2.

3- srGAP2 as a regulator of radial migration in the cortex. Determining the signaling pathways that regulate srGAP2 activity may prove very useful to understand how radial migration is regulated. Recently, Semaphorin 3A was shown to act as a chemoattractive cue for radial migration (Chen et al., 2008) it would be interesting to see if this pathway may act to modulate srGAP2 activity during radial migration.

srGAP2 may be regulated by autoinhibition. We would like to test this model by mutational analysis to residues flanking the SH3 domain. This model is intriguing in part because the SH3 domains of the srGAP family have been shown to associate with regulators of the actin cytoskeleton such as WAVE-1 and N-WASP, suggesting that srGAP2 activity could be regulated by molecules that ultimately cooperate with the F-BAR domain to mediate membrane protrusion.

Chapter 4: General Methods

MATERIAL AND METHODS

Animals

Mice were used according to a protocol approved by the Institutional Animal Care and Use Committee (IACUC) at the University of North Carolina-Chapel Hill and in accordance with NIH guidelines. Time-pregnant females were maintained in a 12 hr light/dark cycle and obtained by overnight breeding with males of the same strain. Noon following breeding is considered as E0.5.

Histochemistry and In situ hybridization

In situ hybridization was done as previously described (Mattar et al., 2004)

Dissociated cortical neuron culture

Cultured neurons and brain sections were stained as described previously (Ghosh and Polleux 2002). The following antibodies were used chicken anti-GFP (Upstate), mouse anti-Tuj1 (β-III tubulin) (Sigma), mouse anti-nestin (BD Bioscience), mouse anti-MAP2 (a/b isoforms) Clone AP20 (Sigma), rabbit anti-srGAP2 (Gift of Gong Ju, Shanghai JiaoTong University), and F-actin was labeled using alexa-546 phalloidin (Sigma). All images were captured using a LEICA TCS SL confocal microscope. For staining of endogenous srGAP2 in acutely dissociated neurons, cells were fixed in 4% paraformaldehyde for 30 minutes. The cells were then washed with PBS three times. They were then permeabilized with .05% triton-x 100 for 20 minutes and washed again in PBS. They were then incubated in blocking buffer (5% bovine serum albumin (BSA) in PBS) for 30 minutes and incubated with srGAP2-A2 antibody (1:200 in .2% BSA in PBS) overnight. For F-actin staining, phalloidin was added at 1:200. Cells were subsequently washed in .2% BSA in PBS and the appropriate alexa-

conjugated secondary antibodies (Molecular Probes) were used at 1:2000 in .2% BSA in PBS for 30 minutes. Cells were then washed and slides were mounted.

Sequence Alignments

Sequence alignments for srGAPs were obtained using MUSCLE (Edgar, 2004). Human srGAP2 (gi|48427907|sp|O75044.2) Mouse srGAP2 (image:BC030547), Human srGAP1 (NP_065813.1), Mouse srGAP1 (NP_001074506.1), Human srGAP3 (NP_055665.1), Mouse srGAP3 (NP_536696.4), Xenopus srGAP (NP_001087899.1), C.elegans (NP_502179.1). Secondary structure was obtained for srGAP2 using hhpred (Soding et al., 2005) (http://toolkit.tuebingen.mpg.de/hhpred), Bioinfobank Metaserver (http://meta.bioinfo.pl) and PromaS3D (Pei et al., 2008) (http://prodata.swmed.edu/promals3d/promals3d.php). Structural alignments srGAP2 and F-BAR domains were obtained using hhpred (Soding et al., 2005) Bioinfobank Metaserver and PromalS3D (Pei et al., 2008). Mouse FBP17 (NP_062279.1), Mouse Syndapin1 (CAQ52060.1), Mouse FCHO2 (NP_766179.1), Mouse PSTPIP2 (CAJ18516.1), Mouse Fer (AAB18988.1)

Constructs

All constructs were cloned into pCIG2 vector (Hand et al., 2005), which contains a (cDNA)-IRES-EGFP under the control of a CMV-enhancer/chicken-®β-actin promoter. srGAP2 (IMAGE clone# BC030457) was first mutagenized using Quickchange (Stratagene) to repair a point mutation at position 596 to avoid premature stop in transcription. srGAP2 was then subcloned into pEGFP-N1 (Clontech). The entire srGAP2-EGFP cassette was then subcloned into pCIG2 replacing the IRES-EGFP resulting in pCIG2::srGAP2-EGFP. srGAP2 was also cloned into pNeuroD-EGFP vector. All subsequent constructs were cloned

similarly. F-BAR (aa1-501), srGAP2$^{\otimes\delta F\text{-}BAR}$ (aa502-1045), srGAP2^{R527L}, srGAP2^{W765A}, srGAP2$^{\otimes\delta C\text{-}term}$, and srGAP2* (dha5 shRNA resistant, base pairs mutation T898C, A900G, and C904T) were generated by mutagenesis using Quickchange (Stratagene). F-BAR$^{\otimes\delta 49}$ was generated by fusing amino acids (1-452) of human srGAP2 (accession number NM_015326) to the c-terminus of clone BC112927. This clone is a partial human duplication of the F-BAR of srGAP2 present in Chromosome 1p12 and encoding only the first nine exons (out of twenty-two in the original full length human srGAP2 (Sassa and Polleux, unpublished results). The first nine exons present in the 1p12 duplication encode for the F-BAR with the last 49 amino acids of the C-terminus are deleted, hence the name F-BAR$^{\otimes\delta 49}$ due to a splicing defect (Sassa and Polleux, unpublished results). This splicing defect also results in the addition of seven additional amino acids to the deleted C-terminus that are not normally present in the F-BAR of srGAP2, as they arise from intronic sequence.

COS7 cell culture, transfections, staining and filopodia measurements

COS7 cells were cultured in DMEM + 10%FBS 2mM L-glutamine and penicillin/streptomycin. For transfections, cells were plated in 6 well dishes and lipofectamine 2000 (4microL) was mixed with 2micrograms of DNA in Opti-mem and added to cells for 3hrs. After 3hrs, serum-free media was replaces with DMEM + 10%FBS and cells were cultured for 24hrs. After 24hrs, cells were trypsanized and replated on poly-l-lysine coated coverslips and cultured for an additional 24hrs. Cells were then fixed using 4% paraformaldehyde. Cells were then washed 3 times in PBS, then blocked/permeablized in .3% triton-X 100 in PBS + 5% BSA (PBS-T) for 20 minutes. Cells were then incubated with alexa-546 phalloidin (1:200) in PBS-T overnight. Finally, cells were then washed 3 times in PBS-T and mounted.

To determine filopodia number, cells were imaged using LEICA TCS SL confocal microscope, 63x/1.4NA oil immersion objective. 2x zoomed images were taken of representative cells from each construct. Images were then imported to NIH ImageJ. Using the segmented line tool, a perimeter was drawn around the cells. The presence of filopodia was determined by counting the number of consecutive pixels on the line drawn around the cell perimeter and normalized by dividing the total number of filopodia by the cell perimeter (filopodia/microns).

For cytochalasin-D treatments, COS7 cells were transfected with F-BAR-EGFP and cultured for 48hrs. Cells were then treated with ã□□ cytochalasin D for 30 minutes. To observe the presence of F-actin, cells were fixed and stained with phalloidin. To observe dynamics, control, untreated cells were imaged for 10 minutes (picture taken every 10 seconds) and cytochalasin-D treated cells were imaged for 27 minutes (picture taken every minute).

For transferring uptake assay, COS7 cells were serum starved for one hour at 4 degrees in the presence of alexa-647 transferrin. Cells were then warmed to 37 degrees to allow uptake of transferrin and fixed and treated as described above.

Protein purification

srGAP2 (amino acids 1-785) and the F-BAR (amino acids 22-501) were cloned into pLIC vectors and expressed in *Escherichia coli* BL21 (DE3) cells. Proteins were then purified on a Ni2+ affinity column. Proteins were further purified by cation exchange chromatography, using a Source S column, and concentrated in 20 mM Tris buffer, pH 8, 150 mM NaCl, 1 mM DTT and 5% glycerol. GAP (amino acids 502-676) and GAP^{R527L} domain of srGAP2 was cloned into pGex-4T3 (Amersham). Recombinant GST-fusion proteins were then purified using glutathione sepharose and resuspended in 20 mM Tris buffer, pH 8, 150 mM NaCl, 1

mM DTT and 5% glycerol.

In vitro GAP assay

In vitro fluorescent-based GAP assay was performed as described previously (Shutes and Der, 2006).

Liposome Preparation

Folch Fraction I Brain Lipid Extract from bovine brain (B1502) in chloroform was obtained from Sigma-Aldrich (St. Louis, MO) and used without further purification. 10 mg of total lipid were added to a glass vial and dried at room temperature under streaming argon while vortexing in order to form a thin lipid film around the tube surface. The lipids were re-dissolved in absolute hexane, dried under argon again while vortexing, and then dessicated *in vacuo* for >2 hours to remove the last traces of chloroform. The dried lipid film was then pre-hydrated at RT with water-saturated N2 for 2 minutes until the film became transparent. Buffer (50mM KCl/10mM/HEPES/1mM DTT, pH 7.4) was added to the hydrated lipid film to a final lipid concentration of 2 mg/ml. The vial was sealed under argon and incubated at RT for 2 h, and then gently rocked overnight to disperse the lipids into solution.

Liposome tubulation assays

The liposomes described above were first subjected to 10 cycles of freeze-thaw, and then used immediately or stored in aliquots at -80°C. The liposomes were then equilibrated at RT for 1 hour before adding protein (either FBP17 F-BAR domain or srGAP2 F-BAR) at a lipid-to-protein ratio of 2:1 mass/mass and final concentrations of 0.2 mg/ml (lipid) and 0.1 mg/ml (protein). The tubulation reaction incubated for 30 minutes at RT before negative staining, as described below. In order to introduce the recombinant purified F-BAR into the

liposomes, 250 μl of the tubulation reaction subjected to 5 seconds of bath sonication at RT, immediately after adding protein. Following sonication, the sample allowed to incubate for another 30 minutes before negative staining, as described below.

Electron Microscopy

Continuous carbon-coated Cu-grids were glow discharged in room air according to standard protocols. 4μL of sample were added and allowed to sit for ~10 seconds before being blotted onto filter paper. The grid surface was then immediately stained with freshly prepared (<15 minutes) 0.8% uranyl formate. Images were acquired using a Philips Tecnai F12 microscope operating at 120 kV using nominal magnifications of 29-50kx, and defocus values of –15,000 to –22,000 Å. Images were recorded on a Gatan 1K CCD. Image analysis, including tubule diameter measurements, were performed with NIH ImageJ.

shRNA design and validation

shRNA sequences were obtained from Dharmacon Dha2 Sense (5'- GAT CCA ATG GAC TAC TCT CGA AAC TTC AAG AGA GTT TCG AGA GTA GTC CAT TTC TTT TTT GGA AA-3') Dha2 Anti-sense (AGC TTT TCC AAA AAA GAA ATG GAC TAC TCT CGA AAC TCT CTT GAA GTT TCG AGA GTA GTC CAT TG) and Dha5 Sense (5'- GAT CCG CTA TCT GCT GAA TTA AAT CTT CAA GAG AGA TTT AAT TCA GCA GAT AGG ATT TTT TGG AAA-3') Dha5 Anti-sense (AGC TTT TCC AAA AAA TCC TAT CTG CTG AAT TAA ATC TCT CTT GAA GAT TTA ATT CAG CAG ATA GCG). These constructs were cloned into psilencer 2.1 (ambion). These shRNA were subsequently cotransfected with srGAP2-EGFP into COS7 cells ((shRNA 1.5μg) and srGAP2-EGFP (.5μg)). Lysates were collected 48hrs. After transfection and level of knockdown was determined by western blot using rabbit □-GFP (Molecular Probes)

Ex Vivo Cortical Electroporation and Primary Cultures

Mouse cortical progenitors were electroporated *ex vivo* at embryonic day (E) E15 as described (Hand et al., 2005). Briefly, cDNA constructs in overexpression experiments (2μg/μl) were injected into the lateral ventricle of each embryo and electroporated using an ECM 830 electroporator (BTX) with four 100 ms pulses separated by 100 ms intervals at 20 V. Following electroporation, cerebral cortices were dissected and enzymatically dissociated as described previously (Polleux and Ghosh, 2002) $1.25x10^5$ cells were plated onto glass coverslips coated with poly-L-lysine and laminin and cultured in serum-free media (Basal Medium Eagle containing both B27 and N2 supplements, L-Glutamine and Penicillin/Streptomycin) and fixed in 4% paraformaldehyde for immunohistochemistry. For shRNA rescue experiments in dissociation a mixture (shRNA 1.5μg/μl) and srGAP2-EGFP* (0.5μg/μl) was injected into lateral ventricle. For slice cultures, embryonic brains were electroporated and dissected as described above. The brains were then embedded in 3% low temperature gelling agarose and 250 μm-thick vibratome sections were cut using a LEICA VT1000S vibratome and placed on poly-L-lysine/laminin coated transwell inserts and cultured organotypically using an air interface protocol (Polleux and Ghosh, 2002). ShRNA expressing sections were cultured for 3 days in vitro and cDNA expressing sections were cultured for 5 days in vitro.

Time Lapse confocal microscopy of cortical sections

Using a Leica TCS-SL confocal microscope (mounted on a DM-IRE2 inverted microscope stand) and equipped with a X-Y motorized Märzhäuser stage, time-lapse confocal microscopy was performed by imaging multiple Z-stacks at different positions on a given set of electroporated slices (using X-Y motorized stage) at a specific frequency for each

experiment. Slices were cultured on confocal inserts (Millipore) and imaged using a long distance 20x/0.4 NA objective. For shRNA expressing sections, pictures were taken repetitively at a frequency of 1 picture every 12 minutes for 4hrs. In the case of srGAP2 over-expression experiments, sections were imaged every 16 minutes for a maximum of 10hrs 24 minutes. Slight drifts of the slices were corrected using an image registration tool developed in ImageJ (Turboregand Stackreg- P. Thévenaz- Univ. Lausanne).

Quantification of neuron migration and neurite branching.

For shRNA treated slices, the extent of cell migration was analyzed as described previously (Hand et al., 2005). In cDNA expressing sections, migration was assayed in 3 different ways: (1) high magnification pictures were taken of the cortical plate and IZ and we quantified the ratio of cells/□m^2 CP/ cells/μm^2 in the IZ. (2) For branching measurements, high magnification images were obtained of neurons migrating in layer 5/6 in various conditions. Number of branches protruding from the leading process were then counted. (3) We measured the percentage of cells in the IZ (defined by Draq5 staining) with $\geq$3 neurites over the total number of GFP+ in the IZ to determine the percentage of cells that did not migrate because they could not make a single leading process (i.e. multipolar). For cell speed measurements in shRNA treated slices, nuclei position was tracked manually during each frame using NIH ImageJ. Cell speed was calculated using Microsoft Excel and speed was reported in □icron/hr. Neurite branching was quantified using NIH ImageJ.

ACKNOWLEDGMENTS

We thank the members of the Polleux and Bear labs for helpful comments. We thank Schumman lab (Pierre Mattar) for in situ hybridization and original srGAP2 cDNA. We thank Gong Ju and Wei-Lin Jin for the srGAP2 antibody. We thank the Sondek (Rafael Rojas) and

Der (Adam Shutes) labs for technical assistance with protein purification and fluorescent GTP hydrolysis assay. We thank Brenda Temple for technical assistance with protein modeling and sequence analysis. We thank Vinzenz Unger, Carsten Mim and Pietro De Camilli for helpful discussions. This work was supported by a Pre-doctoral Research Training Fellowship from the Epilepsy Foundation (AF) and a NIH MSTP award TG 5T32GM07205 (AF), a NIH Predoctoral Fellowship 5F31NS052969-03 (SG), UNC Developmental Biology Training Grant (T32 HD046369) (JCB) and a Pew Scholar award in Biomedical Sciences (FP) and the NINDS Institutional Center Core Grant to Support Neuroscience Research (P30 NS45892-01) (FP).

REFERNCES

Aspenstrom, P., Fransson, A., and Richnau, N. (2006). Pombe Cdc15 homology proteins: regulators of membrane dynamics and the actin cytoskeleton. Trends Biochem Sci *31*, 670-679.

Ayala, R., Shu, T., and Tsai, L.H. (2007). Trekking across the brain: the journey of neuronal migration. Cell *128*, 29-43.

Bai, J., Ramos, R.L., Ackman, J.B., Thomas, A.M., Lee, R.V., and LoTurco, J.J. (2003). RNAi reveals doublecortin is required for radial migration in rat neocortex. Nat Neurosci *6*, 1277-1283.

Bear, J.E., Loureiro, J.J., Libova, I., Fassler, R., Wehland, J., and Gertler, F.B. (2000). Negative regulation of fibroblast motility by Ena/VASP proteins. Cell *101*, 717-728.

Bear, J.E., Svitkina, T.M., Krause, M., Schafer, D.A., Loureiro, J.J., Strasser, G.A., Maly, I.V., Chaga, O.Y., Cooper, J.A., Borisy, G.G.*, et al.* (2002). Antagonism between Ena/VASP proteins and actin filament capping regulates fibroblast motility. Cell *109*, 509-521.

Bellenchi, G.C., Gurniak, C.B., Perlas, E., Middei, S., Ammassari-Teule, M., and Witke, W. (2007). N-cofilin is associated with neuronal migration disorders and cell cycle control in the cerebral cortex. Genes Dev *21*, 2347-2357.

Benhayon, D., Magdaleno, S., and Curran, T. (2003). Binding of purified Reelin to ApoER2 and VLDLR mediates tyrosine phosphorylation of Disabled-1. Brain Res Mol Brain Res *112*, 33-45.

Billuart, P., Bienvenu, T., Ronce, N., des Portes, V., Vinet, M.C., Zemni, R., Roest Crollius, H., Carrie, A., Fauchereau, F., Cherry, M.*, et al.* (1998). Oligophrenin-1 encodes a rhoGAP protein involved in X-linked mental retardation. Nature *392*, 923-926.

Burnette, D.T., Schaefer, A.W., Ji, L., Danuser, G., and Forscher, P. (2007). Filopodial actin bundles are not necessary for microtubule advance into the peripheral domain of Aplysia neuronal growth cones. Nat Cell Biol *9*, 1360-1369.

Cappello, S., Attardo, A., Wu, X., Iwasato, T., Itohara, S., Wilsch-Brauninger, M., Eilken, H.M., Rieger, M.A., Schroeder, T.T., Huttner, W.B.*, et al.* (2006). The Rho-GTPase cdc42 regulates neural progenitor fate at the apical surface. Nat Neurosci *9*, 1099-1107.

Caspi, M., Atlas, R., Kantor, A., Sapir, T., and Reiner, O. (2000). Interaction between LIS1 and doublecortin, two lissencephaly gene products. Hum Mol Genet *9*, 2205-2213.

Causeret, F., Terao, M., Jacobs, T., Nishimura, Y.V., Yanagawa, Y., Obata, K., Hoshino, M., and Nikolic, M. (2008). The p21-Activated Kinase Is Required for Neuronal Migration in the Cerebral Cortex. Cereb Cortex.

Chae, T., Kwon, Y.T., Bronson, R., Dikkes, P., Li, E., and Tsai, L.H. (1997). Mice lacking p35, a neuronal specific activator of Cdk5, display cortical lamination defects, seizures, and adult lethality. Neuron *18*, 29-42.

Chan, D.C., Bedford, M.T., and Leder, P. (1996). Formin binding proteins bear WWP/WW domains that bind proline-rich peptides and functionally resemble SH3 domains. EMBO J *15*, 1045-1054.

Chen, G., Sima, J., Jin, M., Wang, K.Y., Xue, X.J., Zheng, W., Ding, Y.Q., and Yuan, X.B. (2008). Semaphorin-3A guides radial migration of cortical neurons during development. Nat Neurosci *11*, 36-44.

Chen, L., Liao, G., Yang, L., Campbell, K., Nakafuku, M., Kuan, C.Y., and Zheng, Y. (2006). Cdc42 deficiency causes Sonic hedgehog-independent holoprosencephaly. Proc Natl Acad Sci U S A *103*, 16520-16525.

Chitu, V., Pixley, F.J., Macaluso, F., Larson, D.R., Condeelis, J., Yeung, Y.G., and Stanley, E.R. (2005). The PCH family member MAYP/PSTPIP2 directly regulates F-actin bundling and enhances filopodia formation and motility in macrophages. Mol Biol Cell *16*, 2947-2959.

Chitu, V., and Stanley, E.R. (2007). Pombe Cdc15 homology (PCH) proteins: coordinators of membrane-cytoskeletal interactions. Trends Cell Biol *17*, 145-156.

Costa, M.R., Wen, G., Lepier, A., Schroeder, T., and Gotz, M. (2008). Par-complex proteins promote proliferative progenitor divisions in the developing mouse cerebral cortex. Development *135*, 11-22.

Curran, T., and D'Arcangelo, G. (1998). Role of reelin in the control of brain development. Brain Res Brain Res Rev *26*, 285-294.

D'Arcangelo, G., Miao, G.G., Chen, S.C., Soares, H.D., Morgan, J.I., and Curran, T. (1995). A protein related to extracellular matrix proteins deleted in the mouse mutant reeler. Nature *374*, 719-723.

Dent, E.W., Barnes, A.M., Tang, F., and Kalil, K. (2004). Netrin-1 and semaphorin 3A promote or inhibit cortical axon branching, respectively, by reorganization of the cytoskeleton. J Neurosci *24*, 3002-3012.

Dent, E.W., Kwiatkowski, A.V., Mebane, L.M., Philippar, U., Barzik, M., Rubinson, D.A., Gupton, S., Van Veen, J.E., Furman, C., Zhang, J.*, et al.* (2007). Filopodia are required for cortical neurite initiation. Nat Cell Biol *9*, 1347-1359.

des Portes, V., Francis, F., Pinard, J.M., Desguerre, I., Moutard, M.L., Snoeck, I., Meiners, L.C., Capron, F., Cusmai, R., Ricci, S.*, et al.* (1998). doublecortin is the major gene causing X-linked subcortical laminar heterotopia (SCLH). Hum Mol Genet *7*, 1063-1070.

Di Cristo, G. (2007). Development of cortical GABAergic circuits and its implications for neurodevelopmental disorders. Clin Genet *72*, 1-8.

Doherty, G.J., and McMahon, H.T. (2008). Mediation, modulation, and consequences of membrane-cytoskeleton interactions. Annu Rev Biophys *37*, 65-95.

Dotti, C.G., Sullivan, C.A., and Banker, G.A. (1988). The establishment of polarity by hippocampal neurons in culture. J Neurosci *8*, 1454-1468.

Eberth, A., Lundmark, R., Gremer, L., Dvorsky, R., Koessmeier, K.T., McMahon, H.T., and Ahmadian, M.R. (2009). A BAR domain-mediated autoinhibitory mechanism for RhoGAPs of the GRAF family. Biochem J *417*, 371-377.

Endris, V., Wogatzky, B., Leimer, U., Bartsch, D., Zatyka, M., Latif, F., Maher, E.R., Tariverdian, G., Kirsch, S., Karch, D.*, et al.* (2002). The novel Rho-GTPase activating gene MEGAP/ srGAP3 has a putative role in severe mental retardation. Proc Natl Acad Sci U S A *99*, 11754-11759.

Fox, J.W., Lamperti, E.D., Eksioglu, Y.Z., Hong, S.E., Feng, Y., Graham, D.A., Scheffer, I.E., Dobyns, W.B., Hirsch, B.A., Radtke, R.A.*, et al.* (1998). Mutations in filamin 1 prevent migration of cerebral cortical neurons in human periventricular heterotopia. Neuron *21*, 1315-1325.

Francis, F., Koulakoff, A., Boucher, D., Chafey, P., Schaar, B., Vinet, M.C., Friocourt, G., McDonnell, N., Reiner, O., Kahn, A.*, et al.* (1999). Doublecortin is a developmentally regulated, microtubule-associated protein expressed in migrating and differentiating neurons. Neuron *23*, 247-256.

Frost, A., De Camilli, P., and Unger, V.M. (2007). F-BAR proteins join the BAR family fold. Structure *15*, 751-753.

Frost, A., Perera, R., Roux, A., Spasov, K., Destaing, O., Egelman, E.H., De Camilli, P., and Unger, V.M. (2008). Structural basis of membrane invagination by F-BAR domains. Cell *132*, 807-817.

Gallo, G., and Letourneau, P.C. (1998). Localized sources of neurotrophins initiate axon collateral sprouting. J Neurosci *18*, 5403-5414.

Gallo, G., and Letourneau, P.C. (2004). Regulation of growth cone actin filaments by guidance cues. J Neurobiol *58*, 92-102.

Ge, W., He, F., Kim, K.J., Blanchi, B., Coskun, V., Nguyen, L., Wu, X., Zhao, J., Heng, J.I., Martinowich, K.*, et al.* (2006). Coupling of cell migration with neurogenesis by proneural bHLH factors. Proc Natl Acad Sci U S A *103*, 1319-1324.

Gilmore, E.C., Ohshima, T., Goffinet, A.M., Kulkarni, A.B., and Herrup, K. (1998). Cyclin-dependent kinase 5-deficient mice demonstrate novel developmental arrest in cerebral cortex. J Neurosci *18*, 6370-6377.

Gleeson, J.G., Allen, K.M., Fox, J.W., Lamperti, E.D., Berkovic, S., Scheffer, I., Cooper, E.C., Dobyns, W.B., Minnerath, S.R., Ross, M.E.*, et al.* (1998). Doublecortin, a brain-specific gene mutated in human X-linked lissencephaly and double cortex syndrome, encodes a putative signaling protein. Cell *92*, 63-72.

Gleeson, J.G., Lin, P.T., Flanagan, L.A., and Walsh, C.A. (1999). Doublecortin is a microtubule-associated protein and is expressed widely by migrating neurons. Neuron *23*, 257-271.

Goh, K.L., Cai, L., Cepko, C.L., and Gertler, F.B. (2002). Ena/VASP proteins regulate cortical neuronal positioning. Curr Biol *12*, 565-569.

Govek, E.E., Newey, S.E., Akerman, C.J., Cross, J.R., Van der Veken, L., and Van Aelst, L. (2004). The X-linked mental retardation protein oligophrenin-1 is required for dendritic spine morphogenesis. Nat Neurosci *7*, 364-372.

Govek, E.E., Newey, S.E., and Van Aelst, L. (2005). The role of the Rho GTPases in neuronal development. Genes Dev *19*, 1-49.

Guerrini, R., and Marini, C. (2006). Genetic malformations of cortical development. Exp Brain Res *173*, 322-333.

Gupta, A., Sanada, K., Miyamoto, D.T., Rovelstad, S., Nadarajah, B., Pearlman, A.L., Brunstrom, J., and Tsai, L.H. (2003). Layering defect in p35 deficiency is linked to improper neuronal-glial interaction in radial migration. Nat Neurosci *6*, 1284-1291.

Gupta, A., Tsai, L.H., and Wynshaw-Boris, A. (2002). Life is a journey: a genetic look at neocortical development. Nat Rev Genet *3*, 342-355.

Gupton, S.L., and Gertler, F.B. (2007). Filopodia: the fingers that do the walking. Sci STKE *2007*, re5.

Habermann, B. (2004). The BAR-domain family of proteins: a case of bending and binding? EMBO Rep *5*, 250-255.

Hand, R., Bortone, D., Mattar, P., Nguyen, L., Heng, J.I., Guerrier, S., Boutt, E., Peters, E., Barnes, A.P., Parras, C.*, et al.* (2005). Phosphorylation of Neurogenin2 specifies the migration properties and the dendritic morphology of pyramidal neurons in the neocortex. Neuron *48*, 45-62.

Heng, J.I., Nguyen, L., Castro, D.S., Zimmer, C., Wildner, H., Armant, O., Skowronska-Krawczyk, D., Bedogni, F., Matter, J.M., Hevner, R.*, et al.* (2008). Neurogenin 2 controls cortical neuron migration through regulation of Rnd2. Nature.

Henne, W.M., Kent, H.M., Ford, M.G., Hegde, B.G., Daumke, O., Butler, P.J., Mittal, R., Langen, R., Evans, P.R., and McMahon, H.T. (2007). Structure and analysis of FCHo2 F-BAR domain: a dimerizing and membrane recruitment module that effects membrane curvature. Structure *15*, 839-852.

Hiesberger, T., Trommsdorff, M., Howell, B.W., Goffinet, A., Mumby, M.C., Cooper, J.A., and Herz, J. (1999). Direct binding of Reelin to VLDL receptor and ApoE receptor 2 induces tyrosine phosphorylation of disabled-1 and modulates tau phosphorylation. Neuron *24*, 481-489.

Horesh, D., Sapir, T., Francis, F., Wolf, S.G., Caspi, M., Elbaum, M., Chelly, J., and Reiner, O. (1999). Doublecortin, a stabilizer of microtubules. Hum Mol Genet *8*, 1599-1610.

Itoh, T., and De Camilli, P. (2006). BAR, F-BAR (EFC) and ENTH/ANTH domains in the regulation of membrane-cytosol interfaces and membrane curvature. Biochim Biophys Acta *1761*, 897-912.

Itoh, T., Erdmann, K.S., Roux, A., Habermann, B., Werner, H., and De Camilli, P. (2005). Dynamin and the actin cytoskeleton cooperatively regulate plasma membrane invagination by BAR and F-BAR proteins. Dev Cell *9*, 791-804.

Kakimoto, T., Katoh, H., and Negishi, M. (2006). Regulation of neuronal morphology by Toca-1, an F-BAR/EFC protein that induces plasma membrane invagination. J Biol Chem *281*, 29042-29053.

Kawauchi, T., Chihama, K., Nabeshima, Y., and Hoshino, M. (2003). The in vivo roles of STEF/Tiam1, Rac1 and JNK in cortical neuronal migration. EMBO J *22*, 4190-4201.

Kawauchi, T., Chihama, K., Nabeshima, Y., and Hoshino, M. (2006). Cdk5 phosphorylates and stabilizes p27kip1 contributing to actin organization and cortical neuronal migration. Nat Cell Biol *8*, 17-26.

Konno, D., Yoshimura, S., Hori, K., Maruoka, H., and Sobue, K. (2005). Involvement of the phosphatidylinositol 3-kinase/rac1 and cdc42 pathways in radial migration of cortical neurons. J Biol Chem *280*, 5082-5088.

Kutsche, K., Yntema, H., Brandt, A., Jantke, I., Nothwang, H.G., Orth, U., Boavida, M.G., David, D., Chelly, J., Fryns, J.P.*, et al.* (2000). Mutations in ARHGEF6, encoding a guanine nucleotide exchange factor for Rho GTPases, in patients with X-linked mental retardation. Nat Genet *26*, 247-250.

Kwiatkowski, A.V., Rubinson, D.A., Dent, E.W., Edward van Veen, J., Leslie, J.D., Zhang, J., Mebane, L.M., Philippar, U., Pinheiro, E.M., Burds, A.A.*, et al.* (2007). Ena/VASP Is Required for neuritogenesis in the developing cortex. Neuron *56*, 441-455.

Lambert de Rouvroit, C., and Goffinet, A.M. (2001). Neuronal migration. Mech Dev *105*, 47-56.

Lew, J., Huang, Q.Q., Qi, Z., Winkfein, R.J., Aebersold, R., Hunt, T., and Wang, J.H. (1994). A brain-specific activator of cyclin-dependent kinase 5. Nature *371*, 423-426.

Li, X., Chen, Y., Liu, Y., Gao, J., Gao, F., Bartlam, M., Wu, J.Y., and Rao, Z. (2006). Structural basis of Robo proline-rich motif recognition by the srGAP1 Src homology 3 domain in the Slit-Robo signaling pathway. J Biol Chem *281*, 28430-28437.

Lim, K.B., Bu, W., Goh, W.I., Koh, E., Ong, S.H., Pawson, T., Sudhaharan, T., and Ahmed, S. (2008). The Cdc42 effector IRSp53 generates filopodia by coupling membrane protrusion with actin dynamics. J Biol Chem *283*, 20454-20472.

Linkermann, A., Gelhaus, C., Lettau, M., Qian, J., Kabelitz, D., and Janssen, O. (2009). Identification of interaction partners for individual SH3 domains of Fas ligand associated members of the PCH protein family in T lymphocytes. Biochim Biophys Acta *1794*, 168-176.

Luo, L. (2002). Actin cytoskeleton regulation in neuronal morphogenesis and structural plasticity. Annu Rev Cell Dev Biol *18*, 601-635.

Magdaleno, S., Keshvara, L., and Curran, T. (2002). Rescue of ataxia and preplate splitting by ectopic expression of Reelin in reeler mice. Neuron *33*, 573-586.

Mattar, P., Britz, O., Johannes, C., Nieto, M., Ma, L., Rebeyka, A., Klenin, N., Polleux, F., Guillemot, F., and Schuurmans, C. (2004). A screen for downstream effectors of Neurogenin2 in the embryonic neocortex. Dev Biol *273*, 373-389.

Mattila, P.K., and Lappalainen, P. (2008). Filopodia: molecular architecture and cellular functions. Nat Rev Mol Cell Biol *9*, 446-454.

Mattila, P.K., Pykalainen, A., Saarikangas, J., Paavilainen, V.O., Vihinen, H., Jokitalo, E., and Lappalainen, P. (2007). Missing-in-metastasis and IRSp53 deform PI(4,5)P2-rich membranes by an inverse BAR domain-like mechanism. J Cell Biol *176*, 953-964.

Mitin, N., Betts, L., Yohe, M.E., Der, C.J., Sondek, J., and Rossman, K.L. (2007). Release of autoinhibition of ASEF by APC leads to CDC42 activation and tumor suppression. Nat Struct Mol Biol *14*, 814-823.

Moon, S.Y., and Zheng, Y. (2003). Rho GTPase-activating proteins in cell regulation. Trends Cell Biol *13*, 13-22.

Nagano, T., Morikubo, S., and Sato, M. (2004). Filamin A and FILIP (Filamin A-Interacting Protein) regulate cell polarity and motility in neocortical subventricular and intermediate zones during radial migration. J Neurosci *24*, 9648-9657.

Nagano, T., Yoneda, T., Hatanaka, Y., Kubota, C., Murakami, F., and Sato, M. (2002). Filamin A-interacting protein (FILIP) regulates cortical cell migration out of the ventricular zone. Nat Cell Biol *4*, 495-501.

Ng, J., Nardine, T., Harms, M., Tzu, J., Goldstein, A., Sun, Y., Dietzl, G., Dickson, B.J., and Luo, L. (2002). Rac GTPases control axon growth, guidance and branching. Nature *416*, 442-447.

Nguyen, L., Besson, A., Heng, J.I., Schuurmans, C., Teboul, L., Parras, C., Philpott, A., Roberts, J.M., and Guillemot, F. (2006a). p27kip1 independently promotes neuronal differentiation and migration in the cerebral cortex. Genes Dev *20*, 1511-1524.

Nguyen, L., Besson, A., Roberts, J.M., and Guillemot, F. (2006b). Coupling cell cycle exit, neuronal differentiation and migration in cortical neurogenesis. Cell Cycle *5*, 2314-2318.

Niethammer, M., Smith, D.S., Ayala, R., Peng, J., Ko, J., Lee, M.S., Morabito, M., and Tsai, L.H. (2000). NUDEL is a novel Cdk5 substrate that associates with LIS1 and cytoplasmic dynein. Neuron *28*, 697-711.

Nimnual, A.S., Taylor, L.J., and Bar-Sagi, D. (2003). Redox-dependent downregulation of Rho by Rac. Nat Cell Biol *5*, 236-241.

Noctor, S.C., Martinez-Cerdeno, V., Ivic, L., and Kriegstein, A.R. (2004). Cortical neurons arise in symmetric and asymmetric division zones and migrate through specific phases. Nat Neurosci *7*, 136-144.

Ohshima, T., Hirasawa, M., Tabata, H., Mutoh, T., Adachi, T., Suzuki, H., Saruta, K., Iwasato, T., Itohara, S., Hashimoto, M.*, et al.* (2007). Cdk5 is required for multipolar-to-bipolar transition during radial neuronal migration and proper dendrite development of pyramidal neurons in the cerebral cortex. Development *134*, 2273-2282.

Olson, E.C., Kim, S., and Walsh, C.A. (2006). Impaired neuronal positioning and dendritogenesis in the neocortex after cell-autonomous Dab1 suppression. J Neurosci *26*, 1767-1775.

Peter, B.J., Kent, H.M., Mills, I.G., Vallis, Y., Butler, P.J., Evans, P.R., and McMahon, H.T. (2004). BAR domains as sensors of membrane curvature: the amphiphysin BAR structure. Science *303*, 495-499.

Pollard, T.D., and Borisy, G.G. (2003). Cellular motility driven by assembly and disassembly of actin filaments. Cell *112*, 453-465.

Polleux, F., and Ghosh, A. (2002). The slice overlay assay: a versatile tool to study the influence of extracellular signals on neuronal development. Sci STKE *2002*, PL9.

Raftopoulou, M., and Hall, A. (2004). Cell migration: Rho GTPases lead the way. Dev Biol *265*, 23-32.

Rajnicek, A.M., Foubister, L.E., and McCaig, C.D. (2006). Growth cone steering by a physiological electric field requires dynamic microtubules, microfilaments and Rac-mediated filopodial asymmetry. J Cell Sci *119*, 1736-1745.

Reiner, O., Albrecht, U., Gordon, M., Chianese, K.A., Wong, C., Gal-Gerber, O., Sapir, T., Siracusa, L.D., Buchberg, A.M., Caskey, C.T.*, et al.* (1995). Lissencephaly gene (LIS1) expression in the CNS suggests a role in neuronal migration. J Neurosci *15*, 3730-3738.

Ridley, A.J., Schwartz, M.A., Burridge, K., Firtel, R.A., Ginsberg, M.H., Borisy, G., Parsons, J.T., and Horwitz, A.R. (2003). Cell migration: integrating signals from front to back. Science *302*, 1704-1709.

Saarikangas, J., Hakanen, J., Mattila, P.K., Grumet, M., Salminen, M., and Lappalainen, P. (2008). ABBA regulates plasma-membrane and actin dynamics to promote radial glia extension. J Cell Sci *121*, 1444-1454.

Saarikangas, J., Zhao, H., Pykalainen, A., Laurinmaki, P., Mattila, P.K., Kinnunen, P.K., Butcher, S.J., and Lappalainen, P. (2009). Molecular mechanisms of membrane deformation by I-BAR domain proteins. Curr Biol *19*, 95-107.

Scita, G., Confalonieri, S., Lappalainen, P., and Suetsugu, S. (2008). IRSp53: crossing the road of membrane and actin dynamics in the formation of membrane protrusions. Trends Cell Biol *18*, 52-60.

She, B.R., Liou, G.G., and Lin-Chao, S. (2002). Association of the growth-arrest-specific protein Gas7 with F-actin induces reorganization of microfilaments and promotes membrane outgrowth. Exp Cell Res *273*, 34-44.

Sheldon, M., Rice, D.S., D'Arcangelo, G., Yoneshima, H., Nakajima, K., Mikoshiba, K., Howell, B.W., Cooper, J.A., Goldowitz, D., and Curran, T. (1997). Scrambler and yotari disrupt the disabled gene and produce a reeler-like phenotype in mice. Nature *389*, 730-733.

Shimada, A., Niwa, H., Tsujita, K., Suetsugu, S., Nitta, K., Hanawa-Suetsugu, K., Akasaka, R., Nishino, Y., Toyama, M., Chen, L.*, et al.* (2007). Curved EFC/F-BAR-domain dimers are joined end to end into a filament for membrane invagination in endocytosis. Cell *129*, 761-772.

Shutes, A., and Der, C.J. (2006). Real-time in vitro measurement of intrinsic and Ras GAP-mediated GTP hydrolysis. Methods Enzymol *407*, 9-22.

Sigal, Y.J., Quintero, O.A., Cheney, R.E., and Morris, A.J. (2007). Cdc42 and ARP2/3-independent regulation of filopodia by an integral membrane lipid-phosphatase-related protein. J Cell Sci *120*, 340-352.

Simpson, K.J., Selfors, L.M., Bui, J., Reynolds, A., Leake, D., Khvorova, A., and Brugge, J.S. (2008). Identification of genes that regulate epithelial cell migration using an siRNA screening approach. Nat Cell Biol.

Soderling, S.H., Binns, K.L., Wayman, G.A., Davee, S.M., Ong, S.H., Pawson, T., and Scott, J.D. (2002). The WRP component of the WAVE-1 complex attenuates Rac-mediated signalling. Nat Cell Biol *4*, 970-975.

Stossel, T.P., Condeelis, J., Cooley, L., Hartwig, J.H., Noegel, A., Schleicher, M., and Shapiro, S.S. (2001). Filamins as integrators of cell mechanics and signalling. Nat Rev Mol Cell Biol *2*, 138-145.

Suetsugu, S., Murayama, K., Sakamoto, A., Hanawa-Suetsugu, K., Seto, A., Oikawa, T., Mishima, C., Shirouzu, M., Takenawa, T., and Yokoyama, S. (2006). The RAC binding domain/IRSp53-MIM homology domain of IRSp53 induces RAC-dependent membrane deformation. J Biol Chem *281*, 35347-35358.

Tanaka, T., Serneo, F.F., Higgins, C., Gambello, M.J., Wynshaw-Boris, A., and Gleeson, J.G. (2004a). Lis1 and doublecortin function with dynein to mediate coupling of the nucleus to the centrosome in neuronal migration. J Cell Biol *165*, 709-721.

Tanaka, T., Serneo, F.F., Tseng, H.C., Kulkarni, A.B., Tsai, L.H., and Gleeson, J.G. (2004b). Cdk5 phosphorylation of doublecortin ser297 regulates its effect on neuronal migration. Neuron *41*, 215-227.

Toyo-oka, K., Shionoya, A., Gambello, M.J., Cardoso, C., Leventer, R., Ward, H.L., Ayala, R., Tsai, L.H., Dobyns, W., Ledbetter, D.*, et al.* (2003). 14-3-3epsilon is important for neuronal migration by binding to NUDEL: a molecular explanation for Miller-Dieker syndrome. Nat Genet *34*, 274-285.

Trommsdorff, M., Gotthardt, M., Hiesberger, T., Shelton, J., Stockinger, W., Nimpf, J., Hammer, R.E., Richardson, J.A., and Herz, J. (1999). Reeler/Disabled-like disruption of neuronal migration in knockout mice lacking the VLDL receptor and ApoE receptor 2. Cell *97*, 689-701.

Tsai, J.W., Bremner, K.H., and Vallee, R.B. (2007). Dual subcellular roles for LIS1 and dynein in radial neuronal migration in live brain tissue. Nat Neurosci *10*, 970-979.

Tsai, J.W., Chen, Y., Kriegstein, A.R., and Vallee, R.B. (2005). LIS1 RNA interference blocks neural stem cell division, morphogenesis, and motility at multiple stages. J Cell Biol *170*, 935-945.

Tsai, L.H., Delalle, I., Caviness, V.S., Jr., Chae, T., and Harlow, E. (1994). p35 is a neural-specific regulatory subunit of cyclin-dependent kinase 5. Nature *371*, 419-423.

Tsai, L.H., and Gleeson, J.G. (2005). Nucleokinesis in neuronal migration. Neuron *46*, 383-388.

Tsujita, K., Suetsugu, S., Sasaki, N., Furutani, M., Oikawa, T., and Takenawa, T. (2006). Coordination between the actin cytoskeleton and membrane deformation by a novel membrane tubulation domain of PCH proteins is involved in endocytosis. J Cell Biol *172*, 269-279.

Wang, Q., Kaan, H.Y., Hooda, R.N., Goh, S.L., and Sondermann, H. (2008). Structure and plasticity of Endophilin and Sorting Nexin 9. Structure *16*, 1574-1587.

Wong, K., Ren, X.R., Huang, Y.Z., Xie, Y., Liu, G., Saito, H., Tang, H., Wen, L., Brady-Kalnay, S.M., Mei, L.*, et al.* (2001). Signal transduction in neuronal migration: roles of GTPase activating proteins and the small GTPase Cdc42 in the Slit-Robo pathway. Cell *107*, 209-221.

Yao, Q., Jin, W.L., Wang, Y., and Ju, G. (2008). Regulated shuttling of Slit-Robo-GTPase activating proteins between nucleus and cytoplasm during brain development. Cell Mol Neurobiol *28*, 205-221.

Yohe, M.E., Rossman, K.L., Gardner, O.S., Karnoub, A.E., Snyder, J.T., Gershburg, S., Graves, L.M., Der, C.J., and Sondek, J. (2007). Auto-inhibition of the Dbl family protein Tim by an N-terminal helical motif. J Biol Chem *282*, 13813-13823.

Yoshizawa, M., Kawauchi, T., Sone, M., Nishimura, Y.V., Terao, M., Chihama, K., Nabeshima, Y., and Hoshino, M. (2005). Involvement of a Rac activator,P-Rex1, in neurotrophin-derived signaling and neuronal migration. J Neurosci *25*, 4406-4419.